GKSS FORSCHUNGSZENTRUM in der HELMHOLTZ-GEMEINSCHAFT

Identification of geomorphological dynamics from bathymetric time series acquired by radar

(Vom Coastal Research Laboratory, Forschungs- und Technologiezentrum Westküste BÜSUM, der Christian-Albrechts-Universität zu Kiel als Diplomarbeit angenommen)

Author:
N. Alamsyah

ISSN 0344-9629

HELMHOLTZ | GEMEINSCHAFT

wissen schafft nutzen

GKSS 2008/9

GKSS 2008/9

Identification of geomorphological dynamics from bathymetric time series acquired by radar

(Vom Coastal Research Laboratory, Forschungs- und Technologiezentrum Westküste BÜSUM, der Christian-Albrechts-Universität zu Kiel als Diplomarbeit angenommen)

Author:

N. Alamsyah

(Institute of Coastal Research)

GKSS-Forschungszentrum Geesthacht GmbH · Geesthacht · 2008

Die Berichte der GKSS werden kostenlos abgegeben.
The delivery of the GKSS reports is free of charge.

Anforderungen/Requests:

GKSS-Forschungszentrum Geesthacht GmbH
Bibliothek/Library
Postfach 11 60
21494 Geesthacht
Germany
Fax.: +49 4152 87-17 17

Als Manuskript vervielfältigt.

ISSN 0344-9629

GKSS-Forschungszentrum Geesthacht GmbH · Telefon (04152) 87-0
Max-Planck-Straße 1 · 21502 Geesthacht / Postfach 11 60 · 21494 Geesthacht

GKSS 2008/9

Identification of geomorphological dynamics from bathymetric time series acquired by radar

(Vom Coastal Research Laboratory, Forschungs- und Technologiezentrum Westküste BÜSUM, der Christian-Albrechts-Universität zu Kiel als Diplomarbeit angenommen)

Novrizal Alamsyah

117 pages with 34 figures and 2 tables

Abstract

The remote sensing techniques are being used for monitoring the phenomena at the coastal region. The nautical X-band Radar which is mounted in the List West of Sylt by the Department of Radar Hydrography of GKSS Research Centre is used to determine important hydrographic parameter and the water depth. In this thesis, the theoretical accuracy of the Dispersive Surface Classificator (DiSC) used for the analysis of ground based X-band radar image sequences is estimated by the chi-squared distribution to construct the confidence limit of variance. The analyzed data are used for the identification of the tidal cycle and the monitoring of the impact of a severe storm as well the summer period effect on the sediment bedforms. The inversion of local wave in space and time proved that the in situ gauge can be simulated. The comparison between DiSC and tidal gauge water level has a significant correlation (corr = 0.77) at the selection area (81 neighboring cells). The morphodynamic evolution of the ship channel in Lister Tief is also examined. The long term comparison, February to October 2002, has proved that in the area of investigation, there are dynamic but stabilized sediment structures. Generally, it is proven that the characteristic of the channel (slope, absolute depth, width) have great variability and strong dependencies to short period, severe phenomena, such as a storm and to the seasonal impact of the normal, tidal water circulation. Both effects are important for the monitoring of the coastal evolution and protection. Finally, the ground based X-band radar could be characterized as a method for the operational monitoring of the coastal zone.

Identifikation von morphodynamischen Prozessen aus bathymetrischen Zeitserien mittels landgestützten Radars

Zusammenfassung

Fernerkundungstechniken werden unter anderem benutzt, um physikalishe Phänomene der Küstenregionen zu beobachten. Das nautische X-band-Radar, welches auf der Nordseeinsel Sylt, nahe dem Leuchtturm List West, installiert ist, wird von der Abteilung Radarhydrographie des GKSS-Forschungzentrums dazu verwendet, wichtige, hydrographische Parameter, wie die

lokale Wassertiefe, zu erfassen. In dieser Arbeit wird die theoretische Genauigkeit der Dispersive Surface Classificator(DiSC)-Software zur Analyse von landbasierten Radarsequenzen durch Chi-squared-Verteilung abgeschätzt, um einen glaubwürdigen Toleranzgrenzwert zu erzeugen. Die analysierten Daten werden dazu benutzt, um einen Tidezyklus zu identifizieren, den Einfluss von Sturmereignissen zu überwachen und ebenso den Effekt auf den Meeresboden während des Sommers zu beobachten. Die Invertierung der lokalen Wellen in Raum und Zeit beweist, dass In situ-Messungen simuliert werden können. Ein Vergleich zwischen DiSC- und Tide-Pegelwerten zeigt einen signifikanten Zusammenhang (corr = 0.77) im ausgewählten Gebiet (81 benachbarte Zellen). Die morphodynamische Entwicklung des Tidekanals Lister Tief wurde ebenfalls untersucht. Ein Langzeitvergleich von Februar bis Oktober 2002 hat bewiesen, dass im beobachteten Gebiet dynamische aber stabile Sedimentstrukturen existieren. Im Allgemeinen wurde bewiesen, dass die hydrodynamischen Charakteristika des Lister Tiefs (Gefälle, Wassertiefen, Breite) hoch variable und stark abhängig von Phänomenen mit kurzer Periode, wie Stürmen und dem saisonalen Einfluss der normalen Tidezirkulation, sind. Beide Effekte sind wichtige Parameter bei der Überwachung der Küstenentwicklung und des Küstenschutzes. Abschließend kann gesagt werden, dass das landgestützte X-band-Radar eine Methode ist, um eine operationelle Überwachung der Küstenregion zu gewährleisten.

Manuscript received / Manuskripteingang in TKP: 20. August 2008

Table of Contents

Tables and Figures

Acknowledgements

First of all, I would like to thank my supervisor Dr. F. Ziemer for giving me the opportunity to work at the Department of Radar Hydrography (KOR) of GKSS Center. This thesis would not have been possible without kind support, the critiques, the probing questions, and the remarkable patience from him. I am also truly and deeply thankful to Professor R. Mayerle, Director of the Master Course Coastal Geosciences and Engineering, University of Kiel for permitting me to pursue my thesis at GKSS and contribute as supervisor.

I am also very grateful to S. Flampouris, PhD student at KOR, for giving me guidance, and helping me to find solutions for my problem. His ability to explain scientific makes my life easier to writing thesis. I also want to thank M. Cycewski and S. Sedlacek, for tutoring me in PV-Wave programming and their help in practical problem. I also want to acknowledge G. Schymura for providing measurement data.

Finally, I would like my special thanks for my parents who always giving me totally support in my whole life. I also can’t forget Mirna Sophia who always gives me encouragement to do my best in all matter in my life.

Notations

σ^2	variance
μ	mean
∂	partial derivation operator
$\vec{k}$	2D wavenumber vector of sea-surface waves (rad m^{-1}, rad m^{-1})
$\vec{r}$	spatial vector
$\vec{u}_c$	2D near-surface current vector (ms^{-1}, ms^{-1})
C_G	group velocity of sea-surface waves (ms^{-1}, ms^{-1})
C_p	phase velocity of a sea-surface wave (ms^{-1}, ms^{-1})
d	water depth (m)
f	frequency (s^{-1})
ω	circular frequency (s^{-1})
g	gravitational acceleration
k	wavenumber (rad m^{-1}), magnitude
k_x, k_y, k_z	Cartesian wavenumber components (rad m^{-1})
t	time (s)
x,y,z	spatial coordinates (m)
Θ	3D spatio-temporal domain (m, m, s)
Ω	3D wavenumber-frequency domain (rad m^{-1}, rad m^{-1} rad s^{-1})
λ	wavelength (m)
θ	incidence angle
τ	waveperiod
ζ	sea-surface elevation (m)
ς	intrinsic dispersion of sea-surface waves (rad s^{-1})
ς^+, ς^-	positive and negative solution of dispersion (rad s^{-1})
P_r	received signal power
P_t	power
G_t	gain
R	distance
A_e	effective aperture area
λ_s	scattering wave length
λ_r	electromagnetic wave

1. Introduction

The coastal zone plays an important role to the welfare of human and economy which are inextricably linked to the features and activities that occur within this dynamic region. More than 44 % of the world population lives within 150 km of the coast. In 2001 over half the world population lived within 200 km of a coastline (UNEP 2006). The spatial and temporal variations of coast on all scales affect lives and environment significantly. As the coastal communities grow, the pressure of the environment is increasing due to the human activities such as economical and recreation activities. Therefore, the monitoring of oceanographic phenomena, the protection and the development of the coastal zone of socio-economical interest are required.

The knowledge of the bathymetry is one of the most important factors for coastal and marine activity because the changes of the bathymetry have direct influence on the human activities. The attainment of spatial and temporal bathymetries is part of the oceanographic routine; the methods are from rope and plummet to sonar and echo sounding and nowadays by the development of the remote sensing and concrete wave theory, since the first trips of exploration the bathymetric data is a requirement (FLAMPOURIS 2006). Thus long term monitoring using a variety of coastal monitoring systems is needed to better understand coastal phenomena and assess the sustainability of the coasts.

1.1 Objective

The main focus of the investigation is the application of ground based X-band radar on determination of water level and bathymetry.

The objectives of this study are:

1. Identification of the tidal signal at the DiSC results by integrating tide gauge measurement and wind influence.
2. Accuracy of the method and the application of DiSC results as virtual tidal gauge.

3. Comparison of depth and slope over two cross sections to identify the morphodynamic changes in the area of investigation.

The long-term goals are the improvement of DiSC system as oceanographic instrument and operational system for the bathymetric monitoring of coastal regions.

1.2 Background

The sea state and the tidal currents act as forces which induce morphodynamic changes in coastal waters and on the coastline. The knowledge of the bathymetry, at the near shore area and over various spatial and temporal scales, is important for understanding such an interactive regime. Traditional surveying methods of qualifying the depth are inherent labor intensive as they involve manual deployment of expensive instrument over the area of interest. Even with sophisticated depth measuring device like sonar altimeters and global positioning satellite units, the process remains costly in terms of both time and money. Satellite till now are not applicable in coastal area. It is not feasible to use these methods to cover large spatial distance (MISRA, KENNEDY, and KIRBY 2001). Therefore, there is urgent need for a cost-effective remote sensing method, which allows the retrieval of the geo dynamics.

For the last three decades, the RADAR (RAdio Detecting And Ranging) remote sensing is flourished. The first civil system was the CODAR of NOAA (BARRICK 1977), a high frequency system which concerns mainly the measurement of ocean wave and currents. Since the first system of CODAR then there are several projects around the world based on spatial and temporal structure analysis of radar images of the sea surface. The algorithm have been evolved to measure the wave direction spectra within a 2 km^2 patch of the sea using a nautical radar which permit to provide sea state parameters such as significant wave height and peak period. At least two companies commercialized this radar system, the Wave Monitoring System (WaMoS), developed by GKSS research center in Germany (ZIEMER 1991 & 1995, ZIEMER & DITTMER 1994 and NIETO BORGE 1999) and the Marine Radar Wave Extraction (WAVEX), developed by the MIROS AS company in Norway (GRONLIE, 1995 and GANGESKAR & GRONLIE 2000).

The microwave remote sensing method such as ground based X-band radar is suitable for monitoring the waves in coastal zone, with the wave field ranging from few meters to few hundred meters. Therefore, the ground based X-band radar is the adopted wave and current measurement tool. The advantage of deployment nautical X-band radar systems can typically be made in severe storm without high risk of damage the instrument. Nautical X-band radar is not impeded by most weather or light conditions. The only exception is heavy rainfall that increases the background noise in a way that no “signal” is detectable.

For the implementation of the objective, the input data are retrieved by using a remote sensing method (X-band radar) and the Dispersive Surface Classificator (DiSC) software. From the acquired image sequences, hydrographic parameters, such as the water depth (OUTZEN 1998, WOLFF et al.1999) are determined. DiSC is an algorithm that analyses image sequences for the determination of the physical parameters on a local spatial scale, it consist a local analysis method, which allow the analysis of inhomogeneous image sequences of a dynamic and dispersive surface. The method used to date, used the noise to signal ratio, are based on the analysis of radar backscatter signal variance spectra calculated by modulus of a 3D Fast Fourier Transformation (3D FFT) performed on the image sequences. The waves phase maps are estimated and inversed in local scale for the determination of the bathymetry.

The raw radar data were acquired by X-band radar which was mounted at the island Sylt Isle close to the lighthouse List West, a coastal area with high morphodynamical activity, as there is a sand bar which could change the impact hydrodynamic effectively. The radar data is mounted from the 2001 until 2007 with gaps in data acquisition. For the same period, there are available wave buoy data (GKSS), water level data (ALR) and wind data acquired at the radar position. As the DiSC method is applicable during storm period, the available meteorological data have been analyzed and according to them the analysis period of the thesis have been chosen. The thesis is focused on the investigation of the bathymetric surveys during three different periods in 2002. The occurred bathymetries constitute a time series every 0.5h with a total of 24 steps (one period) and 1h with total 12 steps (two periods) each one tidal cycle.

1.3 Outline

The thesis is consisted by seventh chapters. In the first chapter the introduction is described the background of thesis. In the second chapter the study is described the literature on which the thesis based reviewed. The third chapter describes the principles of the mechanism of radar to determine the wave field characteristics and the DiSC (Dispersive Surface Clasificator). In the fourth chapter, the methodology of the thesis is presented. The achievements procedure by the thesis are presented in chapter fifth to seventh where the results are illustrated, discussed and the initial queries are fulfilled.

2. Literature Review

2.1 The Study Area

The island of Sylt is the northernmost outpost in Germany and sits on the West coast of Schleswig-Holstein at North Sea coast of German Bight. Sylt has a length 35 km from north to south and a width up to 13 km from east to west, its surface is 99 km^2. The length of the sandy coastline in North-South direction is about 40 km. The narrowest point of the island is less than 400 m wide. The island was once part of the mainland, and is still shrinking owing to erosion due to the sea state, which is common for most islands and shorelines in the region, which are slowly but constantly changing.

The tide in area of Sylt is semi-diurnal with a maximum tidal heave of approximately 2 m, which cause cross shore transport through the gaps between barier island of German Bight. The longshore transport along the coast is overlaid by wave impact and also alternates in direction, which is obvious at the shape Sylt. The island grows northward as well as southward by spit prolongation in both directions. The nearshore area is characterized by a longshore bar, which is located approximately 300 m seaward of the shoreline. During storm surges, with a water level rise of more than 2 m, the protective effect of the bar (crest height approximately 3 m) is lost and waves pass over the bar without breaking. According to geological estimates, the west coast of Sylt has receded approximately 13 km over a period of 7000 years (1.8 m/year). Since monitoring started (1870) the recession rate has been 0.9 m/year. Over this period, the underwater profile has been shifted eastwards, probably without much change in shape. The eroded material has created spits to the north and south of the centre of the island. These are now curtailed by major tidal channels. Tidal currents carry the sand that arrives at the ends of the spits away from the island. Thus, Sylt is a typical example of an open sand system, because eroded material is not returned to the island (HAMM 2002).

Attempts since 1865 to slow down dune recession by various types of groins along large parts of the island have been fairly unsuccessful, as was a seawall (built in 1907) in the middle of the island (Westerland), which needed gradual reinforcement

and extension. Since 1972, repeated beach nourishments have been carried out regularly to protect this seawall and its 3 km-long revetment against under scouring. Since 1950, greater storm surge frequency has caused the mean yearly recession rate to increase from 0.9 m/year (1870–1950) to 1.5 m/year (1950–1985), which is equivalent to an annual loss of 1.5 million m^3 of sand (1/3 to the south and 2/3 to the north). This prompted the coastal authorities ('Amt für Ländliche Räume' in Husum) to initiate a specific coastal protection master plan in 1985, for a period of 35 years (1985–2020), which has recently been updated in 1997. This assumed that the increased storm surge frequency would continue, and with it, the erosion that would endanger the island if no counter-measures was undertaken. All possible alternatives for future coastal protection of the west coast were considered, and their technical, economic and environmental aspects indicated that repeated replenishments in the form of deposits on the beach and shoreface nourishments would provide the most favorable solution. In the updated nourishment concept, it is intended to maintain the coastline in its 1992 position by compensating for the mean yearly sand loss from the coast. The coastline is defined by the dune foot (3.75 m above mean sea level). The order in which various areas have to be nourished is determined by the degree to which the sites along the west coast are endangered (NEWE & DETTE 1995).

The vulnerable island Sylt has a multi-functional socio-economic nature and is covered by a mixture of natural and cultural land uses. Besides high-level standards in living and recreation facilities, Sylt offers unique aspects of a biotope. The area of Sylt consists of national park which is strongly bounded with the ecological environment of Wadden Sea.

The urge of protecting the coastal area at Sylt is a major concern due to the activities within the area. Extensive work had been done for preventing it, since the 1960's effort for protecting was started then it took place intensely at 1980's (APPENDIX I), one of method is sustainable monitoring system. Therefore, the sufficient continuous and accurate data are necessitated for anticipating the problems which will be occurred in Sylt. The significant role of radar Hydrography is to observe and acquire data for systematic assessment of sediment movement with any weather circumstances.

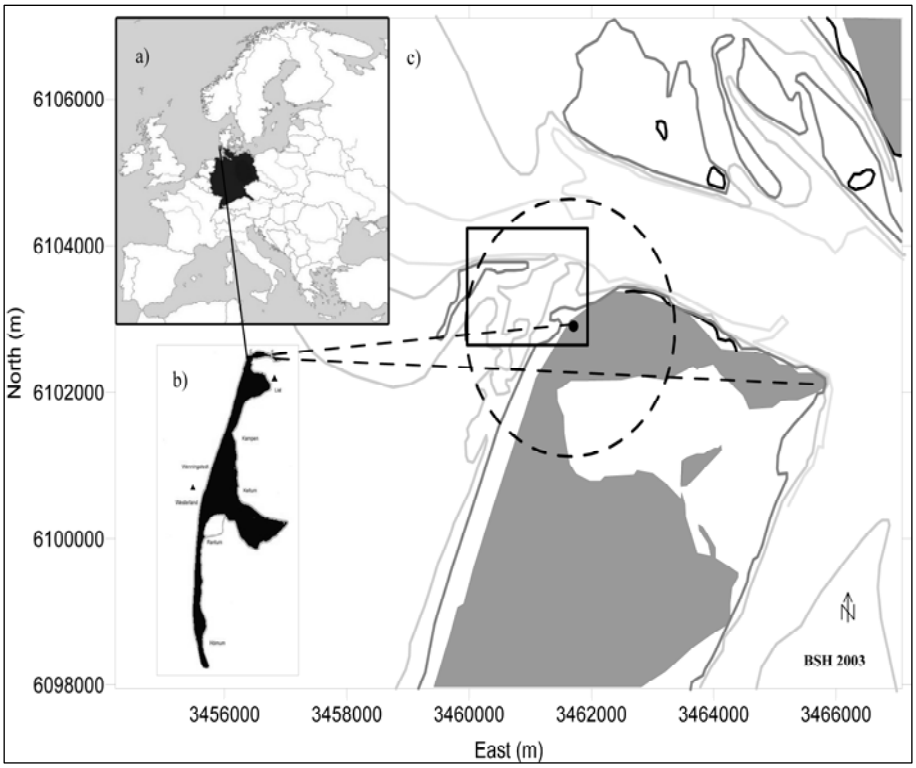

Figure 2.1 Maps for the localization of the area research position, in the black frame on the right map, (FLAMPOURIS 2007).

2.2 Water Level Measurement and the Importance of Remote Sensing

Remote sensing techniques as indirect observation method have great capabilities for monitoring sea state such as water level monitoring. Water level monitoring over long periods of time are particularly helpful in understanding the circulation of the ocean. The measurement of sea level stands out as one of the simplest and most effective methods for establishing long-term global databases of ocean observations.

Bathymetry in the nearshore changes continuously under energetic interactions with shoaling and breaking waves. In the dynamically active coastal area, the bed topography change due to an active interaction between sediment transport and hydrodynamic processes. An accurate knowledge of the ocean floor, particularly in the nearshore region over spatial and temporal scale, is very important in understanding such as interactive regime (MISRA, KENNEDY, and KIRBY, 2002).

Nearshore bathymetry is required to describe depth-induced wave changes and large-scale fluid motions (YOO 2007). Changes in bathymetry can occur on time scales as

short as hours due to the presence of large storms. Data are especially difficult to collect during periods of large waves or strong currents. However, these conditions often represent the most energetic periods for hydrodynamics, morphodynamics, and are the times of greatest scientific interest (HASAN & TAKEWAKA 2007).

The in-situ instruments can record the variation of water surface elevations, velocities, sediment concentration, bottom elevation etc. These instruments are a powerful tool for monitoring nearshore regions. However, the measurements are expensive and limited in spatial extent. Further, during energetic sea states it is not easy to maintain data collection. Remote sensing techniques provide a feasible alternative due to they allow sampling over large spatial extents (meters to kilometers) and temporal scales (seconds to years).

The one of earliest forms of remote sensing is aerial photography which used to image wave field. The utilized of wave-shoaling photographic imagery and the observed reduction of ocean wave phase speed with decreased water depth was used as early as World War II to provide useful estimates of bathymetry in coastal environment (TRIZNA 2001). Nowadays, video camera and radar are becoming popular for continuous monitoring. Video cameras can monitor the sea surface patterns with high temporal resolution typically several images per second. However, the spatial coverage is limited with single camera, which necessitates multiple cameras in order to gain wide coverage. One severe shortcoming is that the use of video cameras is limited to daylight hours and fair atmospheric conditions.

The estimation of hydrodynamic and morphodynamic parameters from video images is just one of a suite of recent techniques. Stockdon and Holman (2000) developed an advanced method to estimate nearshore bathymetry based on video processing. They calculated wavenumber components from the gradient of the wave phase propagation of the dominant incidental band, and a linear dispersion relationship was used to estimate water depths. A similar analysis has been used by Holland (2001) for time series data from bottom mounted pressure sensors. He found that the inclusion of finite amplitude effects in the linear dispersion relationship improved his depth predictions. Piotrowski and Dugan (2002) used a sequence of video images of shoaling ocean waves to retrieve maps of water depth and currents. Some other studies also used inversion techniques to retrieve bathymetry.

Some of the limitation of video imaging can be overcome by using X-band radar. The pixel intensity of the radar image corresponds to the relative amount of backscatter signal from sea surface of the emitted radar beam, which allows its use during night and under slightly rainy and storm conditions as well. Radar image sequences with high spatial resolution and large coverage offer a unique opportunity to study individual waves and wave field in space and time.

Nowadays, the use of X-band radars in coastal studies is becoming popular. Young *et al*. (1985) first described an approach using three-dimension Fourier transform analysis on a sequence of radar images. The resulting wave number spectra were inverted to frequency spectra with information the water depth. Izquierdo *et al.* (2005) compared the ocean wave field derived from X-band radar and wave-rider buoy measurements by spectral analysis. The comparison show a good agreement between variations of significant wave height, peak frequency and mean period obtained from both devises. The estimated directional spectra from their radar observations were broad banded due to coexistence of storm generated swell and wind wave. Bell (1999, 2001) succeeded in determining near-shore bathymetry after analyzing X-band radar images. He applied a linear depth inversion technique, considering peak period of Fast Fourier Transformation (FFT), and wave celerity from cross correlation between sequences of images. Bell *et al.* (2004) used two different type of radar (X-band and MMW radar) to infer water depth and tried to improve further the depth inversion. Hessner *et al*. (1999b) have discussed the use of space-time behavior of the sea surface elevation (with an accuracy of 10% in the significant wave heights) acquired from nautical radars in estimating the water depth. Reichert et al. (1999) and Hessner *et al*. (1999a) have compared sea state measurements acquired from shallow water installation of a remote sensing system based on a nautical X-band radar, to Waverider buoy data, and found that surface current velocities could be estimate to within an accuracy of ± 0.2 m/s.

Recently, Dankert and Rosenthal (2004) developed an empirical inversion method for determination of time series of ocean surface elevation, which maps from X-band nautical radar image sequences in relative deep region. For validation of their result, the wave elevation time series derived from the inverted radar data sets were compared with wave records, and acceptable accuracy was established. Takewaka

and Nishimura (2005) analyzed radar images for run-up analysis during a storm. Takewaka (2005) also analyzed time averaged X-band radar images to quantify shoreline position and inter-tidal foreshore slope, while Ruessink *et al*. (2002) analyzed images to locate near-shore bar crest. Chowdhury (2007) analyzed the correlation between water depth echo sounder measurement and water depth X-band radar deduced. The comparison shows moderate correlation between two depths. Within this thesis, the comparison between water level from X-band radar-deduced and water level from gauge measurement will be analyzed during the storm condition to identify the correlation between both measurements (see, chapter 4).

.

2.3 Erosion and Deposition

The morphodynamical processes in coastal area are affected by tidal currents and sea state, leading to a transport of sand along the seafloor. Vice versa the tidal currents are influenced by changes in the bottom topography (SOULSBY 1997). The continuous observation of areas of high morphodinamycal activity is important in order to warn of such changes in the flood stream situation and to avoid futher change or loss of land (WOLFF et al. 1999).

Morphodinamycal changes can be observed by radar. Radar images the small roughness on the sea surface, causing backscattering (LEE et al. 1995). The sloping bottom induced horizontal gradients in the tidal current, resulting in a variation of the surface roughness (ALPERS & HENNINGS 1984). Another effect resulting in the imaging of the bottom topography is caused by wave breaking in the shallow water (HENNINGS 1988). Therefore, the backscattering indirectly depends on the bathymetry. It is known from the analysis of the satellite images that the observable signatures depend on the tidal currents and the wind situation (VOGELZANG 1997).

In a study by MENN (2002a, b) the effects of eroding and accreting conditions on the structure of beaches were determined. The eroding shore (Sylt/Germany) is coarse grained, steeply profiled and receives high wave energy, while the accreting shore (Rømø/Denmark) is fine grained, flat profiled and receives less wave energy. The former resembles dynamic intermediate beach types and the latter a dissipative beach type (Short & Wright 1983).

The motivation for the observation of the coastal area at Sylt is its high morphodynamical activity. A sand bar between the Lister Landtief and the Lister Tief is the process of breaking, which would change the flood stream situation dramatically. As it is possible to draw conclusion about the bathymetry by interpretation the observation structures, permanent monitoring of the area would allow continuous observation of changes in the bottom topography.

Erosion is almost synonymous to the Sylt Island. The entire coast of Sylt has been severely eroding since a long period of time; accumulation of sand is not seen at any part of the coast. After 1950 the erosion rate in Westerland-Kampen (north of Westerland) has been increasing as compared to the southern area (SISTERMANS & NIEUWENHUIS 2007). During a single storm event it is estimated that about 50,000 cubic meters (± 10%) of sediment is replaced in the area (FLAMPOURIS 2006).

The sediment transport results in a dominant seaward directed cross shore bar, pointing into the German Bight, vice versa this bar steers the tidal current surrounding the north end of Sylt and thus it indirectly steers the sediment transport in the feed back process. The long shore transport along the coast is mainly wave-induced and therefore also alternating in direction. Due to the structural erosion by wave and tide, the adapted main type of coastal protection is beach nourishment at the west coastline of the island, the majoring of this sand being lost during storm surge (AHRENDT 2001).

For the observation of morphodynamic changes at the List Tief area, the changes of slope in the tidal channel from three different time periods will be analyzed (see, chapter 4).

3. Theoretical Background

Remote sensing is the collecting data about sea surface features without coming into direct physical contact with them. The last three decades, the originally technologies developed for military purpose and have been converted for scientific and civil applications. Many of earth observation missions have been successfully carried out providing some useful information. Oceanography, hydrology, geology, forestry and agriculture have been targeted for such applications as hazardous events prevention and territory management. Many of the sea-state parameters for coastal and oceanographic researches are observed by remote sensing techniques, including wave height, water level current field, sea surface temperature, ocean color and surface wind field (FLAMPOURIS 2006).

Ocean wave remote sensing observation can be applied from the several coasts, ship, aircraft or satellite. Surface Ocean waves are measured by several different techniques have become of particular interest in applications where the advantage of remote sensing is to avoiding direct contact with the water surface and avoiding structural interference. The sensor type includes infrared sensor, optic sensor and radar. Radar remote sensing of ocean surface waves may in general be defined as measuring characteristics of the sea surface by means of electromagnetic waves so that the sea surface itself not disturbed. The electromagnetic waves transmitted by the radar antenna are scattered back from the sea surface, modulated in amplitude and phase or frequency by the interaction with the sea surface motion. This modulation carries information about sea characteristics, surface waves and currents. Oceanographic data is extracted from the backscatter signal by sophisticated signal processing and data analysis (SKOLNIK 1990).

The waves are propagating from open sea toward to the coast. During the storm condition, the wave action can cause erosion or deposition at the nearshore area. Therefore, the monitoring of waves at nearshore area is required. These waves can be monitored by ground based X-band radar. The assumptions of the waves are described by linear wave theory and it could be inversed for determination of local bathymetry.

In this chapter, the basic theoretical background of the ground based X-band radar, the linear theory and the connection with DiSC method will be described.

3.1 Microwave Radar Remote Sensing Applied in Oceanography

Radar measures the strength and round-trip time of the microwave signals that are emitted by a radar antenna and reflected off a distance surface or object. The radar antenna alternately transmits and receives pulses at particular microwave wavelengths and polarizations (waves polarized in a single vertical (VV) or horizontal plane (HH)).

Radar can be operated both day and night. This type of system is known as radar active system while passive radar measures the electromagnetic radiation emitted by any radiating source. Microwave radar with wavelength ranging from 0.1 cm to 100 cm, are noted for their ability to penetrate rain, fog and clouds. The spatial resolution of a radar system depends on the transmitted signal in the range and on the antenna pattern in direction (LILLESAMD & KIEFER 1994). The azimuth resolution depends on the microwave wavelength and antenna length; real aperture or the ratio antenna length to microwave length may be improved by either decreasing the wave length of electromagnetic wave or by increasing the antenna length. However, the shorter wavelength radars are affected by sea spray or the rain drops.

Nowadays, remote-sensing techniques at the coastal zone applied to wave and current measurement with coastal radar have become more important. Coastal radar used the microwave radar which has frequency range from 3 to 30 GHz and high frequency radar which has frequency range from 3 to 30 MHz. Both use electromagnetic waves remotely sense ocean surface current and sea states over extended areas. The advantage of microwave radar is easy to install, but does not cover the area as large as it is possible to cover with HF radars. Microwave marine radars originally used for navigation have been developed to measure the ocean waves, such as WaMoS (Waves Monitoring System). WaMoS makes ocean waves and surface currents measurement with microwave marine radar (X-band radar) based on the spatial and temporal structure analysis of radar images of the sea surface (REICHERT et al. 1999). These radar images are generated by the interaction of electromagnetic waves with the surface ripples at grazing incident. The spatial and temporal variability of the sea clutter information is analyzed in order to

extract the wave spectrum and further sea state parameters, such as significant wave height and peak period.

Although the observation range of coastal radars is not as extensive as satellites, the superiority of waves measurement by land-based radar lies in its capability to observe 3D images of the sea state by routine operation, as opposed to 2D observation made from satellite or aircraft. In addition, the wave monitoring systems by coastal radars are relatively easy to install and to operate. Thus it would appear that coastal radars are the potential instruments for the remote sensing activities of waves monitoring, more extensively in the future.

For the present study, the ground based X-band, microwave radar is used. Details of the radar system are tabulated in Table 3.1.

Table 3.1: Properties of the X-Band Furuno 1201 nautical radar (ANONYMOUS 1989).

Properties	Value
Frequency	9410 MHz ± 30 MHz
Pulse repetition Frequency	3 KHz
Antenna type	Slotted Wave Guide
Antenna beam width	0.95º
Polarization	HH
Rotation speed	34-40 cir/min
Output power	5 KW nominal
Pulse length	0.05 μ sec

The antenna rotation time allows imaging successively the ocean surface without the loss of correlation of the image wave fields. This allows acquiring image time series of ocean wave fields, which have the quality to extract wave describing parameters by inverse modeling.

3.1.1 Radar Equation

The way to describe the radar principle is the physical definition, as the single most useful description of the factor influencing radar performance is the radar equation which gives the range of radar in terms of the radar characteristics. One form of this equation gives the received signal power P_r as:

$$P_r = \left(\frac{P_r G_t}{4\pi R^2}\right)\left(\frac{\sigma}{4\pi R^2}\right) A_e \qquad (3.1)$$

The right side has been written as the product of three factors to represent the physical processes taking place. The first factor is the power density at a distance R meters from radar that radiates a power of P_t watts from an antenna of gain G_t. The numerator of the second factor is the target cross section σ in the square meters. The denominator accounts for the divergence on the return path of the electromagnetic radiation with range and is the same as the denominator of the first factor, which accounts for the divergence on the outward path. The product of the first two terms represents the power per square returned to the radar. The antenna of effective aperture area A_e intercepts a portion of this power in an amount given by the product of the three factors.

3.1.2 Sea Clutter

Ocean waves are imaged by a nautical radar because the long surface gravity wave modulate the radar backscatter from the sea surface. Thereby the small scale roughness of the sea surface raises the backscatter of the electromagnetic waves. This phenomenon is called sea clutter (WETZEL 1990).

Bragg scattering is resonant backscatter that occur when electromagnetic energy interacts with waves that have wavelength interacting with transmitted electromagnetic waves. At large angels of incidence, Bragg scattering is responsible for the return, at grazing incidence Bragg scattering criterion being fulfilled by those wave having a wavelength equal to one half the electromagnetic wavelength. Small scale capillary waves on the order of 1 to 3 cm provide the source for Bragg resonant scattering of marine X-band radars. The intensity of backscattered energy is most affected by magnitude of the wind velocity, the incidence angle of the emitted Bragg scattering is strongest when the radar azimuth angle is aligned with the wave direction. This pattern of returned electromagnetic energy is modulated by the large structures, such as swell and wind sea waves.

It would seem a simple matter to characterize sea clutter empirically by direct measurement of radar returns for a wide variety the radar and environmental parameters that appear to affect it. Parameters relating to the radar or its operating configuration, such as frequency, polarization, cell size, and grazing angle, may be specified by the experimenter, but the environmental parameters are quite another matter for two reasons. First, it has not always been clear which environmental variables are important. Even if the importance of an environmental parameter has been recognized, it is often difficult to measure it with accuracy under real sea condition, and there are practical and budgetary limits to obtain open-ocean measurements in sufficient variety to develop any really meaningful statistical models of clutter. Little wonder that many aspects of sea clutter remain frustratingly unidentified (SKOLINK 1990).

It is noted that the appearance of sea clutter depends strongly on the size of the resolution cell or radar footprint. For large cells it appears distributed in range and may be characterized by a surface-averaged cross section with relatively modest fluctuations about a mean value. As the size of the resolution cell is reduced, clutter takes on the appearance of isolated target like, or discrete, returns that vary in time. At these higher resolutions, the distributed clutter is often seen to consist of a dense sequence of discrete returns. When the discrete returns stand well out of the background, as they are seen to do for any polarization but most clearly with horizontal polarization at small grazing angles, they are called sea spikes and are common clutter contaminant in this radar-operating regime.

In 1956, however it is observed that at high frequency (HF) wavelength (tens of meters) scattering appeared to arise from a resonant interaction with sea waves of one-half of the incident wavelength (CROMBIE 1956), i.e., to be of the Bragg type. Reinforced by the theoretical implications of various small wave height approximations and wave tank measurements under idealized conditions, the Bragg model was introduced into the microwave regime by many researchers. This produced a revolution in thinking about the origins of sea clutter because it involved the sea wave spectrum, thus forging a link between clutter physics and oceanography in what became the field of radio oceanography. However, fundamental conceptual problems in applying the Bragg hypothesis in microwave scattering, along with

recent questions about the validity of its predictions and the possibility of alternative scattering hypotheses, have reopened inquiry into the physical origins of sea clutter and how best to model it. This being the case, speculation about models will be kept to a minimum in the sections on the empirical behavior of sea clutter (SKOLNIK 1990).

3.1.2.1 Backscatter Mechanisms

There are various measuring techniques based on the backscatter theories of radar signal. Some are based on the analysis of the backscatter intensity of the return radar signal. Others use both the backscatter intensity and the Doppler spectrum. The mechanism that leads to a scattering of the electromagnetic waves from the sea surface depends on the incident angel. At small incidence angles with respect to the vertical (less than 15°-20°), the main scattering mechanism is quasi-specular, and the roughness scale with govern the backscattering intensity cover all scales from about 3 times the electromagnetic wavelength. At the moderate incident angle from (20° to 70°), the main processes is the so-called “Bragg resonant process” which is generated time by the waves on the surface which are of the same order as the electronic wavelength. At large incidence angles (grazing angle above 70º), the backscattering is more complex, including shadowing effect and other complex mechanisms. In some cases the backscattered signal provides “direct” information on the wavelength of interest, because the Bragg wavelength is of the same order. In other case, marine radars, airborne, or spaceborne real or synthetic aperture radars, the backscatter is related to short wavelength of interest such as X-band radar which is used wave imaging based on Bragg scattering from the small capillary ripples on the surface of the gravity waves.

3.1.2.2 Bragg Backscattering

The radar echo is generated by Bragg scattering, hence wind generated surface ripple (capillary waves) must be present the back scattered signal will be modulated by the large surface gravity waves and gravity wave information is derived from the modulation of backscattered signal.

The Bragg backscattering consists the main theory broadly used for the backscattering of radar, e.g. ground based or naval radars, ERS SAR and in the present paragraph the mechanism is described.

As the incidence angle of radar is oblique to the local mean angle of the ocean surface, there is almost no direct specular reflection except at very high sea states. Therefore it is assumed that at first approximation Bragg resonance is the primary mechanism for backscattering radar pulses. The Bragg equation defines the ocean wavelengths for Bragg scattering as a function of radar wavelength and incidence angle:

$$\lambda_S = \left(\frac{\lambda_r}{2 \sin \theta} \right) \qquad (3.2)$$

where λ_s is the sea surface wavelength, λ_r is the radar wavelength and θ is the incident angel.

The short Bragg-scale waves are formed in response to wind stress. If the sea surface is rippled by a light breeze with no long wave present, the radar backscatter is due to the component of the wave spectrum which resonates with the radar wavelength. The Bragg resonant wave has its crest nominally at right angles to the range direction.

For surface waves with crest at angle to the radar line-of-sight, as shown at the figure, 3.1, the Bragg scattering function is:

$$\lambda_S^{'} = \frac{\lambda_r \sin \phi}{2 \sin \theta} = \lambda_S \sin \phi \qquad (3.3)$$

where: $\lambda_S^{'}$ is the wavelength of the surface waves propagating at the angle ϕ to the radar line of sight.

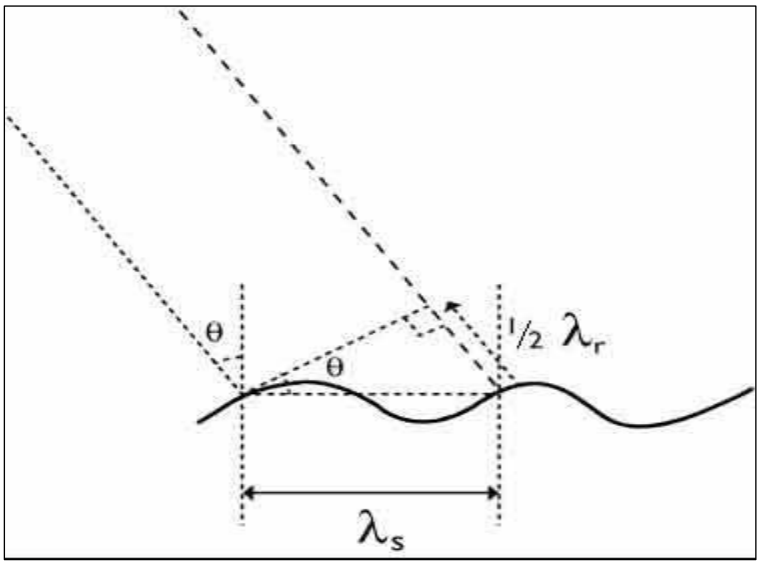

Figure 3.1: Scheme to visualize the relation between scattering wave with the length λ_s and the electronic wave with the length λ_r. The relation between those two is observed by (ESA, 1968) and consist the basic principle of the radar system.

The radars directly image the spatial distribution of the Bragg-scale waves. The spatial distribution may be affected by longer gravity waves, through tilt modulation, hydrodynamic modulation and velocity bunching.
Moreover, variable wind speed, changes in stratification in the atmospheric boundary layer, and variable currents associated with upper ocean circulation features such as fronts, eddies, internal waves and bottom topography affect the Bragg waves.

3.1.3 Modulation Mechanisms

There are several modulation mechanisms that effects the measurements by the radar, the integrated effect of the processes are describe in the next three paragraphs is that one image of low wave field is impressed to the radar signal that is related to the instantaneous sea surface by a Modulation Transfer Function (MTF). For the discussion within this thesis, it is only necessary to localize the position of the moving wave crests and not the retrieve the real shape of the surface. The linear scaled imaging of the wave crests within the radar backscattered fields is not affected by the MTF, thus the intense about it is not real strong.

3.1.3.1 Tilt

Tilt or electromagnetic modulation occurs when a local tilting of the surface changes the local incidence angle and thus the wave on the surface that causes Bragg scattering (WACKERMAN 2000). Tilt modulation is a purely geometrical phenomenon that is created by gravity waves "tilting" the ocean surface towards and away from the radar. Radar backscatter increases as the wave is tilted towards the radar and decrease as the wave is tilted away from the radar. Tilt modulation is most prevalent when the radar beam is perpendicular to the wave front. Tilt modulation provides no contribution to the backscatter if the wave crest is parallel to the radar beam.

3.1.3.2 Hydrodynamics

The sea clutter depends on the hydrodynamic conditions of the area of investigation; the effect the currents on signal is the most investigated. Hydrodynamic modulation is caused by change in shape of small-scale waves that cause Bragg scattering. Capillary waves increase in amplitude, decrease in wavelength on the front of gravity waves and decrease in amplitude, increase in wavelength on the back gravity waves. The modulation of small-scale capillary waves on the front of the wave leads to a higher amount of backscatter on the front part of the wave.

Shipboard observers have reported bands of roaring breakers passing by on an otherwise smooth surface, presumably produced by powerful surface-current shears associated with large amplitude internal waves. The general effect of the current is a change in the surface roughness, which can be expected to give rise to a change in sea clutter cross section (LONG 1990).

3.1.3.3 Shadowing

Radar shadowing as the image can only display that which is along a line of sight to the radar antenna. Shadowing occurs when the crest of wave prevent illumination of the following trough. Thus a "shadow zone" is created between successive crests. Shadowing is the most prevalent modulating mechanism at high angles of incidence (DANKERT and ROSENTHAL 2004).

The shadowing effect at the image sequences of the coastal radar caused by the shape of the waves. The waves are characterized by bright signals from the near slopes and the absence, not illuminated by the radar, of signal by the far slopes. For the sea, it is likely that effects of shadowing become appreciable for angles of incidence closer to horizontal that the crest height and sea wavelength. The shadowing of troughs by crests cause the reduction in expected scattered power. At near grazing incidence angles, when shadowing is appreciable, it is expected that the top of the crests contribute significantly to create the effective reflective surface.

3.2 Sea Surface Waves

Ocean surface waves are mechanical waves that propagate along the interface between water and air. The primarily natural forces are pressure from the atmosphere (especially through the winds), gravity of the Earth and celestial bodies (the moon and the sun), earthquakes, the Coriolis force (due to the Earth's rotation) and surface tension. The characteristics of waves depend on the driving forces. Tidal waves are generated by the response to gravity of the moon and the sun and are rather large-scale waves. Capillary waves, at the other end of the scale, are dominated by surface tension in the water. The restoring force is provided by gravity, and so they are often referred to as surface gravity waves. As the wind blows, pressure and friction forces perturb the equilibrium of the ocean surface. These forces transfer energy from the air to the water, forming waves.

The general concept of the mechanism of wind sea-surface wave generation: if wind skims along the water surface, small perturbations of the near boundary atmospheric pressure field lead to small perturbation of the water surface. The distorted surface allows viscous or turbulent energy transport, leading to the growth of waves. Several theories have developed for detailed explanation of the phenomenon (MILES 1957, HASSELMANN 1962, PHILLIPS 1966) but still it has not totally been clarified. The information about the energy distribution of the waves versus the frequency or the wavelength is illustrated in figure 3.2.

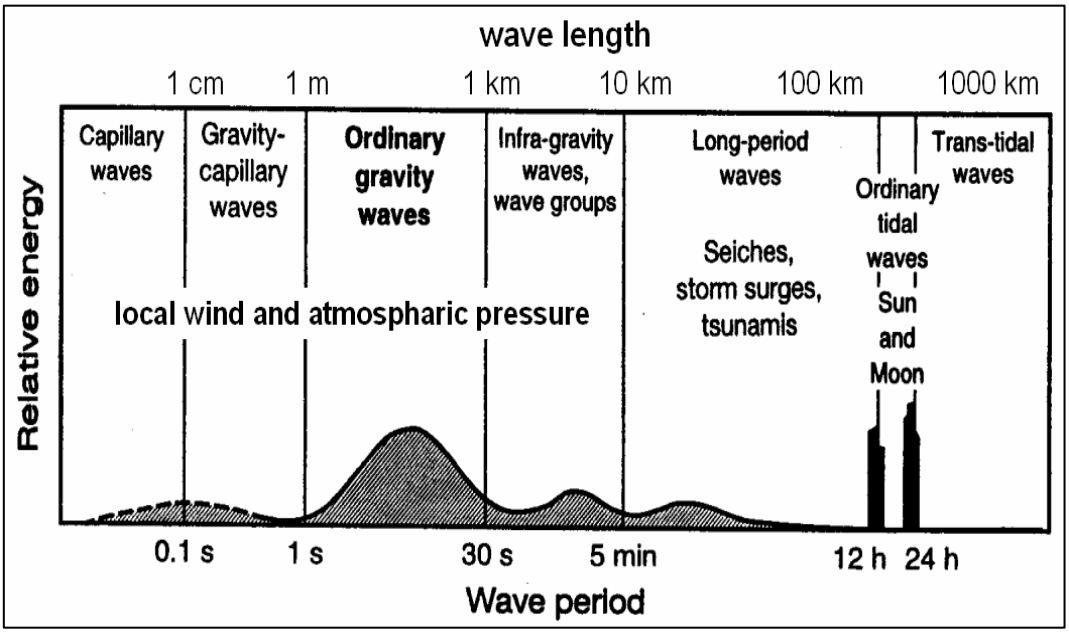

Figure 3.2: Classification of ocean waves and their relative energy.

3.2.1 Linear Wave Theory

A regular wave is defined by sine function or sinusoidal (figure 3.3). In order to fully specify a regular wave, it will be needed its amplitude, ζ, its wavelength λ or the wavenumber $k=2\pi\lambda^{-1}$, its period τ or angular frequency $\omega=2\pi\tau^{-1}$, and in addition its propagation direction θ and phase at a given location and time.

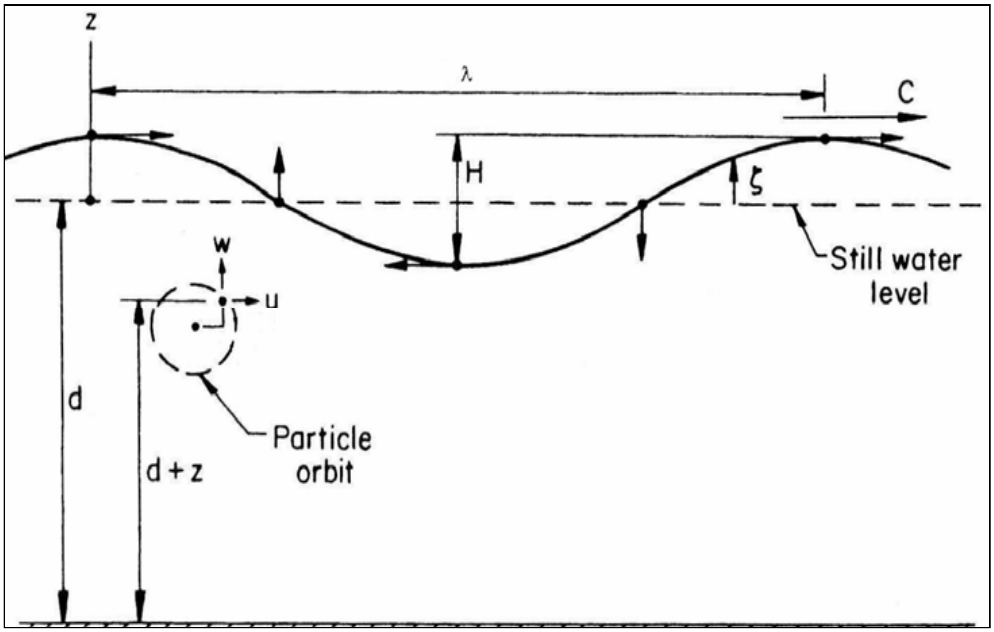

Figure 3.3: A simple sinusoidal wave

A sea surface wave is a plane wave and therefore k and θ can be expressed in Cartesian coordinates as a two-component wave number vector, $k = (k_x, k_y)$. A linear sea surface wave is sinusoidal shape. Deviations from this shape are expressed as nonlinearities. A single sinusoidal plane wave has the form

$$\zeta(\Theta) = \sum S e^{i(\vec{k}\vec{r}-\omega t)} + \sum S_* e^{-i(\vec{k}\vec{r}-\omega t)} \qquad (3.4)$$

Where, ζ is the sea-surface elevation in the spatio-temporal domain Θ= (x, y, t), $S = \zeta_0 e^{i\phi_0}$ is the spectral Fourier coefficient, where ϕ_0 is the initial phase, S* is complex conjugated of S and $\vec{k}$ is the wavenumber vector and $\vec{r} = (x, y)$ is the spatial vector. The expression: $\phi = \phi_0 + \vec{k} \cdot \vec{r} - \omega t$ describe the phase ϕ.

By generalizing the above concept, a wave field is defined as the superposition of single waves and its shape is the sum of n single waves (Figure 3.4).

$$\zeta(\Theta) = \sum S e^{-i(\vec{k}_n r - \omega_n t)} \qquad (3.5)$$

where $\vec{k}_n$ is the n^{th} wavenumber vector, ω_n is the n^{th} frequency and $S_n = \zeta_0 e^{i\phi_0}$, n is the n^{th} Fourier coefficient for the n^{th} wave.

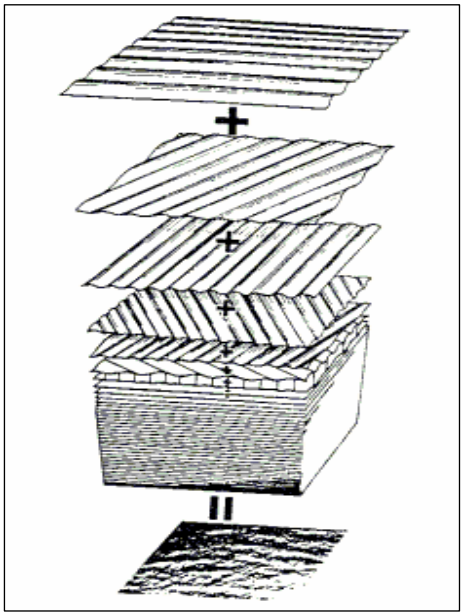

Figure 3.4: Sea-surface obtained from the sum of many sinusoidal waves (derived from Pierson et al. 1995)

3.2.2 Stationarity of Wave Field

In the mathematical science, a stationary process is a stochastic process in which the probability density function of one random variable X does not change over time or position. As a result, parameters such as the mean and variance also does not change over time or position, experimental proved for at least short periods (PRINS 1996). Therefore, the general definition of the stationarity makes clear that for a wave field two conditions must hold to fulfill the criterion of stationarity: the local temporal phase gradient, $\frac{\partial \phi_i}{\partial t}$, have to be invariant in time for considered time period:

$$\frac{\partial \phi_i}{\partial t} = \omega_i \text{ and } \frac{\partial \zeta_{0,i}}{\partial t} = 0 \qquad (3.6)$$

where ϕ_i is the temporally local phase, $\zeta_{0,i}$ is the temporally local amplitude and ω_i is the temporally local frequency, which is constant. If one of the above criteria does not hold for at least one wave of the wave field for the period of the observation, the wave field is instationary.

3.2.3 Homogeneity of wave field

A stochastic process is defined homogeneous in space if the transition probability between any two state values at two given locations depend only the difference between those state values (PRINS 1996).

For a wave field in an oceanic box two condition must hold to fulfill the criterion of homogeneity: the spatially local phase gradients, $\frac{\partial \phi_i}{\partial x}, \frac{\partial \phi_i}{\partial y}$ and the total amplitude, y, have to be invariant in space. Defined for the Cartesian coordinates *(x,y),* the criteria of homogeneity are

$$\frac{\partial \phi_i}{\partial x} = k_{x,i} \text{ and } \frac{\partial \zeta_{0,i}}{\partial x} = 0 \qquad (3.7)$$

And

$$\frac{\partial \phi_i}{\partial y} = k_{y,i} \quad \text{and} \quad \frac{\partial \zeta_{0,i}}{\partial y} = 0 \qquad (3.8)$$

where ϕ_i is the spatial local phase, $\zeta_{0,i}$ is the spatially local amplitude and k_i are the spatially local wavenumber vectors, which are constant. If one of the above criteria does not hold in the considered oceanic box for at least one wave of the wave field, the wave field is inhomogeneous. The above-mentioned processes are inhomogeneous processes. The spectral effects due to inhomogeneous and instationary processes are illustrated in figure 3.5. If a wave field instationary, the global spectral signal is smeared vertically to other frequencies (green dot); if a wave field is inhomogeneous, the global spectral signal is smeared to other wavenumbers horizontally (red dot).

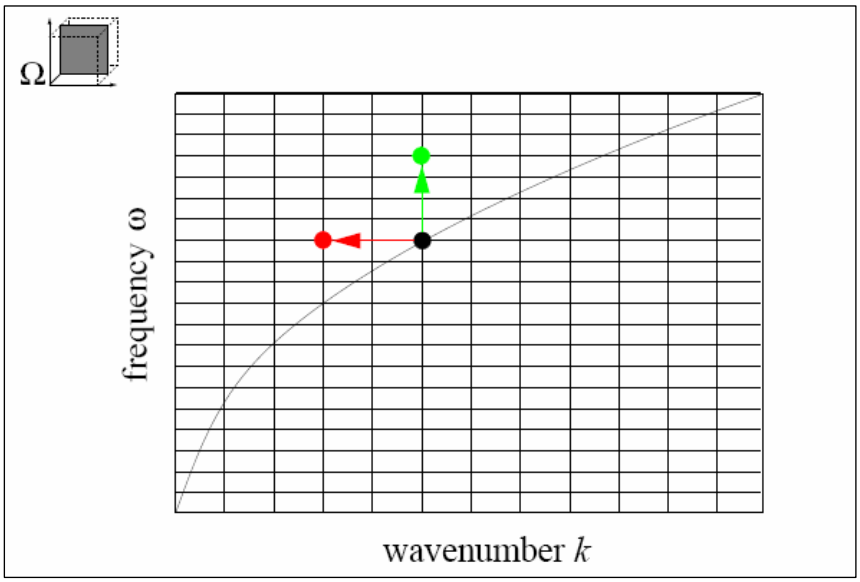

Figure 3.5: spectral instationarity and inhomogeneity illustrated in a 2D k-ω section. (SENET 2004).

3.2.4 Dispersion relation

Assuming a non-viscous, incompressible and homogenous liquid, e.g. water, the dispersion relation of sea surface waves is derived from Eulerian equation of motion,

the continuity equation and the dynamic and kinematic boundary conditions of the dispersion relation is given in (WINKEL 1994).

The phase speed C_p and the group speed C_g are given by

$$C_p = \frac{\omega}{k} \text{ or } C_p = \frac{\lambda}{\tau} \qquad (3.9)$$

And

$$C_g = \frac{d\lambda}{d\tau} \text{ or } C_g = \frac{d\omega}{dk} \qquad (3.10)$$

The phase speed C_p determines the speed of propagation of a single wave component, and the group speed determines the propagation of the wave field's energy. In extremely shallow water which have wavelength $\lambda > 0.1d$, $C_g = C_p$; in the deep water which have wavelength $\lambda < \frac{d}{2}$, the condition $C_g = \frac{C_p}{2}$ holds.

The dispersion relation describes the dynamic relation between wavenumber k and angular frequency ω and determine the phase speed, speed of propagation of a wave. The term "normal" dispersion implies that longer waves have a higher phase speed and shorter waves. This performance holds for capillary waves. The linear dispersion relation for free gravity sea surface waves, if the surface is ignore is given by

$$\widetilde{\omega}(\vec{k}) = \sqrt{gk \tanh(kd)} + \vec{k} \cdot u_c \qquad (3.11)$$

where g is the gravitational acceleration, d is the water depth, u_c is the near surface current.

At the equation (3.11) the first term is called intrinsic frequency, $\varsigma^{\pm} = \sqrt{gk \tanh(kd)}$, and the second term is called the Doppler frequency, $\omega_D = \vec{k} \cdot u_c$, indicates the effect of near surface current. Following (3.11), the accelerations which force an elevated particle to move back to initial position, $\overline{\zeta}$ is $\vec{g}$, this happens to waves longer than 0.1 m. when the waves $\lambda < 0.1$ m, only the surface tension of water has a significant effect of small waves, those waves are called capillary gravity waves and the relation

which describes them take account also the surface tension, in this case they are ignored. The water depth (*d*) and the near surface current vector ($\vec{u}_c$), are free parameters which influence the shape of the dispersion shell in the wavenumber frequency domain (Ω). Therefore the shape of the dispersion shell can be used to inversely determine these parameters.

The dispersion relation generates a shell in the 3DΩ domain. The intrinsic dispersion shell is symmetric about the rotation axis, figure 3.6. The intrinsic dispersion relation has two solutions, ς^+ and ς^-. These two solutions are redundant, a consequence of the symmetrical attributes $\varsigma^+ = -\varsigma^-$ of the Fourier transformation.

Due to the redundancy of the dispersion shell $\varsigma^+(\vec{k})$ and $-\varsigma^-(\vec{k})$ are hermetic and only one of the shell is needed to describe the energy of wave fields in the Ω domain.

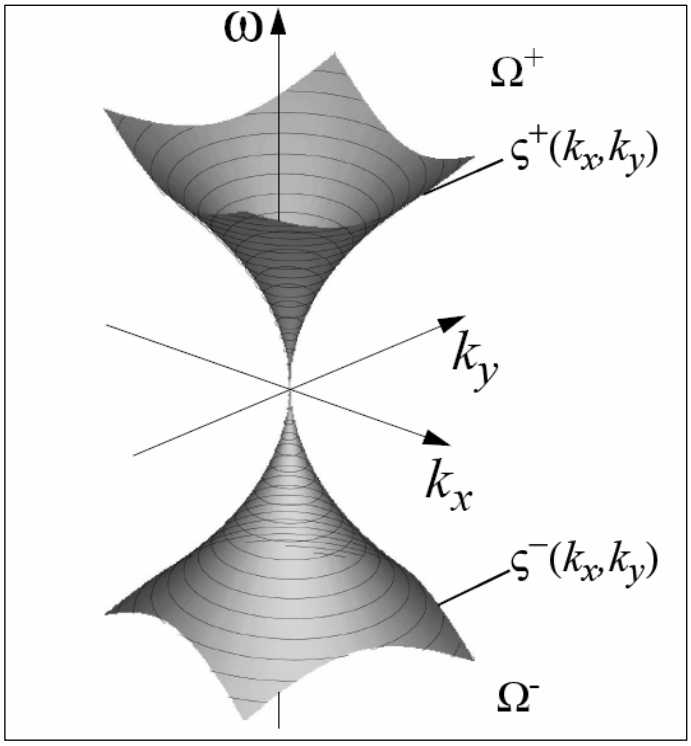

Figure 3.6: Positive and negative dispersion relation of linear deep-water surface-gravity waves in 3DΩ domain, (SENET 2004)

3.2.5 Water Depth and Near Surface Current

If a near surface current, $\vec{u}_c$ is present, waves are Doppler shifted. The Doppler shift, ω_D leads to a frequency shift of ω. If a current is directed in a direction opposite to that a wave, the wave's absolute, in the inertial coordinate system of the observer, frequency is increased and vise versa. The deformation of the dispersion relation due to the Doppler effect is illustrated at figure 3.7c.

For deep-water waves, defined by the condition $d > \frac{1}{2}\lambda$, the approximation tanh(*kd*) ≈ 1 holds and can be substituted into 3.11. By assuming $\vec{u}_c = 0$, the deep-water wave solution is as follows:

$$\zeta^{+}(k) = \sqrt{gk} \qquad (3.12)$$

In shallow waters, where d is small comparing to λ, the shallow water dispersion is:

$$\zeta^{+}(k) = k\sqrt{gk} \qquad (3.13)$$

is obtained when the approximations tanh(kd) ≈ kd and $\vec{u}_c = 0$ are substituted into (3.11).

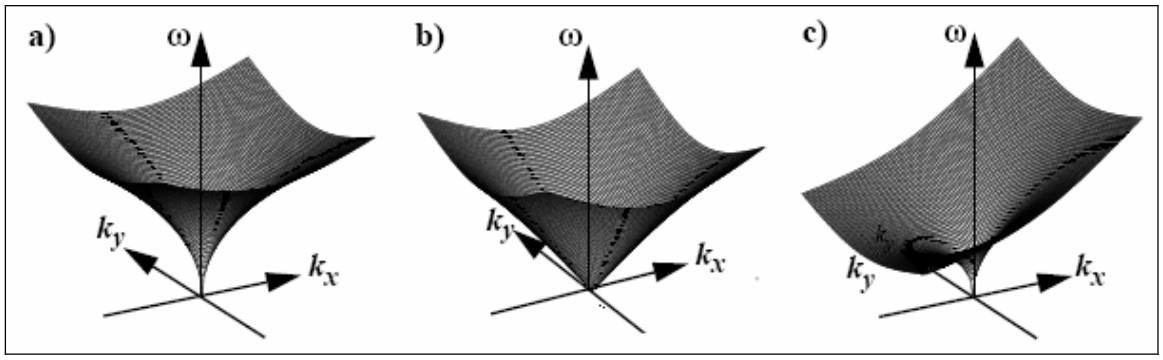

Figure 3.7: Dispersion relation of linear surface-gravity waves in 3D Ω domain: a) intrinsic deep-water dispersion shell, b) intrinsic shallow water dispersion shell and c) Doppler shifted deep-water dispersion shell influenced by near-surface current, (SENET 2004)

3.3 Dispersive Surface Clasificator

The Dispersive Surface Classificator (DiSC), is a recently presented algorithm (SENET et al. 2008), which analyses image sequences for the determination of physical parameters on a local spatial scale, it consists a local analysis method, which allows the analysis of inhomogeneous image sequences of a dynamic and dispersive surface. The basic idea of the method is that in shallow waters wave fields become inhomogeneous due to spatially variable bathymetries. Local change of the wave field, containing the local bathymetry information, therefore must be taken into account.

For analyzing the radar data, software DiSC is used which was developed at the Radar Hydrography Department of the GKSS and commercialized product by Vision 2 Technology GmbH, partner of the Geesthachter Innovation und Technologie Zentrum (GITZ).

The basic steps of DiSC are the following:

- Transformation of the image coordinates from polar to Cartesian.
- Application of 3-D discrete Fourier transformation on the image sequences.
- Decomposition of the complex-valued image spectrum for the separation of the wave signal from the noise and Directional and dispersion separation of the complex-valued spectrum into spectral bins at 2D wavenumber planes of constant frequency by using filtering techniques.
- 2D inverse Fast Fourier Transformation (2D FFT^{-1}) of the spectral bins yielding complex-valued, one-component spatial maps in the spatio-frequency domain.
- Calculation of spatial maps of local wavenumber vectors from the one-component images of constant frequency by using the phase of complex-valued one component images.
- Use of the spatial maps of local wave number vectors and power for the calculation of spatial hydrographic parameter maps.

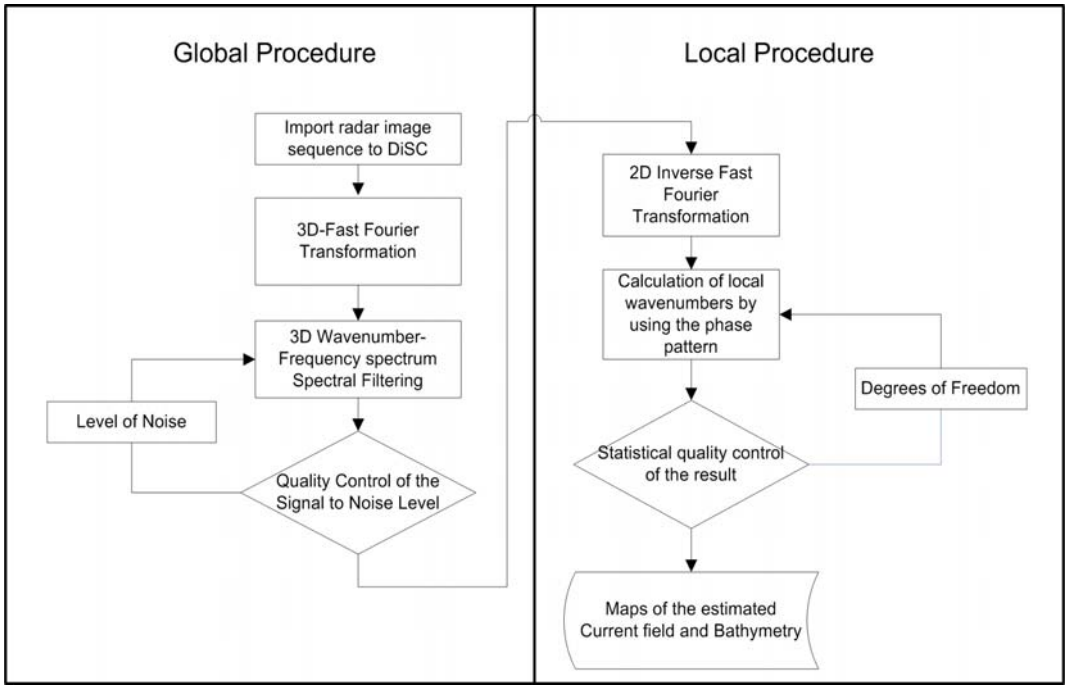

Figure 3.8 Scheme of the procedural and data flow of DiSC (FLAMPOURIS 2007)

3.3.1 Assumptions of DiSC

The requirements for the application of DiSC are, stationarity and validity of the multi component image model (SENET et al.2003).

Stationarity: The image process analyzed by DiSC has to be stationarity. Stationarity implies the temporal invariance of a signal. Assuming stationarity, DiSC can treat the spatial Fourier decomposition of the distinct frequency components independently, with the complex-valued spatial image at a constant frequency.

Validity of the multi-component image model: For inhomogeneous images the amplitude or the spatial phase gradients (i.e. the local-wavenumber vectors) vary. This information is only implicitly included in the coefficients of the Fourier decomposition. To enable explicit analysis, the spatial Fourier decomposition is transformed to an image representation, composed of the superposition of 2D jointly amplitude-frequency-modulated, local coherent, analytic signals, multi-component image model.

3.3.2 Input Parameters

A 3D image sequences as the input data set of the DiSC has to be analyzed, each of the radar image sequence, has three dimension which are the x (easting), the y (northing), and the time t (as number of images), this information are imported at the beginning of the process to the DiSC. In addition to them, the number of pixels at the x and y-axis, the real size of each pixel and the rotation period of the antenna are imported.

3.3.3 The algorithm of DiSC

The signal to noise ratio, broadly used method is based on spectral filtering and the analysis of the real-valued 3D gray variance spectra. The spectral phase, which contains information on the local image structure (OPPENHEIM and LIM 1981), is not used. For the determination of the physical parameters on a local spatial scale, recovers the spatial structure of the image sequence from the complex-valued 3D spectrum. The core of the local analysis method is a decomposition of the complex valued 3D image spectrum, which is followed by a 2D FFT^{-1} into the spatio-frequency domain.

The algorithm is a 5-step method:

1. 3D Fast Fourier Transformation: A discrete 3D Fourier Transformation (3D FFT) can be acquired by the decomposition into 1D FFTs. A 3D FFT using the world and spectral coordinates and the result of process is a discrete complex valued image spectrum of the 3D domain. The discrete grid resolution of the spectrum is calculated the spatio-temporal extension of the initial image sequence. By the 3D FFT, the initial dimension *x, y*, and *t* are transformed to k_x, k_y, and ω. The result of the *x*-dimension is the x-component of global wavenumber, of the y-dimension is the y-component of global wavenumber and of the time t is the frequency. By the result of process, the choice of the power of the backscatter and the minimum and maximum bin, where the energy lays, take place.
2. Spectral decomposition: The aim of the spectral decomposition of the spectral signal of the inhomogeneous wave field is the division of the signal into one-component images containing separated and analyzed parts of the wave field. The spectral decomposition technique DDF-S (Directional Dispersion

Frequency-Separation) is based on the combination of frequency separation taking a k_x - k_y slice of the 3D wavenumber-frequency spectrum and a directional wavenumber band pass filter in $k_x - k_y$ centered on the dispersion shell (dispersion filtering), yielding a spectral DDF bin. The principle of DDF-S is outlined in figure 3.9.

Dispersion filtering is required because of the nonlinearity of radar imaging of the sea surface waves. The nonlinear modulation transfer function (MTF) can be expanded in a Volterra series (CHERRY 1994), creating sum-differences and harmonic signals in addition of the linear fundamental mode in the radar image spectrum. The linear (fundamental) mode is selected by dispersion filtering. The remaining spectral smearing is caused by the inhomogeneity of analyzed area.

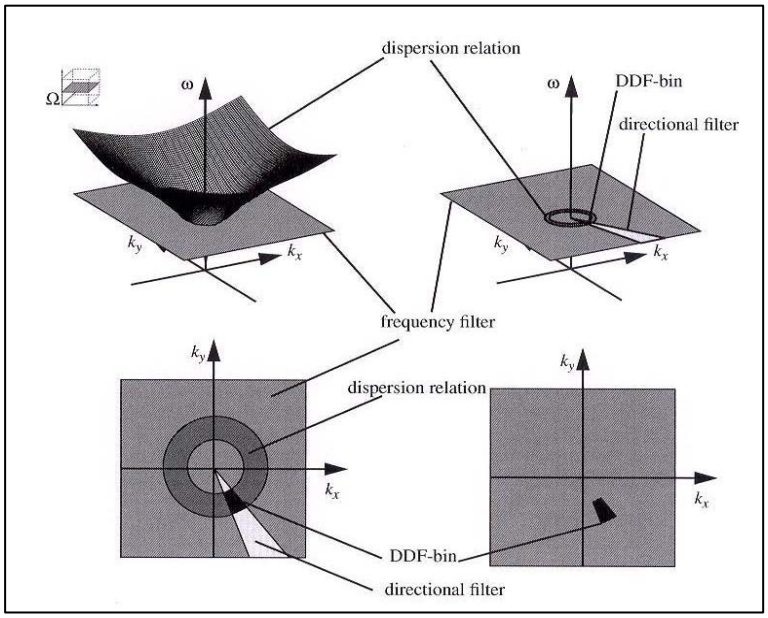

Figure 3.9: Spectral decomposition by filtering (SENET 2004)

3. Inverse 2D FFT: Complex valued one component images are calculated by transforming the filtered frequency slices of wavenumber planes of the 3D image spectrum into the spatial domain, using a 2D FFT^{-1}. The spectral decomposition and inverse 2D FFT yields complex-valued spatial one-component images. These complex-valued one-component images are illustrated as power phase of separate part of the wave field.

4. Calculation of local wavenumber: Determination of spatial maps of local-wavenumber vectors is achieved using the phase of the complex-valued one-component images. Initially an approximate version of the multiple-signal classification algorithm (STOICA and NEHORAI 1989, HAVLICEK et al. 1996) was used to estimate local wavenumber vectors. The method provides complex-valued wavenumber vectors.
5. Calculation of hydrographic parameters maps: In the variance spectrum, the linear portion of signal energy of the waves is localized on the dispersion shell surface waves. Therefore the filling up, the instant depth, of the water mass could be calculated for each grid cell. The only parameter that has to be defined is the minimum number of the regression coordinates that is by default 10. More detail about this technique at (FLAMPOURIS 2006).

4. Methodology

The complete methodology of the investigation is described analytically in this chapter. The methodology is divided into two sections, Data Acquisition (sec. 4.1) and Data Processing (sec. 4.2).

4.1 Data Selection

The first step is the selection of radar data which depends on the purpose of investigation. In this section, the experimental setup, the used radar data for processing and the post processing of the DiSC results are described briefly.

4.1.1 Experimental Setup: Sylt

The radar station was mounted near the lighthouse of List West on the island of Sylt in German bight. The areas covered by radar images are part of List West, Lister Landtief , and Lister Tief. The utilized system for the acquisition of the sea surface is a software-hardware combination, presented by NIETO BORGE et al, (1999), as a part of the Wave Monitoring System (WaMoS), consisting by a Furuno FR 1201 (FURUNO MANUAL 1989), a WaMoS II analog digital converter and a WaMoS II software package for the acquisition of the radar image sequences. The radar is ground-based nautical X-band radar with horizontal polarization (HH), mounted 25m above the NN. The radar was mounted in the year 2000 and the range covered circle of about 2 km radius.
In addition during the observation period a meteorological station was in operation.

4.1.2 Wind Data

Wind parameter is used as indicator of the weather condition in the investigation area. The available row data was mounted from 1999 until 2007, with gaps. It is important to be emphasized here that the intensity of the backscattering depends on the wave conditions and wind, as the generating force is determined. The selection of the analysis wind data during the storm conditions are proposed to identify the influence of the wind in the investigation area.
The wind data was taken from meteorological station of the radar station. Finally, the two data sets at the winter periods with the highest wind velocity of 8 Beaufort (18 m/s)

and one data set at summer period with the highest wind velocity of 6 Beaufort (15 m/s) were chosen to identify the effect of wind behavior toward the water level.

4.1.3 Radar Data

During the period of investigation radar sequences, which consisted by 256 single images were acquired with a time interval of 1.8 s, which is equal to the antenna rotation time. Thus, the total sampling time was approximately 8 minutes. The polar images cover a radius of approximately 2 km, were interpolated to a Cartesian grid with a cell size of 6.82 m x 6.82 m, corresponding to the spatial resolution of the radar. The number of pixel for one image is 288 x 288. The exact specification of the Cartesian grid of the nautical radar image sequences are listed at the table 4.1. The antenna rotation time varies from sampling to sampling but lies near the 1.8s; the reason of the variance is the wind impact to the antenna.

Firstly, the commonly and the most difficult part of the marine sciences is the acquisition data, the rough and many times unforeseen circumstances influence or destroy the equipment, i.e. the lightning consists one of the most common factors of the radar destruction. A second reason is the huge storage capacity that is necessary for the row radar data, every sampling need about 90Mb and only lately the technology permits in small volume high storage capacity which is useful in the field. Also the archiving of all these terabytes of row data confronts several problems, mostly at the hardware; enough data were corrupted by hardware malfunction (FLAMPOURIS 2006).

Finally, the three different storm periods (26^{th}-27^{th} February 2002, 7^{th} March 2002 and 28 October 2002) was chosen for comparison between radar measurements and gauge measurement in the investigation area to identify the tidal signature and morphodynamic changes.

Table 4.1 specification of the Cartesian grid of the ground based nautical radar images sequences.

Number of pixel in x-direction (west-east) N_x	288
Cartesian-grid pixel resolution in x-direction (west-east) Δx	6.82m
Spatial length in x-direction (west-east) X	1964m
Number of pixel in y-direction (south-north) N_y	288
Cartesian-grid pixel resolution in y-direction (south-north) Δ_y	6.82m
Spatial length in y-direction (south-north) Y	1964m
Number of images per image per image sequences N_t	256
Temporal resolution (antenna-rotation time) Δ_t	1.8s
Temporal length of an image sequence T	460s

4.2 Data Processing

After the output data from DiSC processing (processing of bathymetric data) were evaluated. The first step was the optimization of the reliability of the result according to the depth and number regression coordinate. The second step is the identification of the tidal cycle from the calculated sea water level and averaging each time steps of one tidal cycle from the difference time periods (three periods) of analysis for identifying the accuracy of the results and to establish one common reference every one period to make water level values to be comparable. The third is regression analysis between radar and gauge water level; the fourth step is identified the time lag between water level measurement in List Westerland and water level measurement in List Tief; the fifth step is visualized the average bathymetry; the sixth step is defining the cross section at the tidal channel, the seventh step is water depth analysis over the cross section, and the final step is slope analysis over the cross section to identify the morphodynamic changes in the area of investigation. The data processing is illustrated at figure 4.1.

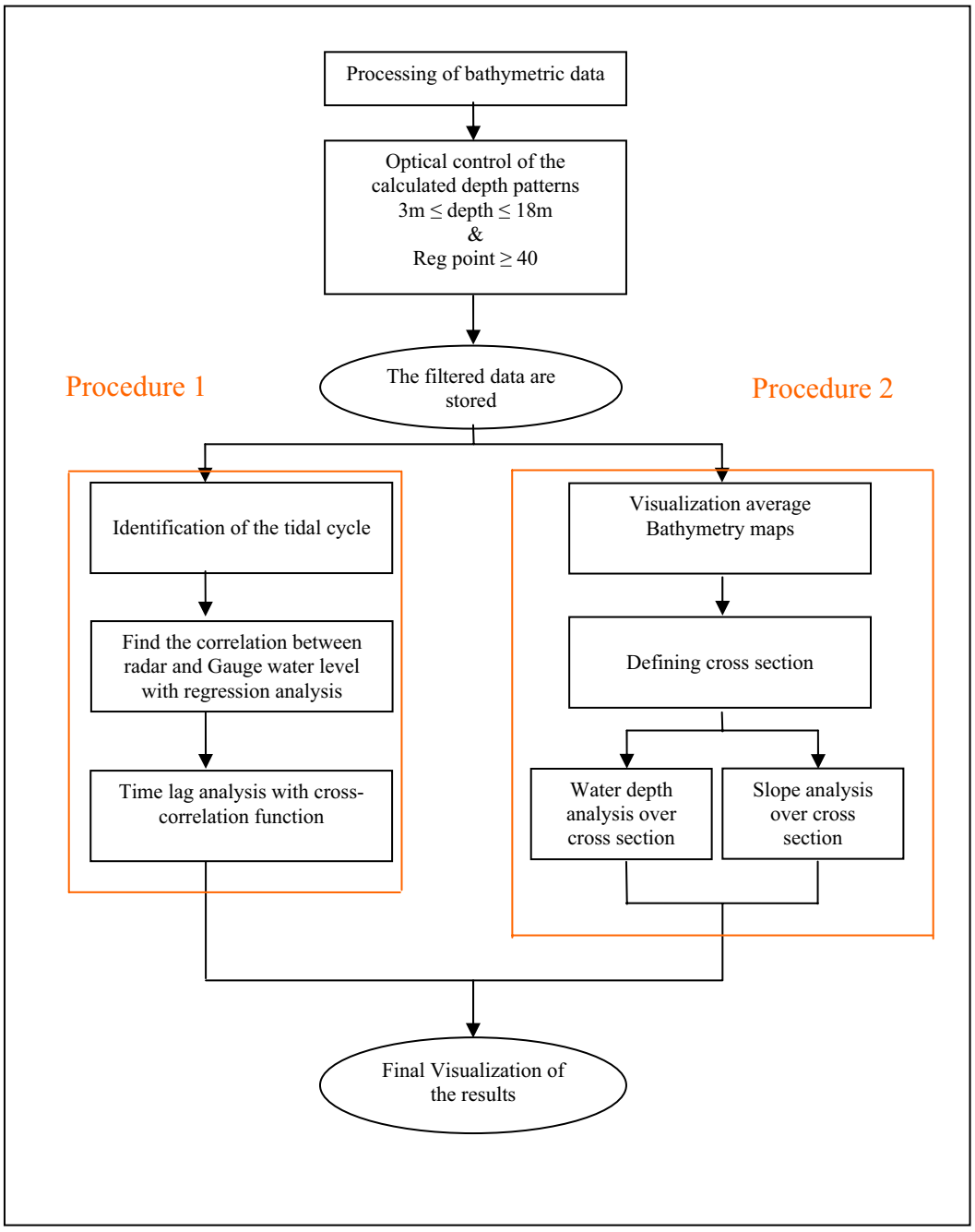

Figure 4.1 Flow chart of data processing consist 2 procedure, procedure 1 as the investigation of theoretical accuracy of DiSC and procedure 2 as the observation of morphodynamic changes.

4.2.1 Export of Data

The final result of DiSC software is a text file, in which are stored the coordinate of every cell for which has been calculated the instantaneous water depth, the number of the regression coordinates, the calculated depth and current vector. For the further processing of the data, it was necessary to export the data to create a new file, which include all the results. For this reason, a programming in the PV-Wave has been developed. FLAMPOURIS (2006) was made the program which is consisted by 6 subroutines, the basic concept is that the complex grid of the area of analysis is created, the coordinates of each of the results and the output is one file where are stored the results at the whole grid. The structure of the program permits to the user to define the check of the number of coordinates and the export any calculated variable, number of regression coordinates depth.

It is evident that the applicability of DiSC depends on the wave condition, as a method requires waves, long enough, to be influenced by the sea bottom. The reason of filtering according the number regression coordinate (<40) is at the low frequencies, the real signal cannot be distinguished from the noise and has nonlinear effects as produced by wave group (SMITH et al.1996). As result, the dispersion relation does not model the waves. Moreover, the program is also filtering the depth less than 4 m, the reason is that the waves are not anymore dispersive at the very shallow area due to wave breaking in the other words the linear wave theory is not valid at the very shallow area.

4.2.2 Identification of the Tidal Signal

The identification of the tidal cycle consist a common (BELL 1999), (ROBINSON et al 2000) way to control the whole series of the image sequence analysis and the comparison with gauge measurement consist strong evidence about the reliability of the results. In this case, the accuracy of DiSC water level result was identified with confidence interval of variance by assuming one grid cell equal one degree of freedom and using 95 % level of confidence. Chi-squared was used to calculate the upper and lower limits as confidence interval of variance. Chi-squared based on the normal distribution which is approached method at the wave field area. ALPERS & HASSELMANN (1978) has proven that the normal distribution is approached method to identify wave characteristic.

The purpose of comparison between tidal gauge and DiSC is to virtualize the parallel trend for both water levels as the tidal signature. Two procedures from DiSC water level was examined as comparison with gauge water level. The first steps for the estimation of the tidal cycle were average the calculated the sea levels of 81 neighboring cells around the point 3460944.34, 6103240.84 (high degree of freedom). To decrease degree of freedom, the chi-squared was used to identify the accuracy of DiSC result at the small area (the area less than at the first step). By decreasing degree of freedom, the variance will be increased. The second step were average the calculated the sea levels of homogenous field area by filtering ± 0.25 m from 81 neighboring cells to define the gentle slope. They have been plotted for the twelve hours (one tidal cycle) of each period of analysis and take to common reference for each time step.

4.2.2.1 Confidence Interval of Variance

The Chi-squared (χ^2) distribution refers to a sum of square random variables, ($X_1^2 + X_2^2 + X_3^2 + \ldots + X_n^2$). Where n is N (0, 1) variable, it is normal with mean (μ) of zero and variance (σ^2) of one. The chi-square distribution (appendix V) is tabulated according to degree of freedom (ν) and has mean (μ) = ν and variance = 2ν.

To find the confidence interval for a sample of n observations, the sample variance is calculated first:

$$s^2 = \frac{1}{n-1}\sum_{i=1}^{n}(x_i - \bar{x})^2 \qquad (4.1)$$

To describe the variability in this function from one sample to the next, one introduces the corresponding random S^2 where:

$$S^2 = \frac{1}{n-1}\sum_{i=1}^{n}(X_i - \bar{X})^2 \qquad (4.2)$$

If the X_i are independent $N(\mu, 1^2)$ random variables, it must be shown that $(n-1)S^2$ is distributed as a chi-square with $\nu = (n-1)$ degree of freedom. The term degree of freedom is used here in the same sense as it in statistical mechanics. Thus, for any set of n observation there will only be $(n-1)$ independent deviation ($X_i - \bar{X}$) since their sum is zero from the definition of the mean.

Usually the observations will be assumed to be N (μ, σ^2). In this case, X_i/σ will be N (μ/σ, 1^2) and so the random variable will have a chi-square probability density function with $\nu = n - 1$.

$$(n-1)\frac{S^2}{\sigma^2} = \frac{1}{\sigma^2}\sum_{i=1}^{n}(X_i - \bar{X})^2 \qquad (4.3)$$

Since $\nu S^2/\sigma^2$ is distributed as χ_ν^2, probability limit of the form

$$\Pr\left\{\chi_\nu\left(1-\frac{\alpha}{2}\right) < \frac{\nu S^2}{\sigma^2} \le \chi_\nu\left(\frac{\alpha}{2}\right)\right\} = 1-\alpha \qquad (4.4)$$

Rearranging it follows that the random variables σ^2/S^2 satisfies

$$\Pr\left\{\frac{\nu}{\chi_\nu(\alpha/2)} < \frac{\sigma^2}{S^2} \le \frac{\nu}{\chi_\nu(1-\alpha/2)}\right\} = 1-\alpha \qquad (4.5)$$

Plot of the upper and lower limits $\nu/\chi_\nu(1-\alpha/2)$ and $\nu/\chi_\nu(\alpha/2)$ are given in the appendix V for $\alpha = 0.01$, 0.05, and 0.2 and for $3 \le \nu \le 100$.

4.2.3 The Regression Analysis of Water Level

Regression analysis is a statistical tool for the investigation of relationships between variables. In this section, Regression analysis is used to show the correlation between radar and gauge water level measurements.

By determining correlation coefficient (corr), it can be shown the significance correlation between both water levels. The corr value has range from 0 to 1, which reveals how closely the correlation is. A trend line is most reliable when its cross correlation value is at or near 1.

To find the correlation coefficient from both water levels, it must be first estimate the covariance: μ_y

$$\mathrm{cov}(x,y) = \frac{1}{n}\sum_{i=1}^{n}(x_i - \mu_x)(y_i - \mu_y) \qquad (4.6)$$

where n is number of observation, x_i is the gauge water level with mean μ_x and y_i is the radar water level with mean μ_y.

So the correlation coefficient:

$$corr_{(x,y)} = \frac{\mathrm{cov}(x,y)}{\sigma_x, \sigma_y} \qquad (4.7)$$

where $corr_{(x,y)}$ is correlation coefficient, σ_x is variance of gauge water level and σ_y is variance of radar water levels.

4.2.4 The Time Lag Analysis between List Westerland and List Tief

The cross-correlation function was used to determine time lag between List Westerland and List Tief water level by comparison the water level in the both area with the same time (local time). The cross-correlation function is defined as:

$$r_{(x,y)}(k) = \frac{\sum_{t=1}^{N-k}(x_t - \bar{x})(y_{k+t} - \bar{y})}{\sqrt{\sum_{t=1}^{N-k}(x_t - \bar{x})^2}\sqrt{\sum_{t=1}^{N-k}(y_{k+t} - \bar{y})^2}} \qquad (4.8)$$

where $r_{(x,y)}(k)$ is cross-correlation function, x_t is the water level in the List Westerland at time *t*, and $\bar{x}$ is the mean of x_t over t. y_{k+t} is the water level in the List Tief at time *k*+*t*, and $\bar{y}$ is the mean of y_{k+t} over *t*. *N* is the number of time points and *k* is the time delay.

The $r_{(x,y)}(k)$ value has range from -1 to 1 which reveals correlation between both measurements. The calculation and comparison of statistical significance values at all delays within one tidal cycle, and define the delay with the largest value as a "lag". The most trivial case of cross-correlation between two stochastic processes occurs when the cross-correlatin function is identically zero for all lags. This implies that the two measurements are completely uncorrelated. If the correlation negative, the two measurements will tend to be mirror images of each other, which is positive change in one measurement are associated with negative changes in the other and independent of each other. If the correlation positive, the two measurements are either both positively correlated or both negative correlated.

The program was used to calculate the difference time lag between List Westerland and List Tief such as PV-Wave. The program consist 3 subroutines. The basic concept is comparing the water level data from each time steps. The routine from PV-Wave is showed in the Appendix IV.

4.2.5 Visualization Average Bathymetry Map

The mean bathymetry for each time period was calculated by averaging the water depth of a tidal cycle. Golden software Surfer was used to construct the bathymetry map for each period, see chapter 5. The bathymetry map consist two-dimensional representation of the three-dimensional data. The first two dimensions are the x (easting) and y (northing) coordinates, and the third dimension, depth, is represented by lines of equal value. The relative spacing of the contour lines denotes the relative slope of the surface. The area between the contour lines contains only grid nodes having depth values within the limits defined by two enclosing contours. The contour interval is defined as the difference between two contours. Each depth value denotes with difference color in the bathymetry map. Depth contour are given at 1 m interval. The grid size of the maps is the same with grid size of the DiSC. It is high possible resolution and the number of cells is 40 x 40.

The assumption of averaging over one tidal cycle is that the mean value of depth is constant. Thus, the comparison between three periods is easier to identify.

4.2.6 Defining Cross Section

After the bathymetry maps were created from the averaging water depth, the next step is the creation of the cross-section in the tidal channel. Two cross-sections were created for each bathymetry map which are cross-section A-B and C-D. The length cross-section A-B is 490.91 m and B-C is 286.6 m (figure 5.5). The points A, B, C, and D lies at the GK coordinate (3461435.28; 6102831.77), (3460944.37; 6103322.68), (3460944.37; 6103363.59), and (3460617.09; 6103690.87) respectively.

4.2.6.1 Depth Analysis over Cross Section

As the water level fluctuates during a tidal cycle, the comparison of water depth over the cross section at three different periods can show the variation of water depth in the tidal channel (figure 5.5).

The common reference is needed as indicator for comparison between the three difference time periods. By calculating the average water depth of 2002 from the tidal gauge in List Westerland as a common reference the comparison of the water level from

different period is possible to investigate. Therefore, the morphodynamic changes can be identified in the area of investigation.

4.2.6.2 Slope Analysis over Cross Section

The identification slope over the cross-section from grid cell to grid cell was calculated. The slope is defined as:

$$\alpha = arctg\left(\frac{\Delta L}{\Delta d}\right) \qquad (4.9)$$

where α is the slope angle in degree, L is the distance over the cross-section and d is water depth over cross-section.

The morphodynamic changes such as erosion or deposition in the area of investigation can be estimated with the comparison of slope between there difference time period (figure 5.6).

5 Results

In the current chapter, the results of the investigation are presented. The methodology of the investigation has been presented, extensively in chapter 4. Three periods of 12 hours (one tidal cycle); period 1: from 26th-27th February 2002, period 2: on 7th March 2002 and period 3: at 28th October 2002 have been chosen. The area of investigation is the ship channel in Lister Tief. The three different periods have been used as example of different wind and wave conditions (see chapter 4.1.2). The area of investigation approximately covers 2.5 km^2.

The results of period 1 are illustrated at figure 5.1; the blue line denotes average water level every 30 minutes of time series derived as DiSC resulting one tidal cycle. In figure 5.1a, each of time series have been normalized by subtracting the mean value of 81 neighboring cells at the point, GK coordinates (3460944.34 m, 6103240.84 m) which covers approximately 0.11 km^2. The bars on the DiSC results show the confidence interval by assuming one grid cell equal to one degree of freedom and using 95% level of confidence, (see chapter 4.2.2). The accuracy of DiSC has been checked by decreasing the degree of freedom. The reason of decreasing the degree of freedom is to increase the variance of averaging data set which is used as interval limit for comparing with tidal gauge. In figure 5.1b, the DiSC result in the homogenous field area by filtering ± 0.25 m from the 81 neighboring cells. The pink line as the gauge measurement denotes the 10 min average every 30 minutes of the time series of water level in Westerland, which have a shifted 1 hour lag due to the distance. All the water level every one time step takes into common reference by subtracting with the average water level values, to obtain the results more reliable.

The comparison between the DiSC result and the gauge measurement on figure 5.1 has the similar general trends. In period 1, water level around homogenous field area (part “b”) is the best result from the other graph.

The results during period 2 which have time steps every one hour is showed at figure 5.2. The comparison between DiSC and gauge water level is exhibited the difference result with the period 1. At the period 2, water level in the homogenous field area (part “b”) is presented the best result.

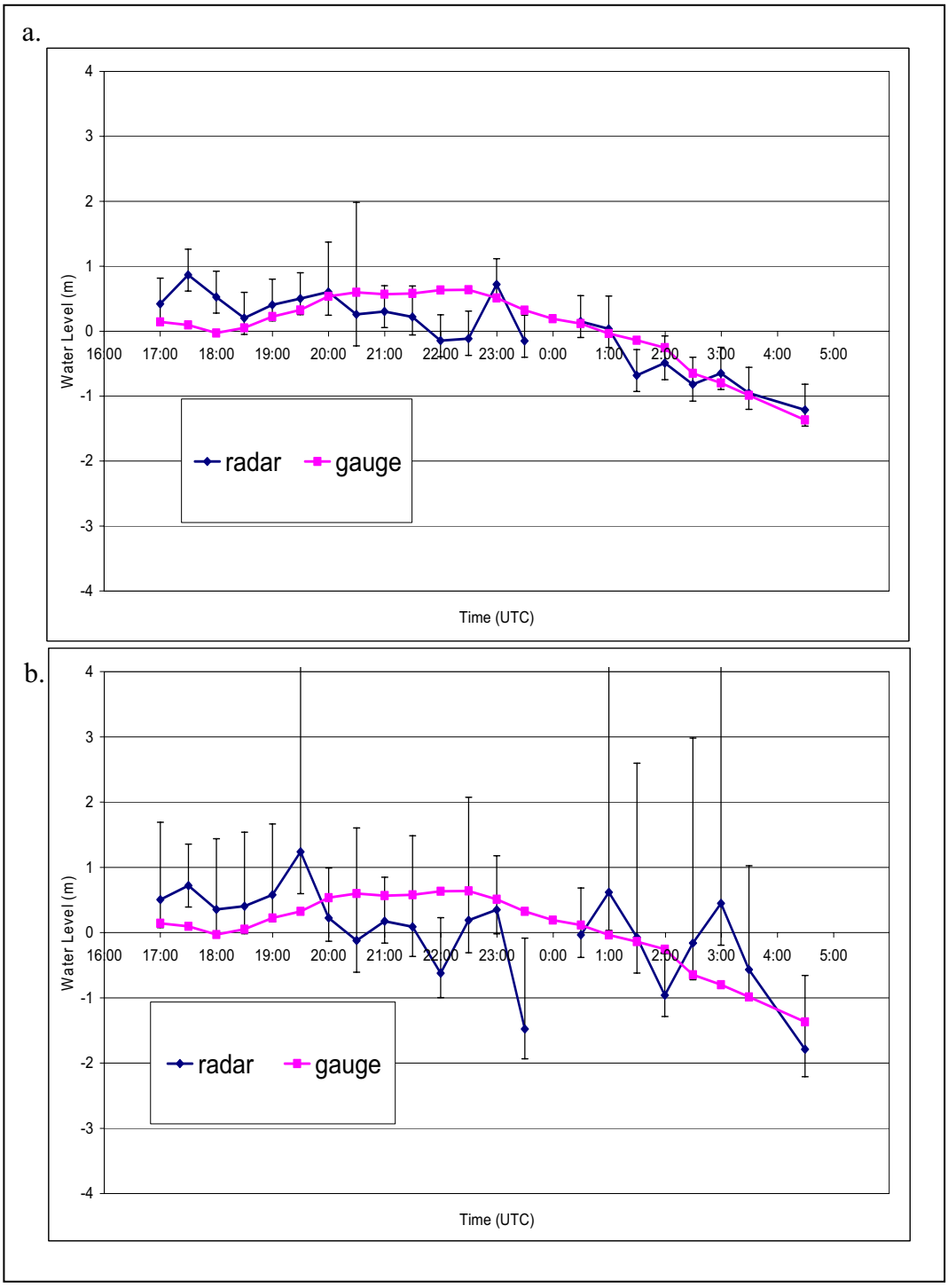

Figure 5.1: Graph representing the tidal cycle during period 1 at 26th-27th February 2002 after subtracting the mean water level of the series from every time step. The pink line is tidal gauge measurement in Westerland and the blue line is the estimated tidal cycle from radar sequences. The bars show confidence interval of variance. a. the average radar water level at the 81 neighboring cells around the point (3460944.34, 6103240.84); b. the average radar water level after filtering with ± 0.25 m at the 81 neighboring cells.

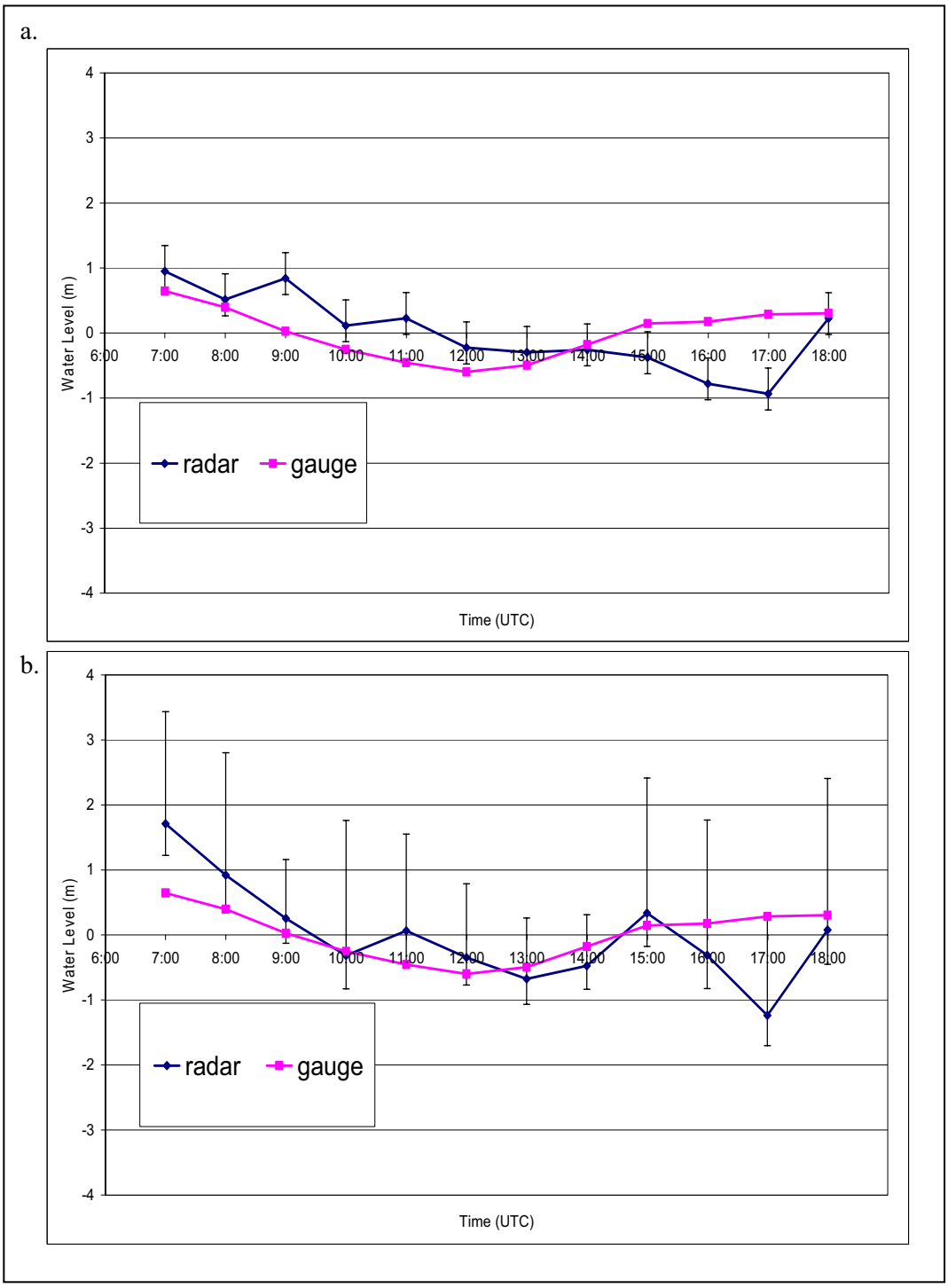

Figure 5.2: Graph representing the tidal cycle during the period 2 at 7th March 2002 after subtracting the mean water level of the series from every time step. The pink line is tidal gauge measurement in Westerland and the blue line is the estimated tidal cycle from radar sequences. The bars show confidence interval of variance. a. the average radar water level at the 81 neighboring cells around the point (3460944.34, 6103240.84); b. the average radar water level after filtering with ± 0.25 m at the 81 neighboring cells.

At the figure 5.1 and 5.2, the confidence interval shows asymetry between upper and lower limits, because they have different behavior as functions of different equation (Appendix V).

We compare in-situ gauge measurements of one tidal cycle with: 1.the water level deduced by the radar measurements in 81 neighboring cells area (blue dots) and 2. The water level at homogenous field area (green dots). Figure 5.3 show these comparisons, the most significant correlation (0.77) was found for water level at 81 neighboring cells.

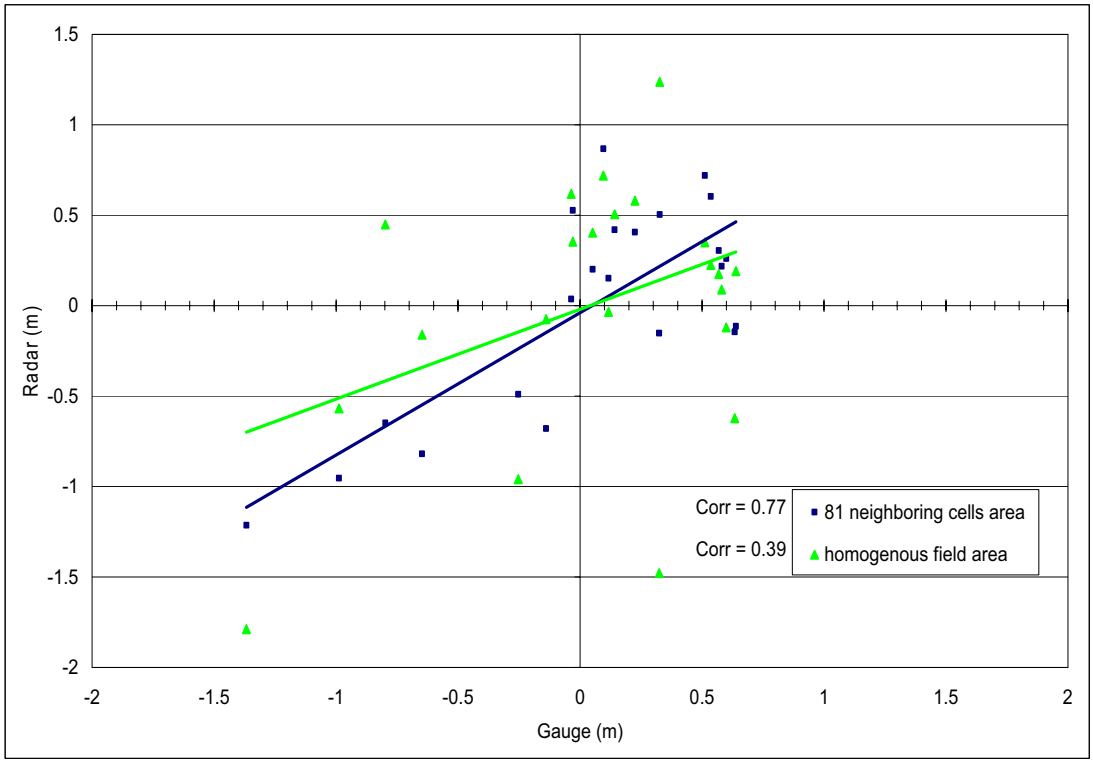

Figure 5.3: The correlation coefficient produced by comparison between gauge water level and radar water level at the whole area, 81 neighboring cells, and homogenous area.

Cross correlation analysis was used to determine the time lag between List Westerland and List Tief, the result of the analysis is illustrated at figure 5.4. The blue bar denotes the cross correlation coefficient from between water levels (DiSC and gauge). During the period 1 (figure 5.4a), the time lag is 1.5 hours. The same result also shows for period 2 (figure 5.4b) which has time lag 1 hour.

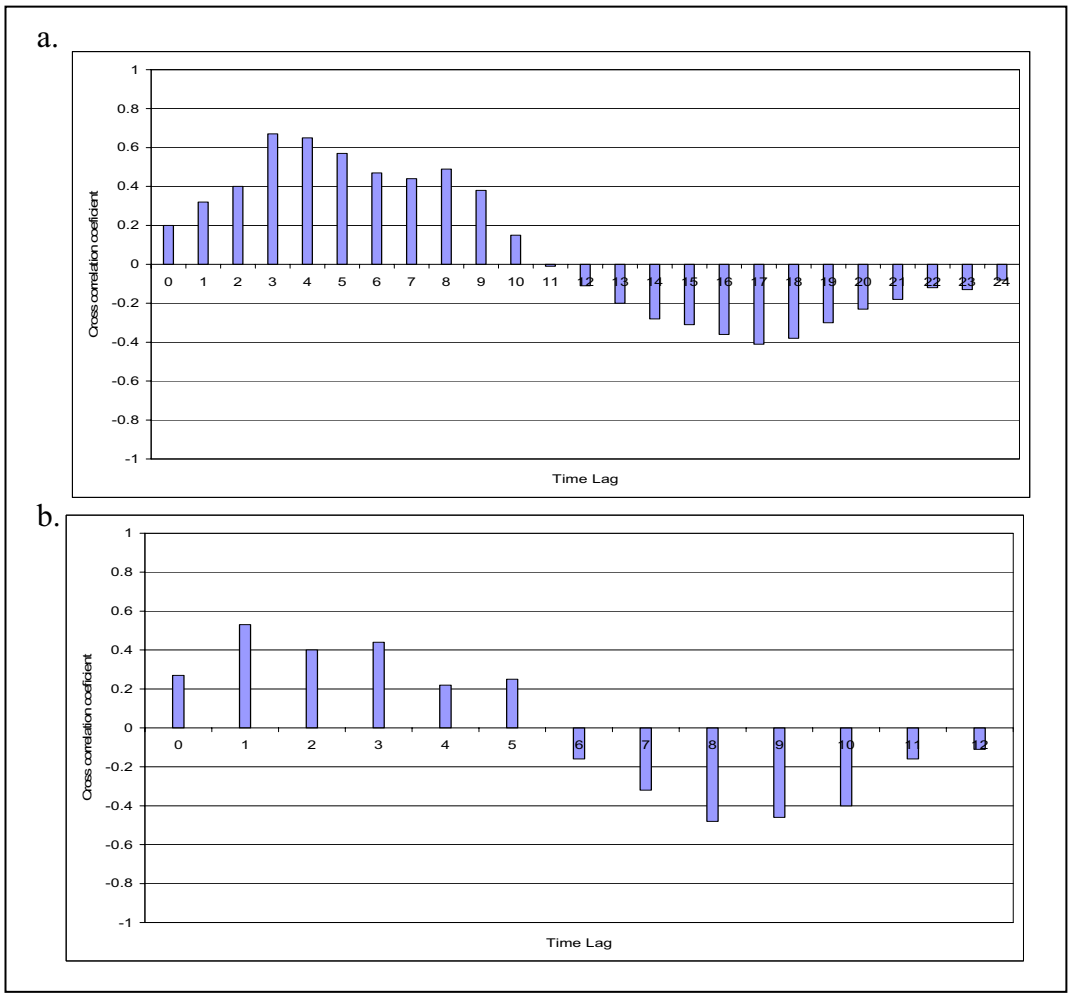

Figure 5.4: Cross correlation analysis between water level in List Tief (radar deduced) and water level in List-Westerland (gauge deduced) with the same local time. The blue bars show the cross correlation coefficient for both water levels. a. cross correlation at 26th-27th February 2002); b. cross correlation at 07th March 2002.

The average bathymetries of time series (one tidal cycle) for three different time observation during the period 1, period 2 and period 3 were calculated. Period 1 at figure 5.5, period 2 and period 3 at Appendix VIII is presented the results of depth calculation. The interval of isolines is 1 m. The R symbol on the bathymetry map indicates the radar position.

For the qualitative observation of sediment deposition or erosion during the three storm periods, are taken the cross sections as indicated in figure 5.5 from A to B and C to D (Appendix VI) which is started in the shallow area (4 m depth) and cross the channel (11 m depth).

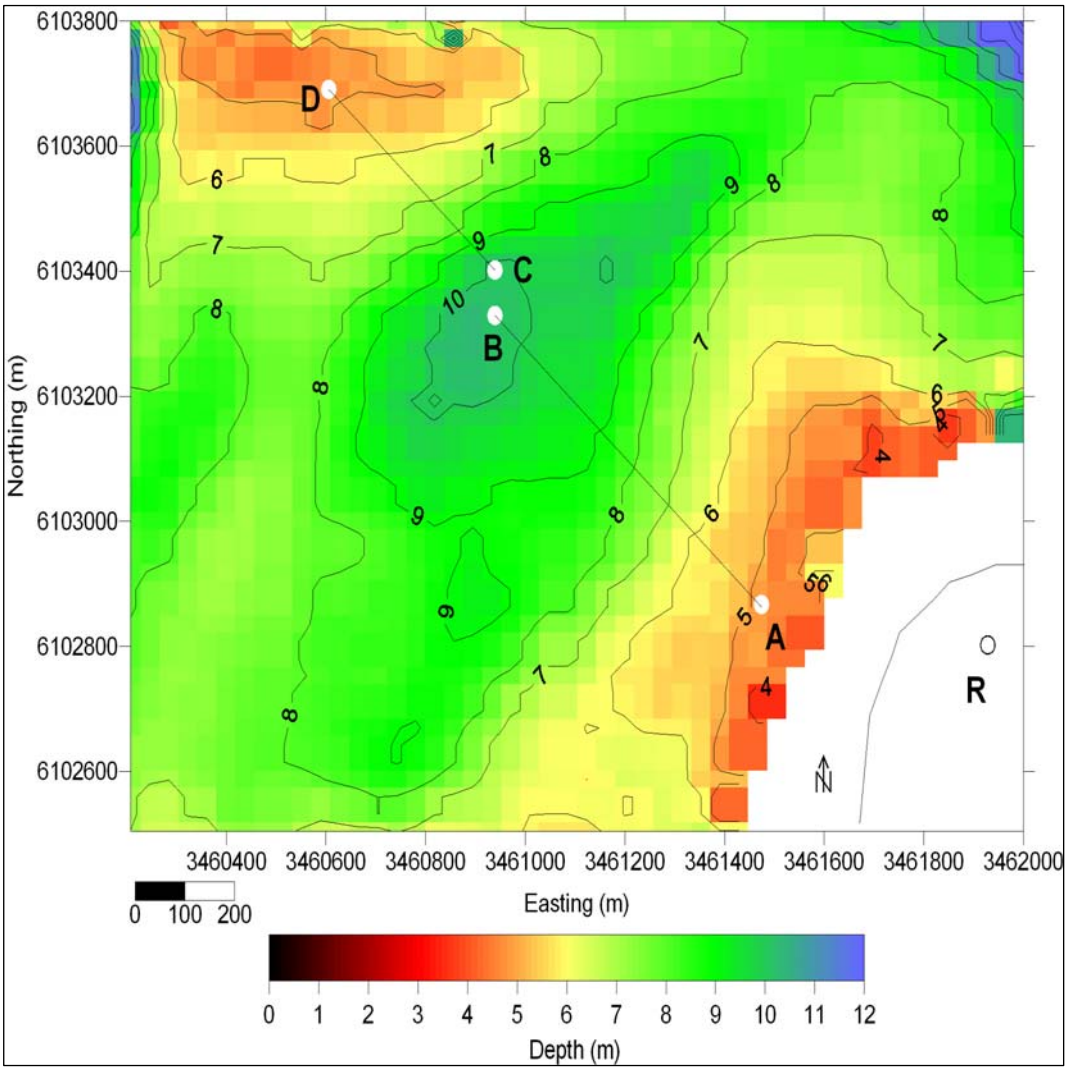

Figure 5.5: Depth of the area of investigation during the storm period (26th-27th February 2002), as a result of averaging the calculated depths for 12 hours. The R symbol is the radar position. The white dot is the cross section A-B and C-D.

For comparison the water depth over cross section, the common reference level is needed; it is calculated by using the simultaneous water depth measurement in Westerland. With this reference the direct comparison is possible. The figure 5.6 is illustrated different water depth at three periods over cross section A-B. The blue line represents the water depth at the period 1, the pink line is period 2 and the green line is period 3. The difference water depth over cross section during period 1, 2 and 3 is approximately 0.5 m at the distance 150 m till 400 m from the point A.

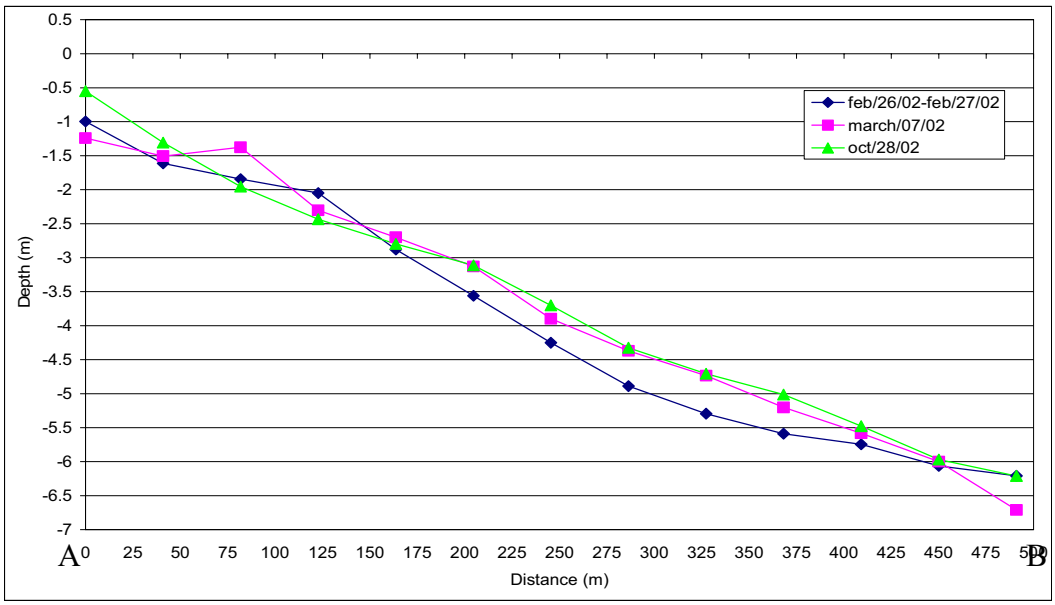

Figure 5.6: The comparison of depth at the cross section A-B during the three difference periods; the reference is defined as the average of water level in 2002.

The slope variation during three difference time periods at the cross section A-B is illustrated at figure 5.7. The blue line represents the slope at period 1, the pink line is period 2 and the green is period 3. The nearshore area which is the east side at the distance 81.81 m was changed significantly at the three periods. At the period 1, period 2 and period 3 the slopes are 0.41, 0.07, and 0.7 (degrees). The changes in the slope for three periods indicate deposition and erosion in the shallow area (4m – 7m).

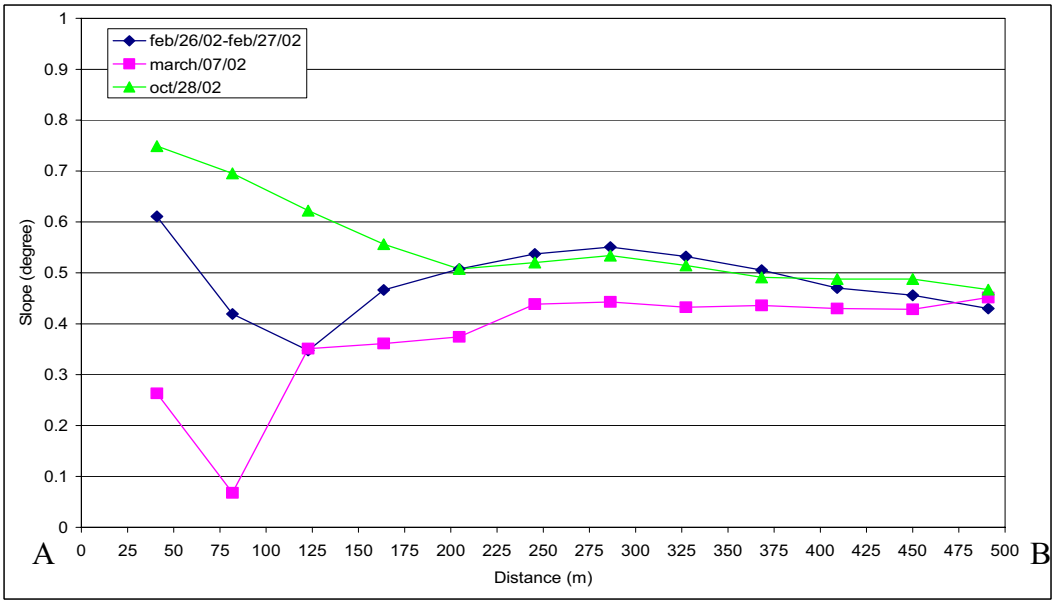

Figure 5.7: The comparison of the slope over the cross section (A to B) for the three different periods.

6. Discussion

The present investigation is constituted by two main parts: 1.The investigation of the theoretical accuracy of DiSC results in its application as radar tidal gauge and, 2. the observation of the morphodynamic changes over the tidal channel.

The water level result every 30 minutes and hourly from different time period is at figure 5.1 and 5.2 respectively. The general comment is the tidal gauge measurement lays always in the confidence limits of the DiSC results; hence in term of statistics, the radar deduced water level is acceptable. The confidence interval proved that the DiSC result could be used as virtual tidal gauge. An interesting result is shown from both periods. At the period 1 and period 2, the best result is illustrated in homogenous field area.

At the period 1 the influences of the gradient in atmospheric pressure to the water level (inversed barometric phenomena) and the wind speed (15-18 m/s) are identified as the addition source of error at least for the first 3 hours of the observation (figure 5.1). For the period 2, the trend of the tidal cycle is identified by DiSC result. The ebbing is monitored satisfactory but during the flooding there is underestimation of the water level during the last 3 hours, probably due to the wind direction which is suddenly changing from the West direction (280º from North) to North-West direction (320º from North) (Appendix III).

The accuracy of DiSC result with gauge measurement is also identified with regression analysis (figure 5.3). At the 81 neighboring cells area shows significant correlation. It is proved that the wave at homogenous area is enough to detect the water depth.

The determination of time lags due to the distance (17 km) by comparing the time series between water level from gauge measurement in List Westerland and water level from radar measurement in List Tief in the same local time shows interesting results (figure 5.4). According to tidal calendar (BUNDESAMT FUR SEECHIFFAHRT UND HYDROGRAPHIE 2002) the time lags between both places is 1 hours. To obtain more precise result about the time lag between two time series, it is necessary to have longer in time observation. The comparison results from period 1 and 2 have also proved that the time lags are 1.5 hours and 1 hour,

respectively. The differences in the time lag could be due to the meteorological conditions and the extensive (0.5 and 1 hours) sampling interval. Thus, the time lags indicate that the water level will have the same tidal phase after 1 hour.

The visualization of mean bathymetry at figure 5.5 is the main product of present investigation at the period 1, hence for the period 2 and 3 at appendix VIII. The bathymetry map shows three distinctive depth regions which are near the shore at the South-East, the channel and the shallow area at the North-West. At the channel which is the deeper part area, the water depths reach approximately 11 m. For the shallow area at the both side, the results is limited to almost 4 m contour lines, due to the limitation of DiSC which uses the dispersion relation as part of the linear wave theory. The algorithm is out of reach at the shallow area due to the propagation of waves is not linear. Therefore the dispersion relation near the shore is not valid.

The cross section is used to determine the morphodynamic changes (figure 5.5). In this thesis, there are two ways to analyze the erosion or deposition over the cross section area. Firstly, the water depth variation over the cross section (figure 5.6) after subtracting with common references is identified. The shallower water depth is in October and the deeper is in February. At the distance 150 m - 400 m the sediment deposition due to the storm is obvious, the period 1 has different water depth approximately 0.5 m with period 2 and 3. The effect of the storm on the berm (100 m from A) was the transportation of it closer to the coast. This phenomenon is unusual as we expect the long waves to immigrate the berm to the deeper area. The comparison between three periods shows the deposition of sediment almost every where, but the sediment source cannot be defined. Probably, the deposition is caused by longshore sediment transport. Secondly, the slope variations over the cross section (figure 5.7) show very interesting results. In the area with depth higher than 8 m, the geomorphological features present common behavior. At the period 2, the effect of the storm on the sediment features is obvious, whereas at the period 1 and 3 have the similar slope at the water depth higher than 8 m and could be assumed the stable condition of the system. The near shore which is the South-East area at the distance 81.81 m was changed significantly at the three periods. The comparison between period 1 and period 2 is shown the deposition at that point. The slope at the period 1 is approximately 0.41º and become 0.07º at period 2 after 8 days. The changes slope

after 8 days is indicated that the sediment almost deposits in everywhere but the most significant at the shallow water area which have water depth around 4m-7m. After 8 months (comparison between period 2 and period 3) the slope at the distance 81.81m becomes steeper 10 times than before (from 0.07º become 0.7º). The changes slope is indicated the erosion along the cross section and the significant results is shown at the near shore area (South-East). The storm brought the sea bottom topography to conservative condition for the summer period.

SENET et al. (2001, 2004) identified the changes bathymetry between 2001 and 2003 for an area of the island of Sylt using ground based radar (figure 6.1). Close to the shore loss sand is obvious, whereas a broad stripe between 200 m and 800 m distance from shore shows a significant increase of sand and at the distance around 1000 m is the sand reduction zone. These results have been verified by conventional observation.

7. Conclusion

The Dispersive Surface Classificator (DiSC) as remote sensing method for interpreting of radar image sequences has been proven to be a powerful tool for coastal remote sensing. The comprehensive DiSC method permits the determination of spatial maps of important hydrographic parameter and the water depth. The technique is particularly useful for monitoring the consequences of a severe storm period, when the other monitoring systems are unusable.

In this thesis the potential of the DiSC algorithm has been examined to extract the additional information on the momentary water level. The accuracy of the chosen method was assessed with the chi-squared distribution to construct the confidence interval of variance. It could be shown that by inversion of the local wave in space and time, the in-situ gauge can be simulated. It is proven that the water level deduced by the radar measurements is not diverging significantly from the tidal gauge. The meteorological conditions, regional and local are important for the accuracy of the method. In addition, the selection area with 81 neighboring cells, as occurred from the method itself, is increasing the significance of the resulted water level. The comparison between DiSC and tidal gauge water level has a significant correlation (Corr=0.77). So, due to the capability of X-band radar to measure water depth, the in-situ measurement in the nearshore area at the two positions in direct vicinity and the closest gauge data can be used, when the time shift of the tidal phase is known.

The morphodynamic changes is also examined, by studying new bathymetry layer along two cross sections at the ship channel in the List Tief. The characteristic of the channel is changing (slope, absolute depth, and width).The slopes along two cross sections are compared during three different periods and it shows the deposition/erosion. The variability of sediment over the cross section is influenced by extreme events (storm) as well as by seasonal phenomena. The long term March to October has proved that in the area of investigation morphodynamic changes also occur during the summer season.

The nautical X-band radar measurement as a remote sensing method for water depth measurement in the coastal area has proven to get reasonable results in the severe

weather condition. The advantage of using an X-band radar system is its ability to monitor the coastal processes remotely and continuously, under calm condition as well as stormy. Hence, the X-band radar is satisfactory to observe the phenomena at the coastal region.

.

References

AHRENDT, K. (2001): Expected effect of climate change on Sylt island: results from a multidisciplinary German project. *Clim. Res*., 18: 141-146.

ANONYMOUS (1989): FURUNO – Operators manuals for FR 1201; Nishimomiya, Japan (FURUNO ELECTRIC CO. LIMITED).

BARRICK, D. E. (1977): Ocean surface current mapped by Radar. *Science* 198: 138-144.

BELL, P.S. (1999): Shallow water bathymetry derived from an analysis of X-band marine radar images of waves. *Coastal Engineering* 37: 513-527.

BELL, P.S. (1998): Bathymetry derived from an analysis of X-band radar marine radar images of waves. *Proceeding of oceanology'98 conference*, Bringhton, England, vol.3. 535-543.

CHERRY, J.A. (1994): Distortion analysis of weakly nonlinear filters using volterra series. Master's thesis, Ottowa Carleton Institute for Electrical ngineering, Ottawa, Canada.

CHOWDHURY, M.Z.R. (2007): Assessment of water flow and the impact on sediment motion in a tidal channel of North Sylt basing on radar observation. Master thesis, Coastal Geosciences and Engineering, CORELAB, University of Kiel, Germany.

CROMBIE, D. D. (1956): Doppler spectrum of sea echo at 13.56 Mc/s. *Nature,* 175: 681-682.

DAVIS, J.C. (2002): Statistics and data analysis in geology (third edition). 638pp.; New York, London, Toronto, Singapore (John willey & Sons).

DANKERT, H. & ROSENTHAL, W. (2004): Ocean surface determination from X-Band radarimage sequences. *Journal of Geophysical Research*, 109, pp C04016.
DANKERT, H. (2004): Measurement of wave, wave groups, and wind fields using nautical radar-image sequences. Dissertation, University of Hamburg, Germany.

DOONG, D. J. (2003): Uncertainty assessment of wave remote sensing, PhD thesis, Department of Hydraulic and Ocean Engineering, National Cheng Kung University, Tainan, Taiwan, Republic of China.

EMERY, W.J & THOMSON, E.R. (2001): Data analysis methods in physical oceanography (second and revised edition). 638pp.; Amsterdam, London, New York, Oxford, Paris, Tokyo (Elsivier).

FLAMPOURIS, S. (2006): Investigation of correlations between radar deduced bathymetries due to the outer impact of a storm in the area “Salzsand”. Master thesis, Coastal Geosciences and Engineering, CORELAB, University of Kiel, Germany.

GANGESKAR, R. & GRONLIE, O. (2000): Wave Height Measurement with a Standard Navigation Ship Radar – Result from Field Trials. In: Proceedings of the Sixth International Conference on Remote Sensing for Marine and Coastal Environments, Charleston, South Carolina.

GRONLIE, O. (1995): Microwave Radar Directional Wave Measurements – MIROS Results. *In*: Proceedings of the WMO/IOC Workshop on Operational Ocean Monitoring using Surface Based Radars, WMO Report no. 32, WMO/TD-No. 694, Geneva.

HASSELMANN, K. (1962): On the non-linear energy transfer in a gravity wave spectrum. 1: General theory. *J. Fluid Mech.*, 12, 481–500.

JAHID HASAN, G.M. & TAKEWAKA, S. (2007). Observation of a stormy wave field with X-band radar and its linear aspect. Department of Engineering Mechanics and Energy, University of Tsukuba, Tsukuba, Ibaraki, Japan.

JENSKINS, G. M. & WATTS, D.G. (1968): Spectral Analysis and Its Applications. 525pp.; San Francisco, Düsseldorf, Johannesburg, London, Panama, Singapore, Sydney, Toronto (Holden-Day).

JOHN, W. (2002). Chi-Square Calculator, Mathematic Detail and Table. (http://www.fourmilab.ch/rpkp/experiments/analysis/chiCalc.html).

LONG, M. W. (1983): Radar Reflectivity of Land and Sea (Second Edition). 385pp.; Dedham (Artech House, Inc).

MISRA, S. K. et al. (2002): An approach to determining nearshore bathymetry using remotely sensed ocean surface dynamics. *Journal Coastal Engineering, 47,* 265-293p.

NIETO BORGE, J. C.; REICHERT, K.; DITTMER, J. & ROSENTHAL, W. (1998): WaMoS II: A wave and current monitoring system, Presented at the COAST 714 conference, Sept., Paris Proceedings.

NIETO BORGE, J.C. & SOARES, C. G. (2000): Analysis of directional wave fields using X-band navigation radar. *Coastal Engineering*, 40, 375-391.

NIETO BORGE, J.C.; REICHERT, K. & DITTMER, J. (1999): Use of nautical radar as wave monitoring instrument. *Coastal Engineering*, 37, 331-342.

PHILLIPS, O.M. (1966): Thy dynamics of the upper ocean (First Edition); Cambridge University Press.

PIERSON, W. J. (1962): The directional spectrum of a wind-generated sea as determined from data obtained by the Stereo Wave Observation Project. *Coll. Eng. NYU Meteorol. Pap*. 2, No. 6.

PIERSON, W. J., NEUMANN, G. & JAMES, R. W. (1955): Practical methods for observing and forecasting ocean waves by means of wave spectra and statistics. US Navy Hydrographic Office Pub., 603.

REISE, K. (2004): Sea-Level Rise and the Future of Barrier Island in the North Sea; in proceedings of SeaLevel Rise and Coastal Defence in the Southern North Sea, Norfolk on 18 March 2004, 38-43p.

ROBINSON, I.S., WARD, N.P., GOMMENGINER, C.P, & TENORIO-GONZALES M.A (2000): Coastal oceanography applications of digital image data from marine radar. *Journal of Atmospheric and Oceanic Technology*, 17, pp. 721-725.

SABINS, F. F. (1987): Remote Sensing, Principles and Interpretation (Second Edition). W.H. Freeman, New York.

SEEMANN, J., ZIEMER, F. & SENET, C. M. (1997): A method for computing calibrated ocean wave spectra from measurements with a nautical X-band radar. Proc. Oceans ’97, Halifax, NS, Canada, MTS/IEEE, 1148–1154.

SEEMANN, J.; SENET, C.M.; WOLFF, U. & ZIEMER, F. (2000a): Nautical X-band radar Image Processing: Monitoring of Morphodynamic Processes in Coastal Waters, Ocean 2000, Conference Proceedings, Rhode Island, USA.

SEEMANN, J.; SENET, C.M.; WOLFF, U.; HATTEN, H. & ZIEMER, F. (2000b): Hydrographic Parameter Maps Retrieved from Nautical Radar Image Sequences of inhomogeneous Water Surfaces. IGARSS”2000, Conference Proceedings, Volume V, pp. 1898-1900, Honolulu, Hawaii.

SEEMANN, J.; SENET, C.M.; ZIEMER, F. (2000c): Local analysis of inhomogeneous Sea surfaces in Coastal waters using Nautical Radar Image Sequences, Mustererkennung 2000, Springer, Berlin, Informatik aktuell, pp. 179-186.

SENET, C., SEEMANN, J. & ZIEMER, F. (2001). The near-surface current velocity determined from image sequences of the sea surface. IEEE Trans. *Geosci. Remote Sens*., 39, 492–505.

SENET, C.M. (2004): Dynamics of Dispersive Boundaries: The determination of Spatial Hydrographic-Parameter Maps from Optical Sea-Surface Image Sequences. PhD thesis, GKSS Research Center, University of Hamburg.

SENET, C.M. & SEEMANN, J. (1999): Old_Pol_2_Cartesian (Computer Program), Internal Resource, Radar Hydrography (KOR), GKSS Research Center GmbH, Geesthacht, Germany.

SENET, C.M. & SEEMANN, J. (2002): Studie II: "Validation". Technical report, GKSS Research Center GmbH, Geesthacht, Germany.

SENET, C.M.; SEEMANN, J. & ZIEMER, F. (2003): Determination of Bathymetric and Current Maps by the Method DiSC Based on the Analysis of Nautical X-Band Radar-Image Sequences of the Sea Surface, (Elsevier Science).

SISTERMANS, P. & NIEUWENHUIS, O. (2007): Isle of Sylt: Isles Scheslwig-Holstein (Germany)-a Case Study of European Initiative for Sustainable Coastal Erosion Management (Eurosion), Amersfoort, The Netherlands. 21p.

SKOLNIK, M. (1990): Radar Handbook (Second Edition). McGraw-Hill, Inc., New York, St. Louis, London, Lisbon, Madrid, Mexico, Paris, Singapore, Sydney, Tokyo, Toronto.

SORENSEN, R. M. (1997): Basic Coastal Engineering (Second Edition). 301p. Kluwer Academic Publishers, Boston, Dordrecht, London.

SOULSBY, R.L. & HUMPHERY, J.D. (1990): Field observations of wave-current interaction at the sea bed, in Water Wave Kinematics, [eds] A. Torum and O.T. Gudmestad, pp. 413-428. Kluwer Academic Publishers, Dordrecht.

Trizna, D, B. (2001): Errors in bathymetric retrieval using linear dispersion in 3-D FFT analysis og image. Transactions on Geoscience and remote sensing, vol. 39, No. 11.

WILLEYWOLFF, U.; SEEMANN, J.; SENET, C.M. & ZIEMER, F. (1999): Analysis of Morphodynamical Processes with a Nautical X-Band Rader, Mustererkennung '99, Springer, Berlin, Ch. Pages 372-380.

YOO, J. (2007): Nonlinear bathymetry inversion based on wave property estimation from nearshore video imagery. PhD thesis, Civil and Environmental Engineering, Georgia Institute of Technology, USA.

YOUNG, I., ROSENTHAL, W., & ZIEMER, F. (1985). A three dimensional analysis of marine radar images for the determination of ocean wave directionality and surface currents. *J. Geophys. Res.,* 90,C1, 1049–1059.

ZIEMER, F. & DITTMER, J. (1994): A System to Monitor Ocean Wave Fields. In: Proceedings of the OCEANS'94, October 13-16: 28-31.

ZIEMER, F. (1991): Directional spectra from shipboard navigation radar during LEWEX. In Directional Ocean Wave Spectra, edited by R.C. Beal, The Johns Hopkins University Press, Baltimore, USA, pp. 80-84.

ZIEMER, F. (1995): An Instrument for the Survey of the Directionality of the Ocean Wave Field. Workshop on Operational Ocean Monitoring using surface based radars, Geneva, WMO/IOC Report No. 32, pp. 81-87.

ZIEMER, F., BROCKMANN, C.; VAUGHAN, A. R.; SEEMANN, J. & SENET, C.M. (2004): Radar Survey of Near Shore Bathymetry within the OROMA project. EARSel eProceedings 3, 2/2004, pp. 282-288.

I. Appendix

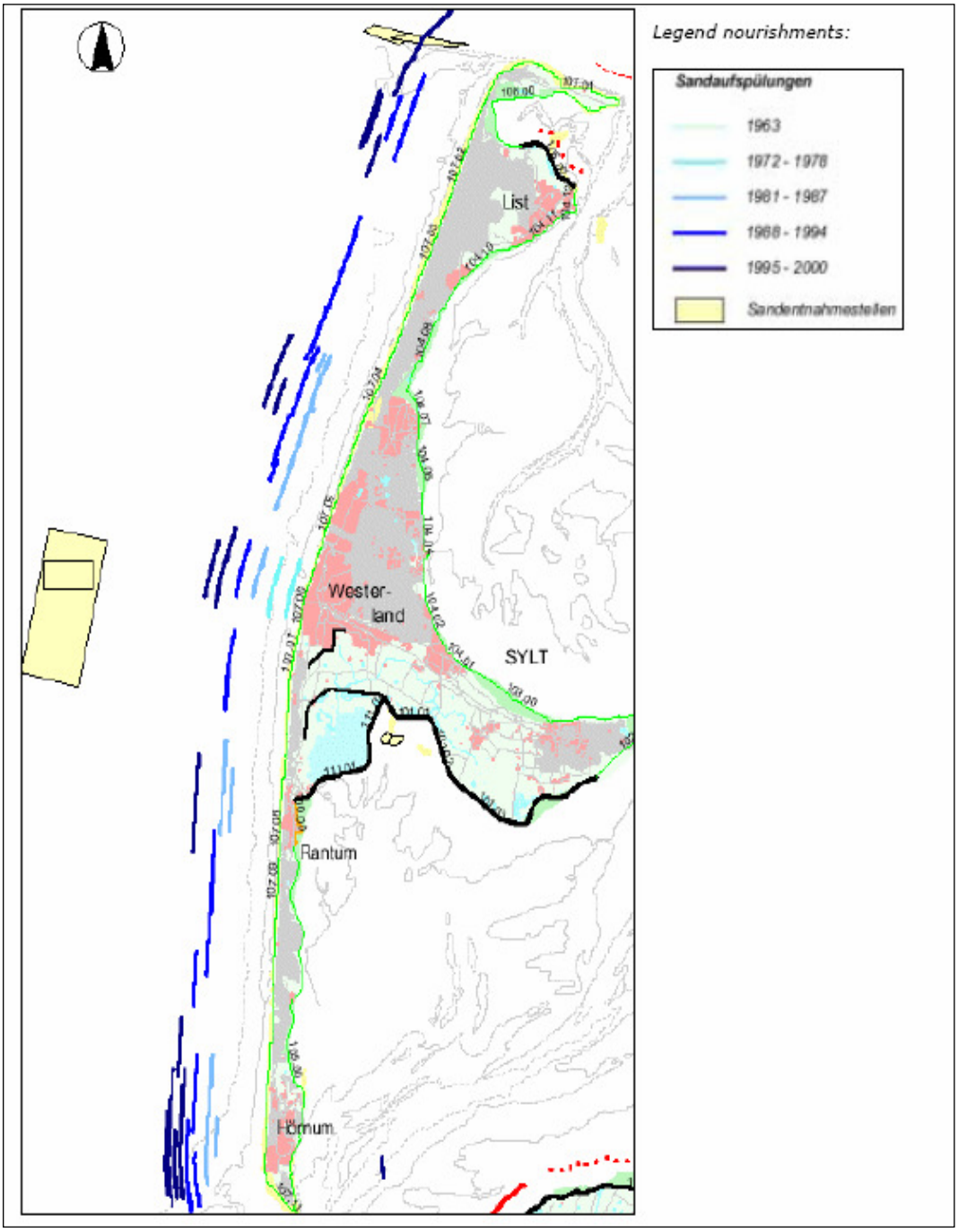

Figure I-1: Sand nourishment at Sylt (GENERALPLAN KUSTENSCHUTZ).

II. Appendix

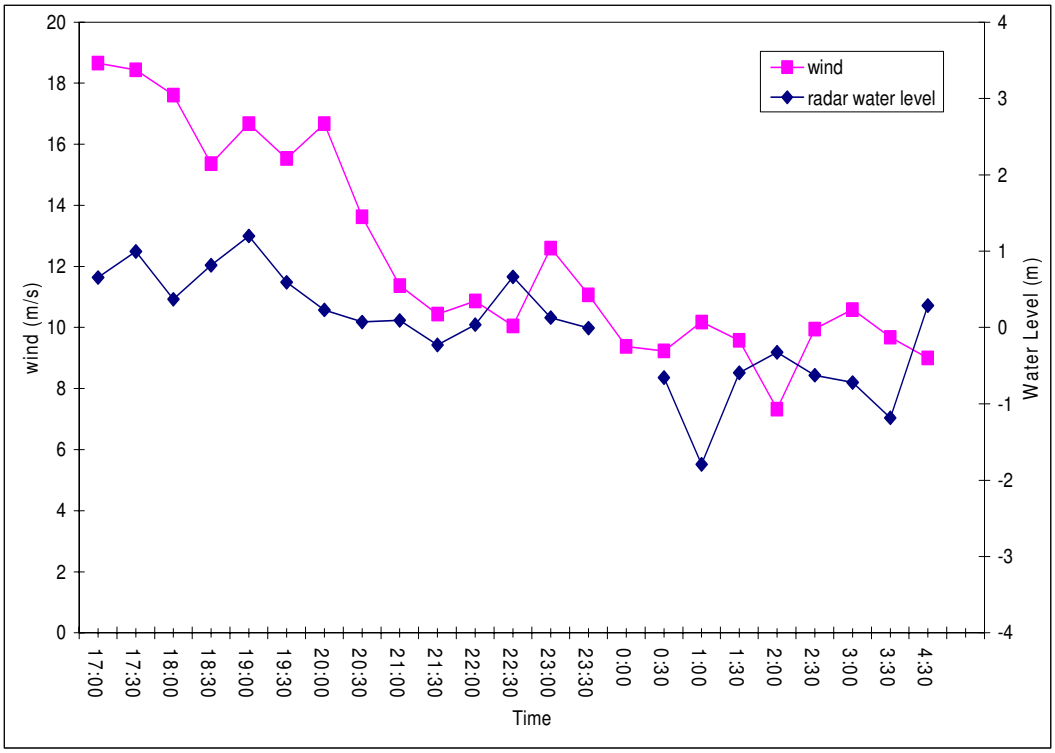

Figure II-1: plot wind speed and water level at the period 1(27 February 2002).

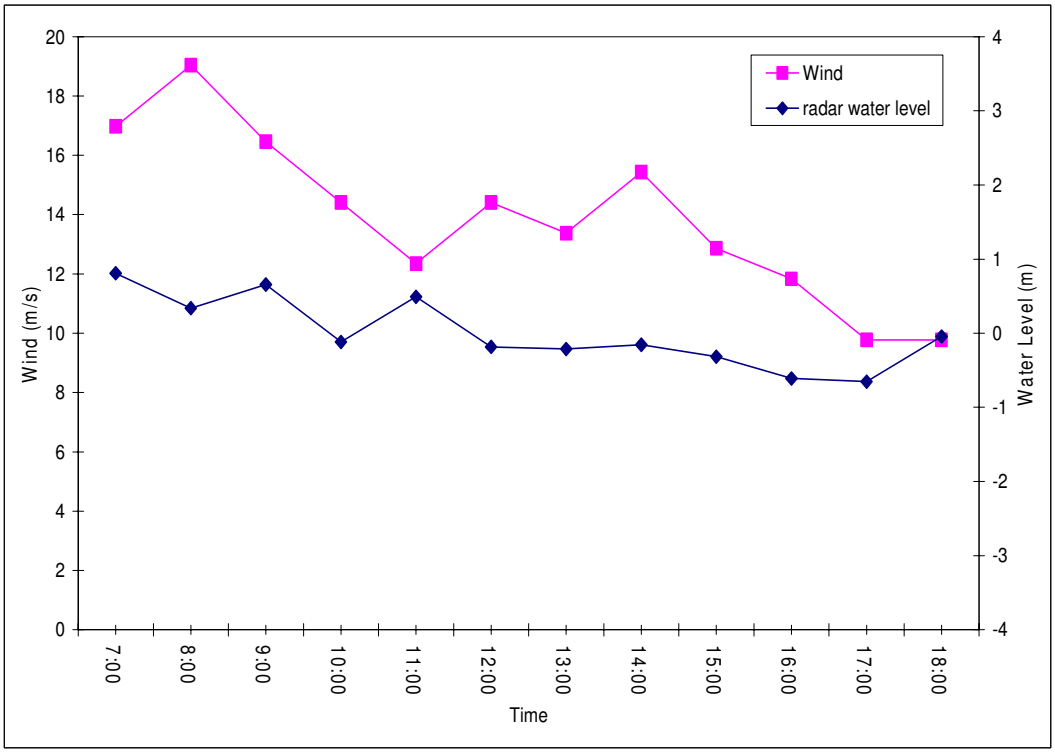

Figure II-2: Plot wind speed and water level at the period 2 (7 March 2002).

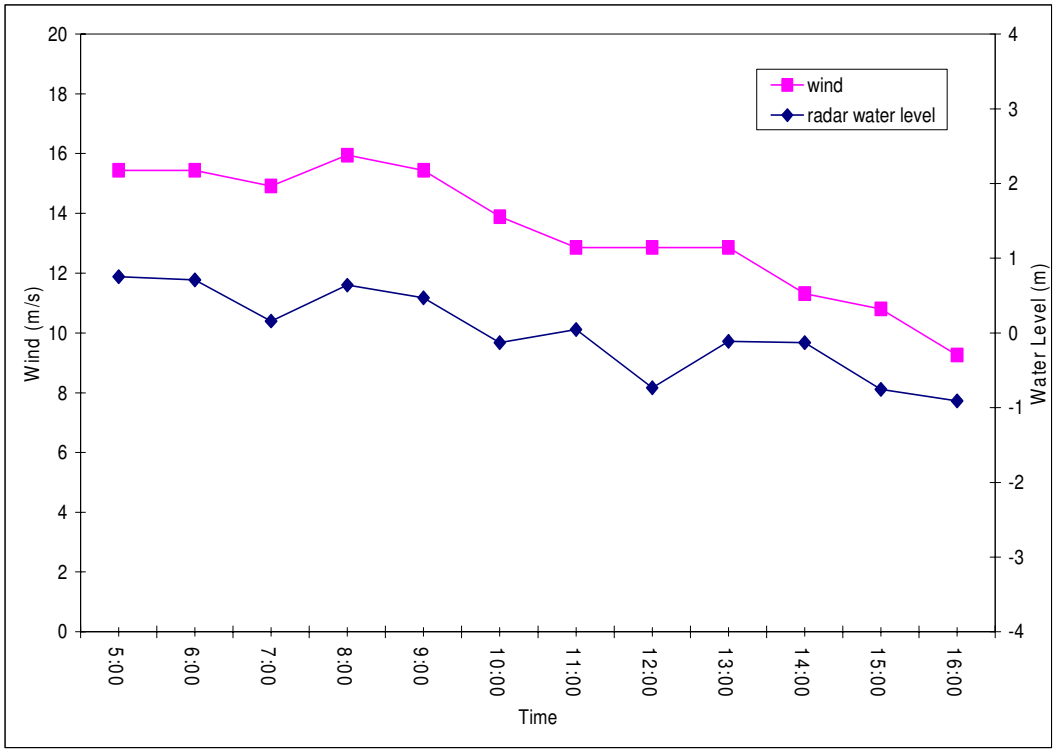

Figure II-3: Plot wind speed and water level at the period 3 (28 October 2002).

III. Appendix

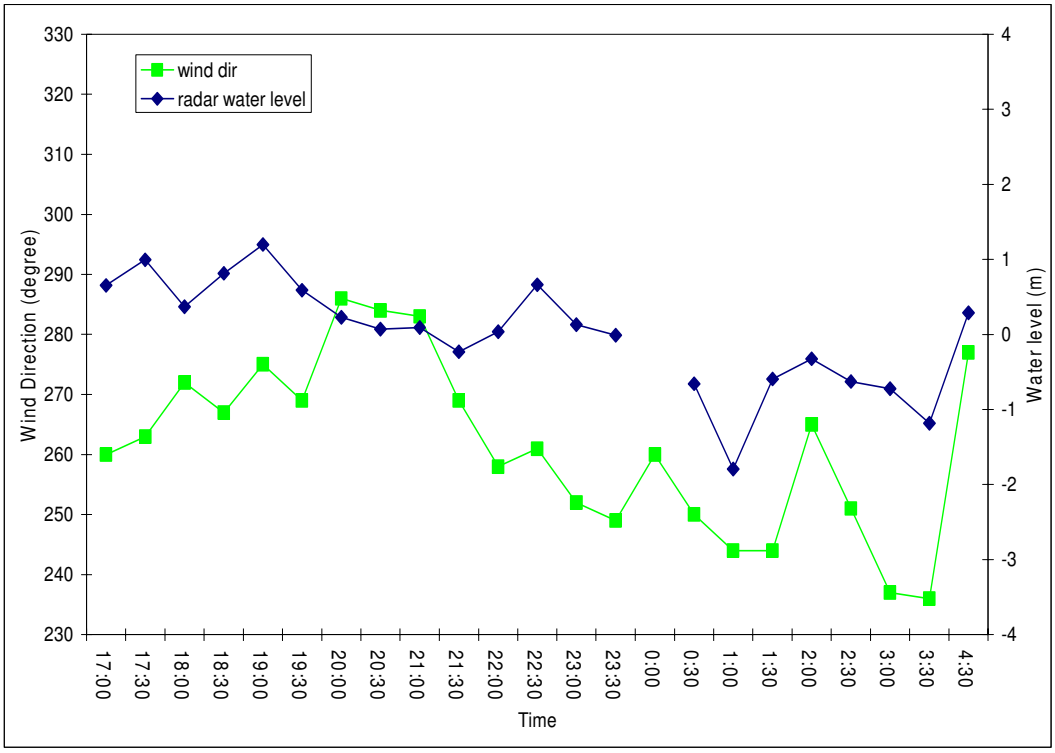

Figure III-1: Plot wind direction and water level at the period 1 (26-27 February 2002).

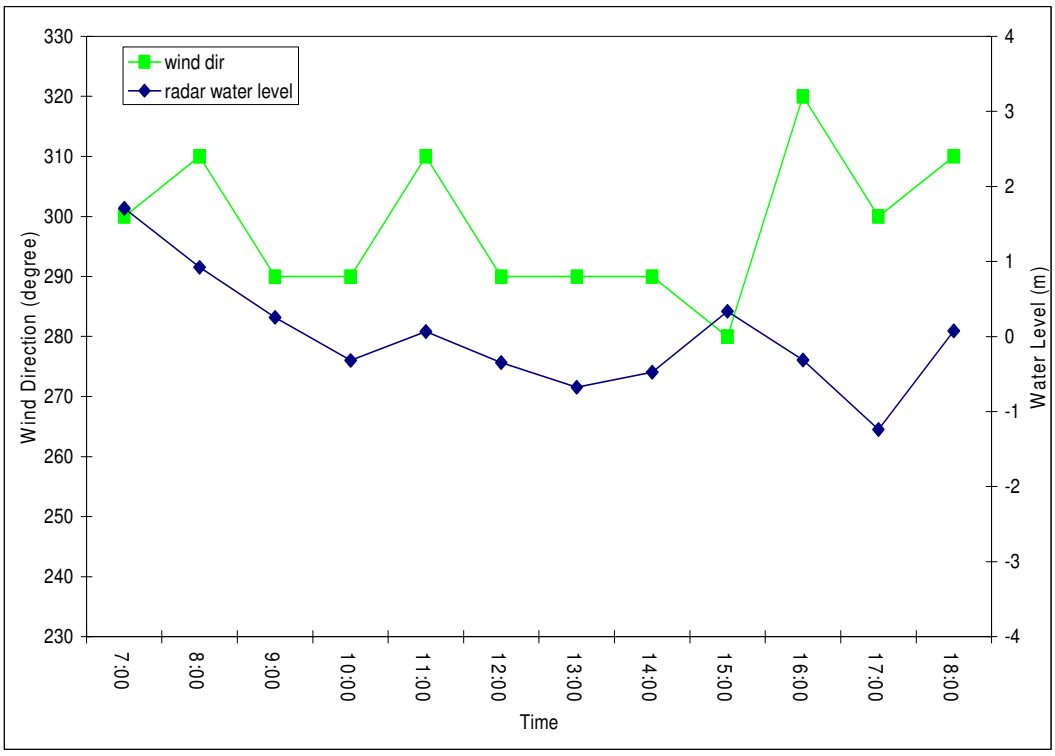

Figure III-2: Plot wind direction and water level at the period 2 (7 March 2002).

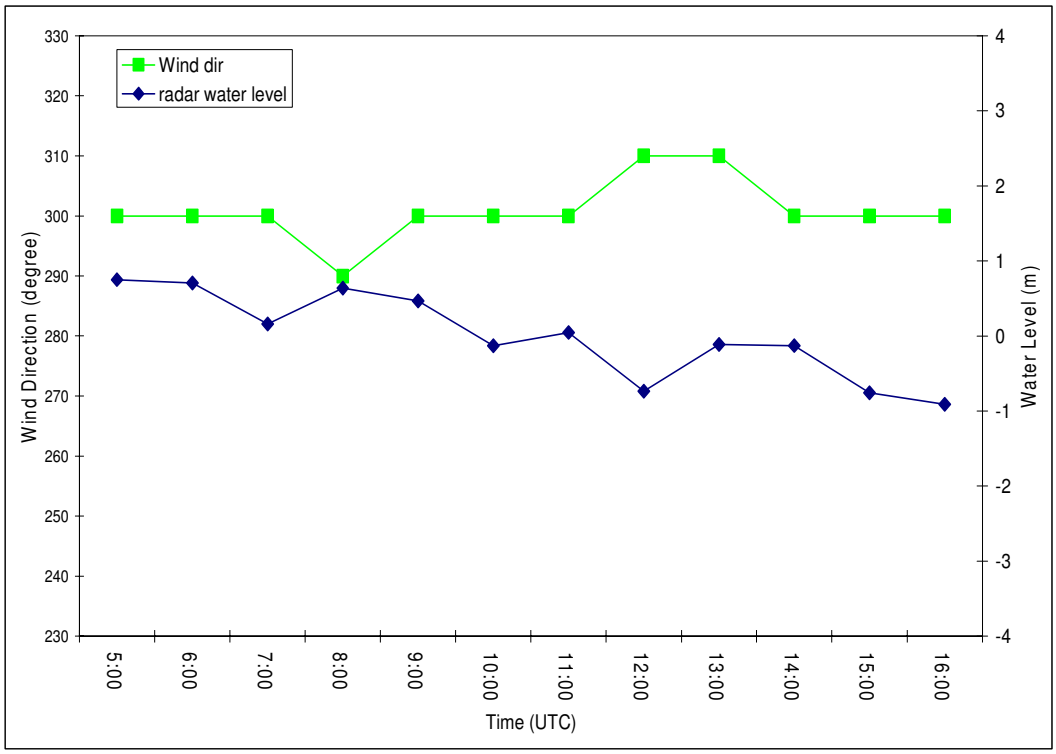

Figure III-2: Plot wind speed and water level at the period 3 (28 October 2002).

IV. Appendix

```
;*****************************************************************************
; PV WAVE Header
;-----------------------------------------------------------------------------
; File name       :       start
; Residency       :
; Programe name   :       After_DiSC_Processing
; Module name     :       Bathymetry
; Version nr      :       1.0
; Date            :       05.11.2005
; Place           :       GKSS / Geesthacht
; Author          :       Stelios F.
; Email           :       stylianos.flampouris@gkss.de
;-----------------------------------------------------------------------------
; Descriptions    :  Initializing the compiling of all the routines
;-----------------------------------------------------------------------------
;
;*****************************************************************************


RETALL
.LOCALS
DELVAR, /ALL
CLOSE, /ALL
DEVICE, /CLOSE

set_plot,'win32'
@stat_startup
@math_startup
;@sigpro_startup
;@ip_startup

.run E:\pv-wave\pro\coordinates
.run E:\pv-wave\pro\datarr_creation
.run E:\pv-wave\pro\filenamed
.run E:\pv-wave\pro\comparison
.run E:\pv-wave\pro\output
surfer_main
```

```
;*****************************************************************************
; PV WAVE Header
;-----------------------------------------------------------------------------
; File name       :       surfer_main
; Residency       :
; Programe name   :       After_DiSC_Processing
; Module name     :       Bathymetry
; Version nr      :       1.1
; Date            :       05.11.2005
; Place           :       GKSS / Geesthacht
; Author          :       Stelios F.
; Email           :       stylianos.flampouris@gkss.de
;-----------------------------------------------------------------------------
; Descriptions    :  The main of the After_DiSC_Processing
;-----------------------------------------------------------------------------
;
;*****************************************************************************

PRO surfer_main

Print, '--------------------------------------
Print, 'The surfer_main is running'

Print, 'By stelios f.

Print, 'GKSS Research Center
Print, '--------------------------------------

WAIT,1

;The subroutine 'coordinates' reads the coordinates of the result
;from DiSC. The coordinates are in meters
        coordinates, linenr
;The subroutine 'datarr_creation' reads the data and creates an array
        datarr_creation, data_arr, linenr
; The subroutine 'filenamed' checks for the existence of the input
; data file and calls two more subroutines the 'comparison' and the
; 'output'
        filenamed, lookfor, data_arr
END
```

```
;*****************************************************************************
; PV WAVE Header
;-----------------------------------------------------------------------------
; File name       :       coordinates
; Residency       :
; Programe name   :       After_DiSC_Processing
; Module name     :       Bathymetry
; Version no      :       1.1
; Date            :       05.11.2005
; Place           :       GKSS / Geesthacht
; Author          :       Stelios F.
; Email           :       stylianos.flampouris@gkss.de
;-----------------------------------------------------------------------------
; Description     :  The subroutine 'coordinates' is reading the coordinates of the resuls from DiSC.
                     The coordinates are in meters


;-----------------------------------------------------------------------------
;
;*****************************************************************************
PRO coordinates, linenr

        Print, '--------------------------------------
        Print, 'The coordinates is running'
        Print, '--------------------------------------


        OPENW,1,'coordinates.txt'
                FOR xcoordinate = DOUBLE(3460208),
DOUBLE(3462171.636),DOUBLE(40.9092) DO BEGIN
                FOR ycoordinate = DOUBLE(6102504.6),
DOUBLE(6104468.236),DOUBLE(40.9092) DO BEGIN
                xcoordinate1 = STRING(xcoordinate - 0.0208,format="(D12.2)")
                ;Print, 'xcoordinate1= ', xcoordinate1
                ycoordinate1 = STRING(ycoordinate - 0.0208,format="(D12.2)")
                ;Print, 'ycoordinate1= ', ycoordinate1
                coordinates = xcoordinate1+' '+ ycoordinate1
                PRINTF,1, coordinates
                ENDFOR ;ycoordinate
                ENDFOR ;xcoordinate
        CLOSE,1

;Counting the lines
        linenr = LONG(0)
        OPENR,1, 'coordinates.txt'
                WHILE (NOT EOF(1)) DO BEGIN
        READF,1,line
                linenr = linenr+1

                ENDWHILE
;print, linenr

        CLOSE,1

END
```

```
;*****************************************************************************
; PV WAVE Header
;-----------------------------------------------------------------------------
; File name       :       datarr_creation
; Residency       :
; Programe name   :       After_DiSC_Processing
; Module name     :       Bathymetry
; Version no      :       1.0
; Date            :       05.11.2005
; Place           :       GKSS / Geesthacht
; Author          :       Stelios F.
; Email           :       stylianos.flampouris@gkss.de
;-----------------------------------------------------------------------------
; Descriptions    :       The datarr_creation reads the data and creates an array
;-----------------------------------------------------------------------------
;
;*****************************************************************************

PRO datarr_creation, data_arr, linenr

        Print, '--------------------------------------
        Print, 'The datarr_creation is running'
        Print, '--------------------------------------

;Creation of data array
        data_arr=DBLARR(linenr,linenr)
        lincnt = 0l
        line = STRARR(1)
        OPENU, 1, 'E:\pv-wave\main\coordinates.txt'
                WHILE (NOT EOF(1)) DO BEGIN
                        READF,1,line
                ; To define the x_coordinate, have to find the position of the
                ;first point ".", so search for it
                        pos_firstpoint = STRPOS(line,'.')
                        x_coordinate = DOUBLE(STRMID(line,pos_firstpoint(0)-7,10))
                data_arr(0,lincnt) = x_coordinate
                ;print,'x = ',x_coordinate
                ; To define the x_coordinate, have to find the position of the
                ;second point ".", so search for it
                        pos_secondpoint =STRPOS(line,'.',pos_firstpoint(0)+1)
                        ;print,'pos_secondpoint=',pos_secondpoint
                y_coordinate = DOUBLE(STRMID(line,pos_secondpoint(0)-7,pos_secondpoint(0)-
pos_firstpoint(0)-1))
                data_arr(1,lincnt) = y_coordinate
                ;print,'y_coordinate=',data_arr(1,lincnt)
                lincnt = lincnt+1
                ENDWHILE
        CLOSE,1
END
```

```
;*****************************************************************************
; PV WAVE Header
;-----------------------------------------------------------------------------
; File name         :       filenamed
; Residency         :
; Programe name     :       After_DiSC_Processing
; Module name       :       Bathymetry
; Version no        :       1.0
; Date              :       05.11.2005
; Place             :       GKSS / Geesthacht
; Author            :       Stelios F.
; Email             :       stylianos.flampouris@gkss.de
;-----------------------------------------------------------------------------
; Descriptions      :        The subroutine 'filenamed' checks for the existence of the input data file
and calls two more subroutines the ‘comparison’ and the ‘output’
;

;-----------------------------------------------------------------------------
;
;*****************************************************************************

PRO filenamed, lookfor, data_arr

        Print, '--------------------------------------
        Print, 'The filenamed is running'
        Print, '--------------------------------------

        fn=LONG(2)
existfiles_strvec = STRARR(1)
;definition of the variables
        FOR day = 28, 29, 1 DO BEGIN
                FOR hour = 0, 23, 1 DO BEGIN
                        FOR shoot = 1,4, 1 DO BEGIN
                                day1 = STRCOMPRESS(STRING(day),/Remove_all)
                                        daylen = STRLEN(day1)
                                                IF daylen LT 2 THEN BEGIN
                                                        day1 = '0'+ day1
                                                ENDIF ELSE BEGIN
                                                        day1 = day1
                                                ENDELSE
                                hour1 = STRCOMPRESS(STRING(hour),/Remove_all)
                                        hourlen = STRLEN(hour1)
                                                IF hourlen LT 2 THEN BEGIN
                                                        hour1 = '0'+hour1
                                                ENDIF ELSE BEGIN
                                                        hour1 = hour1

                                                ENDELSE

                        shoot1 = STRCOMPRESS (STRING(shoot),/Remove_all)
                                shootlen = STRLEN (shoot1)
                                IF shootlen LT 2 THEN BEGIN
                                        shoot1 = '0'+shoot1

                        ENDIF ELSE BEGIN
                                        shoot1 = shoot1

                                        ENDELSE
```

```
                    fname = '10'+day1+hour1+'00_'+shoot1+'_result_6x6.txt'

;Existence of file

                f_path = 'E:/2002_re/Oct/1028/'
                    lookfor = f_path+fname
                ;print, 'lookfor=', lookfor
                    file_exist=FINDFILE(lookfor, count = fe_counter)
                    IF fe_counter EQ 1 THEN BEGIN
                    existfiles_strvec = [existfiles_strvec,file_exist]

                    ;PRINT, lookfor

                    ;PRINT,existfiles_strvec
                ;HAK
                comparison, lookfor, data_arr, fn
        fn=fn+1

                    ENDIF
                ENDFOR ;shoot

                ENDFOR ;hour

          ENDFOR ;day
output, data_arr

END
```

```
;*****************************************************************************
; PV WAVE Header
;-----------------------------------------------------------------------------
; File name         :       coordinates
; Residency         :
; Programe name     :       After_DiSC_Processing
; Module name       :       Bathymetry
; Version no        :       1.1
; Date              :       05.11.2005
; Place             :       GKSS / Geesthacht
; Author            :       Stelios F.
; Email             :       stylianos.flampouris@gkss.de
;-----------------------------------------------------------------------------
; Descriptions      :       The subroutine 'comparison' creates an index which matches the
'coordinates' with the coordinates of the result from DiSC and simultunuously the results are filtered
but the number of regression points (GT 40)
;-----------------------------------------------------------------------------
;
;*****************************************************************************

PRO comparison, lookfor, data_arr, fn

        Print, '--------------------------------------
        Print, 'The comparison number
        Print, fn
        Print, '--------------------------------------

;Creation of the full data array with the correct coordinates..!
        lincnt = 0l
        line = STRARR(1)
        OPENR, 1, lookfor
                WHILE (NOT EOF(1)) DO BEGIN
                        READF,1,line
                                ;print,    line
                ; To define the x_coordinate of the data, have to find the position of the
                ;first point ".", so search for it
                        pos_firstpoint = STRPOS(line,'.')
                                ;print,'pos_firstpoint = ',pos_firstpoint
                        x_coordinate = DOUBLE(STRMID(line,pos_firstpoint(0)-7,10))

                ;print, 'x_coordinate=', x_coordinate

                ; To define the y_coordinate of the data, have to find the position of the
                ;second point ".", so search for it
                        pos_secondpoint = STRPOS(line,'.',pos_firstpoint(0)+1)
                                ;print,'pos_secondpoint = ',pos_secondpoint
                y_coordinate = DOUBLE(STRMID(line,pos_secondpoint(0)-7,pos_secondpoint(0)-
pos_firstpoint(0)-1))
                ;print, 'y_coordinate=', y_coordinate

        ;For qualifying reasons the regression points of each "depth" must be more than 40
        ;So first read the regression points anf if greater than 40,we accept the calculated depth
                pos_secondtab = STRPOS(line,' ',pos_secondpoint(0)+1)
                ;pos_secondtab = STRPOS(line,'    ',pos_secondpoint(0)+1)
                ;print,'pos_secondtab = ',pos_secondtab
                nr_reg_point = DOUBLE(STRMID(line,pos_secondtab(0),4))
                ;print, 'nr_reg_point', nr_reg_point
```

```
                ;To define the depth, have to find the position of the third point "."
                pos_thirdpoint = STRPOS(line,'.',pos_secondpoint(0)+1)
                ;print,'pos_thirdpoint = ',pos_thirdpoin
                        depth = DOUBLE(STRMID(line,pos_thirdpoint(0)-2,5))
                        ;print,'depth =', depth
                IF nr_reg_point(0) LT 40 OR (depth(0)LT 4 OR depth(0) GT 18) THEN BEGIN

                depth=0
                ;print,'depth1 =', depth

                ENDIF ELSE BEGIN

                ;Index
                   x_index = WHERE(      $
                                (data_arr(0,*)  LE x_coordinate(0) + 10.0)    AND $
                                (data_arr(0,*)  GT x_coordinate(0) - 10.0)    $
                                        )
                                        ;PRINT,'x_index', x_index
                if (x_index(0) EQ -1) then STOP

                        y_index = WHERE(          $
                                (data_arr(1,x_index)  LE y_coordinate(0) + 10.0)       AND $
                                (data_arr(1,x_index)  GT y_coordinate(0) - 10.0)       $
                                        )

                                right_line = x_index(y_index)


                                ;PRINT, right_line

                        data_arr(fn,right_line) = depth(0)
                                ;PRINT,'Z=', data_arr(fn,right_line)
        ENDELSE
                lincnt = lincnt+1

                ENDWHILE

        CLOSE,1

END
```

```
;*****************************************************************************
; PV WAVE Header
;-----------------------------------------------------------------------------
; File name         :       coordinates
; Residency         :
; Programe name     :       After_DiSC_Processing
; Module name       :       Bathymetry
; Version nr        :       1.0
; Date              :       05.11.2005
; Place             :       GKSS / Geesthacht
; Author            :       Stelios F.
; Email             :       stylianos.flampouris@gkss.de
;-----------------------------------------------------------------------------
; Description       : The subroutine 'output' extracts the data into two different files.
  The coordinates : coor_result.txt
; The data          : data_result.txt
;-----------------------------------------------------------------------------
;
;*****************************************************************************

PRO output, data_arr

        Print, '--------------------------------------
        Print, 'The output is running'
        Print, '--------------------------------------

;Output subroutine
;Coordinates Output
        OPENW,1, 'E:\pv-wave\main\coordinates.txt'
                for j=0l,2302 do begin
                str_dum1=''
                        for i=0l,2 do begin
                                str_line1 = STRING(data_arr(i,j), format="(D12.2)")
                                str_dum1=str_dum1 + str_line1
                        endfor ; column

                                PRINTF,1,str_dum1
                endfor ; lines
CLOSE,1

;Data Output
        OPENW,1, 'E:\pv-wave\main\data_result.txt'
                for j=0l,2302 do begin
                        str_dum=''
                        for i=2,58 do begin
                                str_line = STRING(data_arr(i,j), format="(D6.2)")
                                str_dum=str_dum + str_line
                        endfor ; column
                        PRINTF,1,str_dum
                endfor ; lines
CLOSE,1

END
```

```
;*****************************************************************************
; PV WAVE Header
;-----------------------------------------------------------------------------
; File name       :       cross_correlation
; Residency       :
; Programe name   :       Cross_correlation_processing
; Module name     :       Water level
; Version nr      :       1.1
; Date            :       03.01.2008
; Place           :       GKSS / Geesthacht
; Author          :       Novrizal Alamsyah
; Email           :       nalamsyah@gkss.de
;-----------------------------------------------------------------------------
; Description     :       Initializing the compiling of all routines
;-----------------------------------------------------------------------------
;
;*****************************************************************************

Retall
.Locals
Delvar, /ALL
Close, /ALL
Device, /Close

set_plot,'win32'
@stat_startup
@math_startup
@sigpro_startup
@ip_startup

.run ../sub/baca_1
.run ../sub/cross_correlation
.run mulai_main
mulai_main
```

```
;*****************************************************************************
;
;-----------------------------------------------------------------------------
; Description       :       The main of the Cross_correlation_processing
;-----------------------------------------------------------------------------
;
;*****************************************************************************
;first step with pv-wave
PRO mulai_main

baca_1,time,Westerland_waterlevel,List_waterlevel,linenr2

cross_correlation,westerland_waterlevel,list_waterlevel,linenr2

END
```

```
;*****************************************************************************
;
;-----------------------------------------------------------------------------
; Description       :       The Subroutine 'baca_1' is reading the water level data
;-----------------------------------------------------------------------------
;
;*****************************************************************************
PRO baca_1,time,Westerland_waterlevel,List_waterlevel,linenr2

path1    ='E:/cross_correlation_data/102802_3.txt'
line     =STRARR(1)
linenr   =LONG(0)
linenr2  =LONG(0)

OPENER,1,path1
                WHILE (NOT EOF(1)) DO BEGIN

                READF,1,line
                linenr = linenr+1
 ENDWHILE

                                CLOSE,1

                time                =STRARR(linenr+1)
                Westerland_waterlevel  =STRARR(linenr+1)
                List_waterlevel       =STRARR(linenr+1)

OPENR,1,path1

                WHILE (NOT EOF(1)) DO BEGIN

                READF,1,line


                time            (linenr2)           =  STRMID(line,0,10)
                        Westerland_waterlevel  (linenr2)     =  STRMID(line,10,13)
                List_waterlevel       (linenr2)          =  STRMID(line,23,13)



                linenr2             = linenr2+1

ENDWHILE
                                CLOSE, 1


;print, 'time= ', time
print, 'Westerland_waterlevel=', Westerland_waterlevel
print, 'List_waterlevel=',List_waterlevel

END
```

```
;*****************************************************************************
;
;-----------------------------------------------------------------------------
; Description       :       Comparison water level data
;-----------------------------------------------------------------------------
;
;*****************************************************************************
PRO cross_correlation,westerland_waterlevel,list_waterlevel,linenr2

linenr2=linenr2+1
cros_res = CROSSCORRELATION (linenr2, westerland_waterlevel,list_waterlevel, 6)

Print, cros_res

END
```

V. Appendix

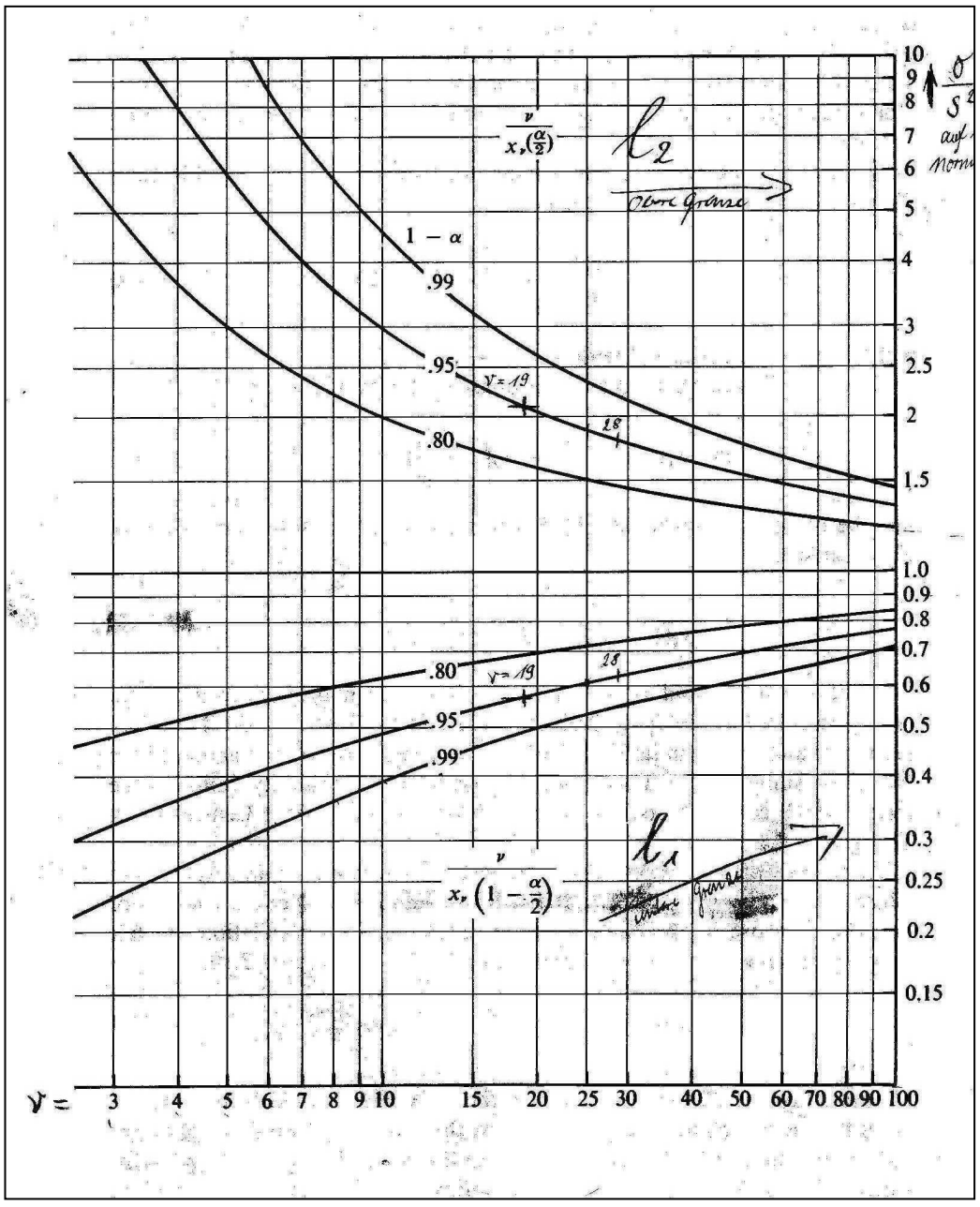

Figure V-1: Plot of upper limit, lower limit ($\frac{\nu}{\chi_\nu(\alpha/2)}, \frac{\nu}{\chi_\nu(1-\alpha/2)}$) vs. ν for $(1-\alpha)$ = 0.80, 0.95, 0.99 (derived from JENKINS and WATTSS (1968), "Spectral Analysis and its Application").

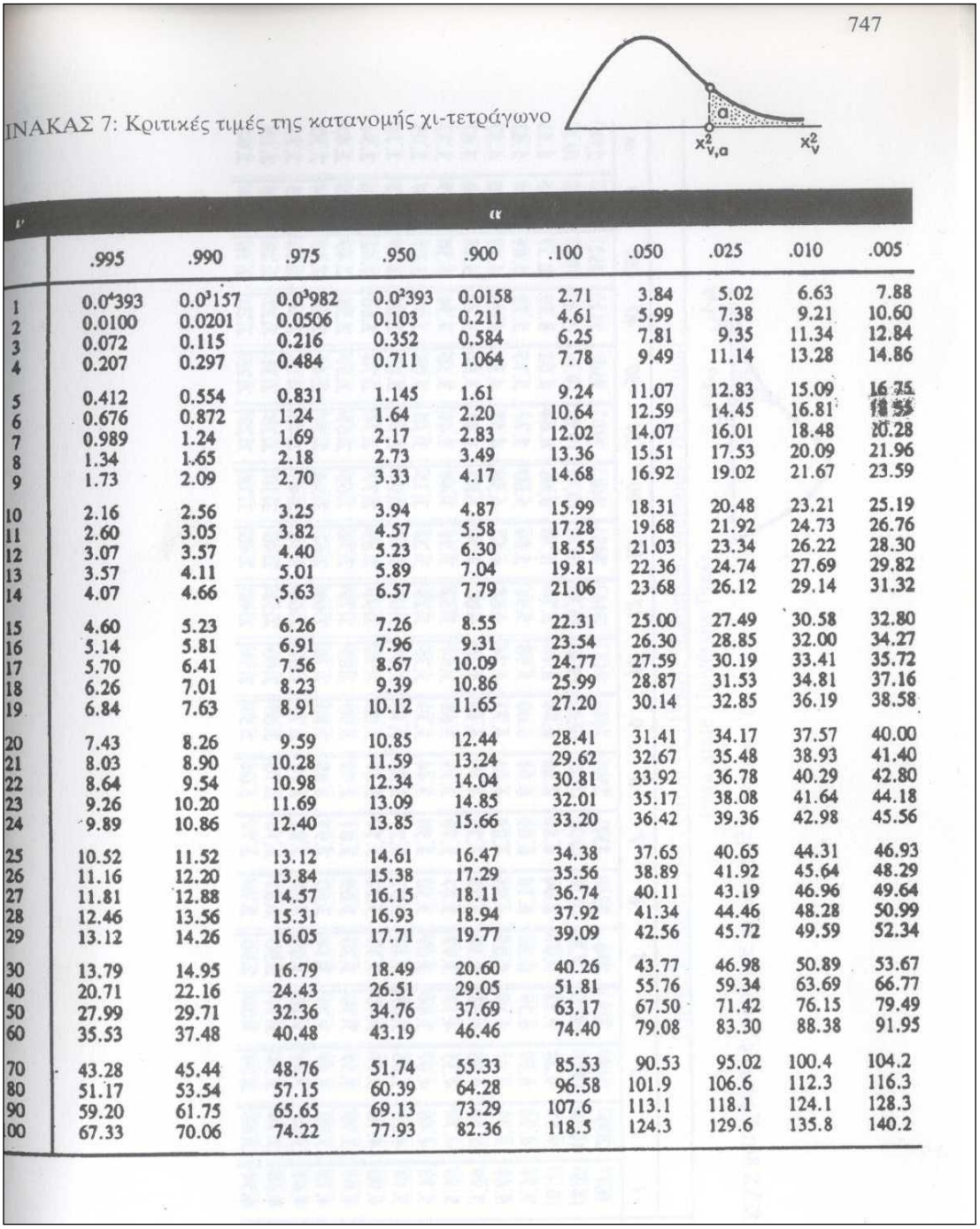

747

ΙΝΑΚΑΣ 7: Κριτικές τιμές της κατανομής χι-τετράγωνο

	.995	.990	.975	.950	.900	.100	.050	.025	.010	.005
1	0.0^4393	0.0^3157	0.0^3982	0.0^2393	0.0158	2.71	3.84	5.02	6.63	7.88
2	0.0100	0.0201	0.0506	0.103	0.211	4.61	5.99	7.38	9.21	10.60
3	0.072	0.115	0.216	0.352	0.584	6.25	7.81	9.35	11.34	12.84
4	0.207	0.297	0.484	0.711	1.064	7.78	9.49	11.14	13.28	14.86
5	0.412	0.554	0.831	1.145	1.61	9.24	11.07	12.83	15.09	16.75
6	0.676	0.872	1.24	1.64	2.20	10.64	12.59	14.45	16.81	18.55
7	0.989	1.24	1.69	2.17	2.83	12.02	14.07	16.01	18.48	20.28
8	1.34	1.65	2.18	2.73	3.49	13.36	15.51	17.53	20.09	21.96
9	1.73	2.09	2.70	3.33	4.17	14.68	16.92	19.02	21.67	23.59
10	2.16	2.56	3.25	3.94	4.87	15.99	18.31	20.48	23.21	25.19
11	2.60	3.05	3.82	4.57	5.58	17.28	19.68	21.92	24.73	26.76
12	3.07	3.57	4.40	5.23	6.30	18.55	21.03	23.34	26.22	28.30
13	3.57	4.11	5.01	5.89	7.04	19.81	22.36	24.74	27.69	29.82
14	4.07	4.66	5.63	6.57	7.79	21.06	23.68	26.12	29.14	31.32
15	4.60	5.23	6.26	7.26	8.55	22.31	25.00	27.49	30.58	32.80
16	5.14	5.81	6.91	7.96	9.31	23.54	26.30	28.85	32.00	34.27
17	5.70	6.41	7.56	8.67	10.09	24.77	27.59	30.19	33.41	35.72
18	6.26	7.01	8.23	9.39	10.86	25.99	28.87	31.53	34.81	37.16
19	6.84	7.63	8.91	10.12	11.65	27.20	30.14	32.85	36.19	38.58
20	7.43	8.26	9.59	10.85	12.44	28.41	31.41	34.17	37.57	40.00
21	8.03	8.90	10.28	11.59	13.24	29.62	32.67	35.48	38.93	41.40
22	8.64	9.54	10.98	12.34	14.04	30.81	33.92	36.78	40.29	42.80
23	9.26	10.20	11.69	13.09	14.85	32.01	35.17	38.08	41.64	44.18
24	9.89	10.86	12.40	13.85	15.66	33.20	36.42	39.36	42.98	45.56
25	10.52	11.52	13.12	14.61	16.47	34.38	37.65	40.65	44.31	46.93
26	11.16	12.20	13.84	15.38	17.29	35.56	38.89	41.92	45.64	48.29
27	11.81	12.88	14.57	16.15	18.11	36.74	40.11	43.19	46.96	49.64
28	12.46	13.56	15.31	16.93	18.94	37.92	41.34	44.46	48.28	50.99
29	13.12	14.26	16.05	17.71	19.77	39.09	42.56	45.72	49.59	52.34
30	13.79	14.95	16.79	18.49	20.60	40.26	43.77	46.98	50.89	53.67
40	20.71	22.16	24.43	26.51	29.05	51.81	55.76	59.34	63.69	66.77
50	27.99	29.71	32.36	34.76	37.69	63.17	67.50	71.42	76.15	79.49
60	35.53	37.48	40.48	43.19	46.46	74.40	79.08	83.30	88.38	91.95
70	43.28	45.44	48.76	51.74	55.33	85.53	90.53	95.02	100.4	104.2
80	51.17	53.54	57.15	60.39	64.28	96.58	101.9	106.6	112.3	116.3
90	59.20	61.75	65.65	69.13	73.29	107.6	113.1	118.1	124.1	128.3
00	67.33	70.06	74.22	77.93	82.36	118.5	124.3	129.6	135.8	140.2

Figure V-2: Table of Chi-Squared (derived from Newbold (1984), "Statistics for Business and Economics").

VI. Appendix

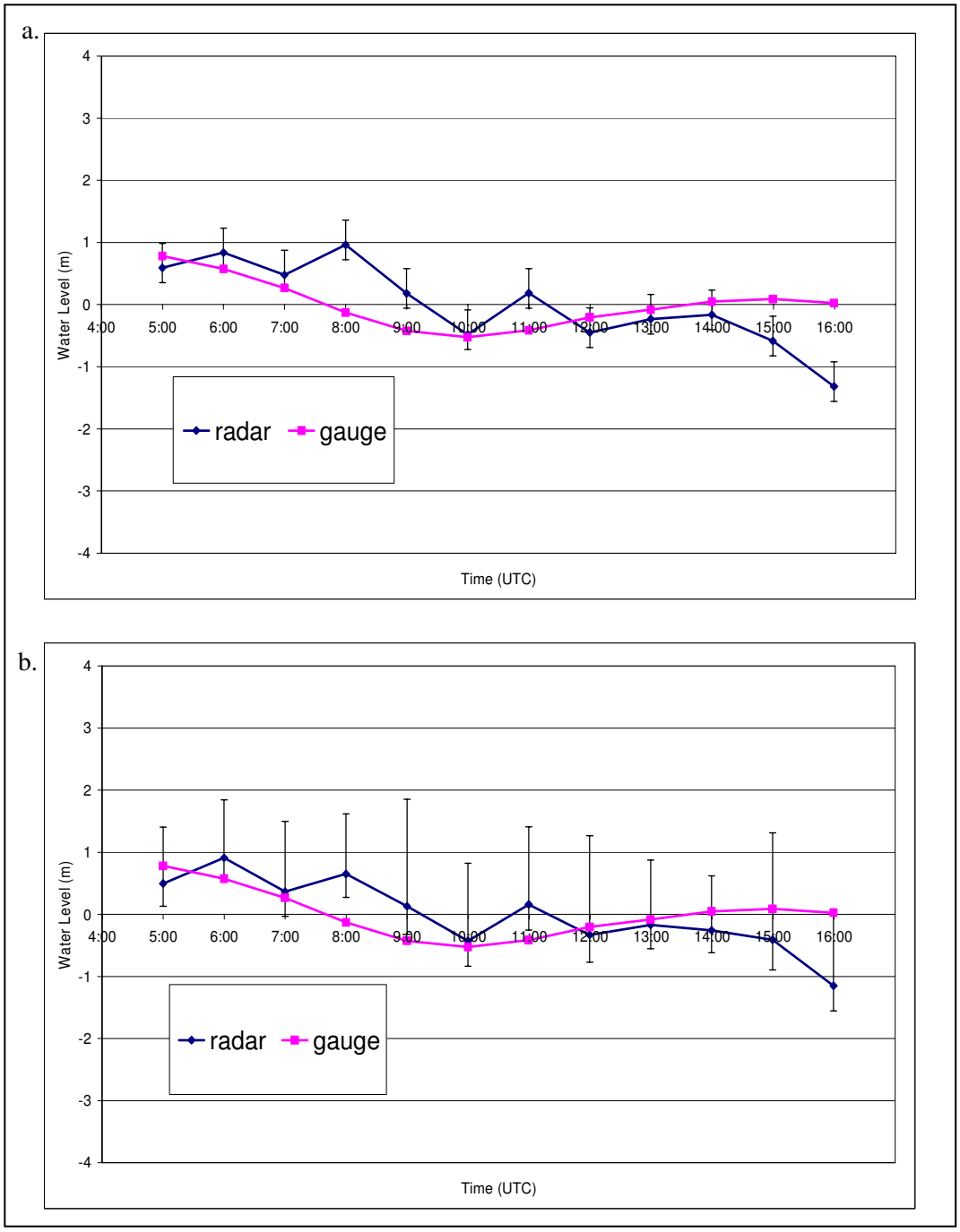

Figure VI-1: Graph representing the tidal cycle during period 3 at 28 October 2002 after subtracting the mean water level of the series from every time step. The pink line is tidal gauge measurement in Westerland and the blue line is the estimated tidal cycle from radar sequences. The bars show confidence interval of variance. a. the average radar water level at the 81 neighboring cells around the point (3460944.34, 6103240.84); b. the average radar water level after filtering with ± 0.25 m at the 81 neighboring cells.

VII. Appendix

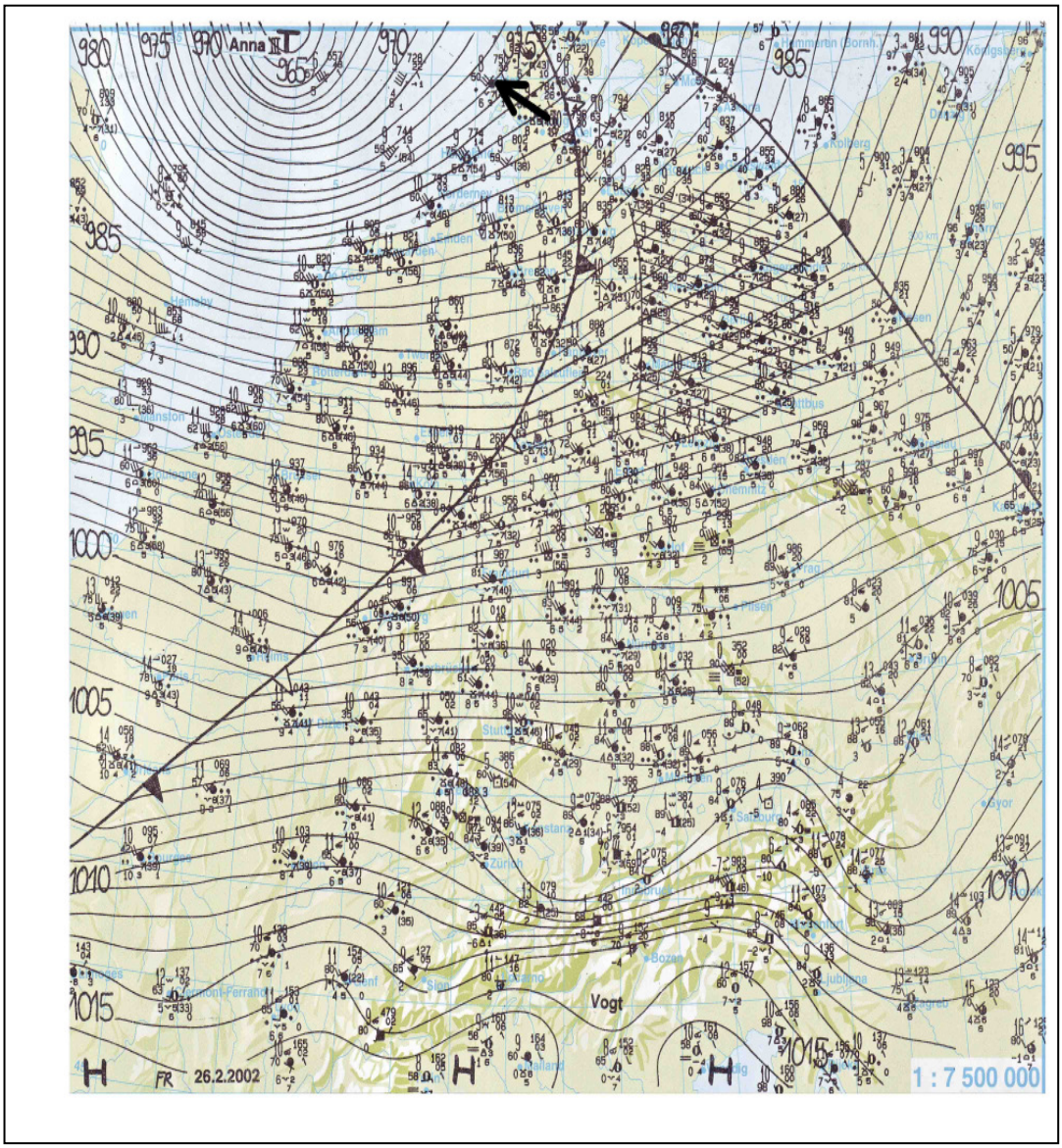

Figure VII-2: Atmospheric pressure (barometric phenomena) (FLAMPOURIS 2008), Sylt is denoted with black arrow.

VIII. Appendix

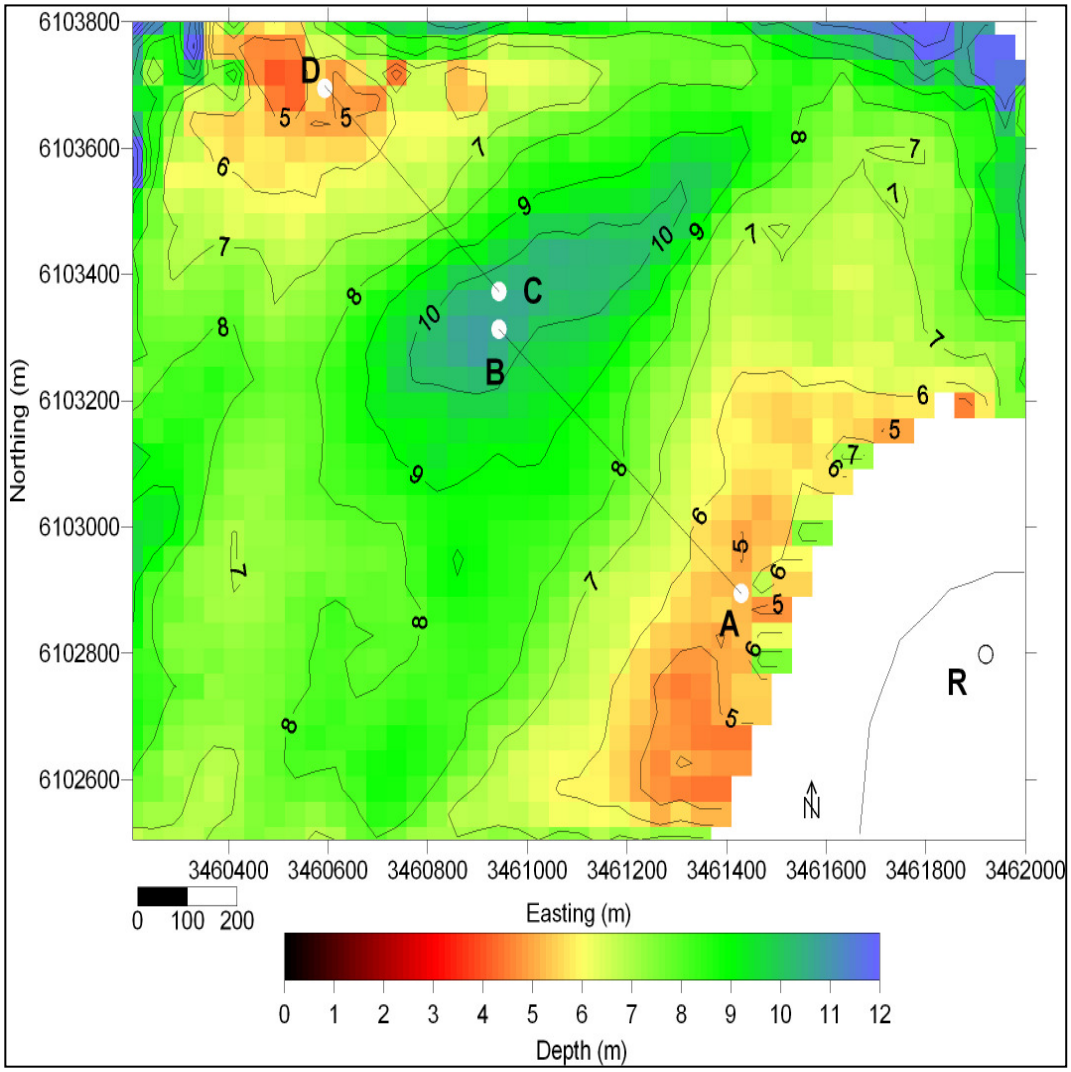

Figure VIII-1: Depth of the area of investigation during the storm period 2 (7 March 2002), as a result of averaging the calculated depths for 12 hours. The R symbol is the radar position. The white dot is the cross section A-B and C-D.

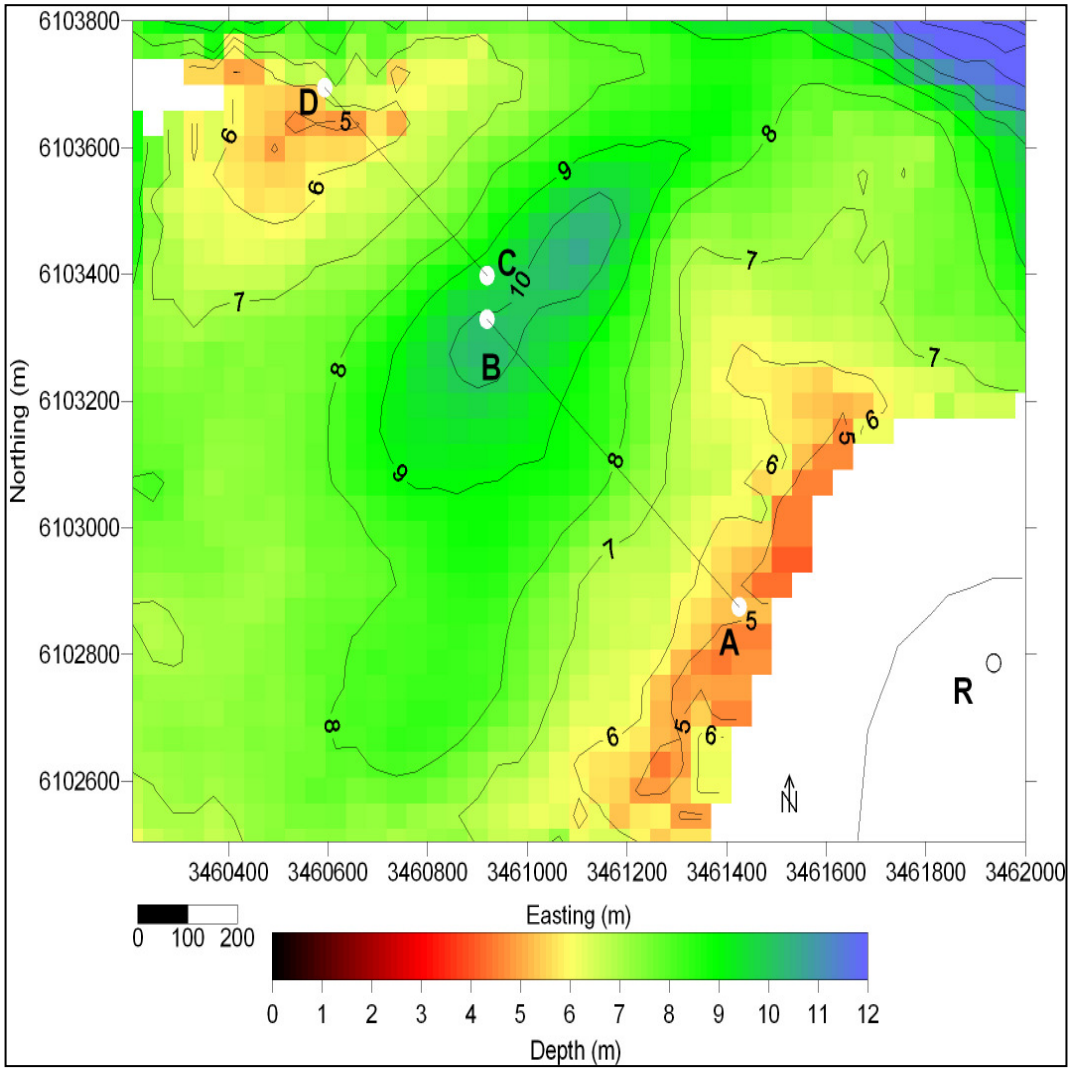

Figure VIII-2: Depth of the area of investigation during the storm period 3 (28 October 2002), as a result of averaging the calculated depths for 12 hours. The R symbol is the radar position. The white dot is the cross section A-B and C-D.

IX. Appendix

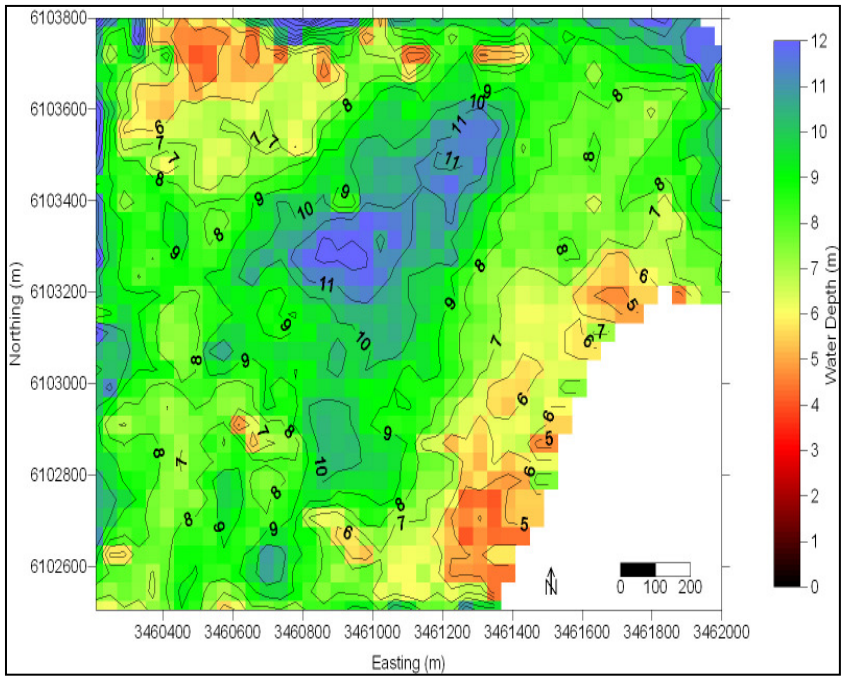

7th March 2002. 07:00

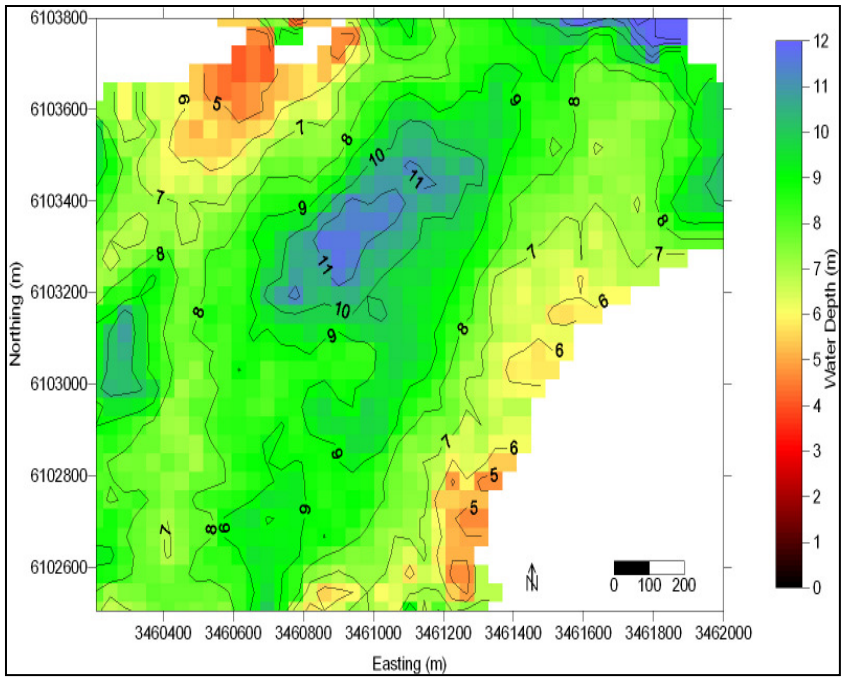

7th March 2002. 08:00

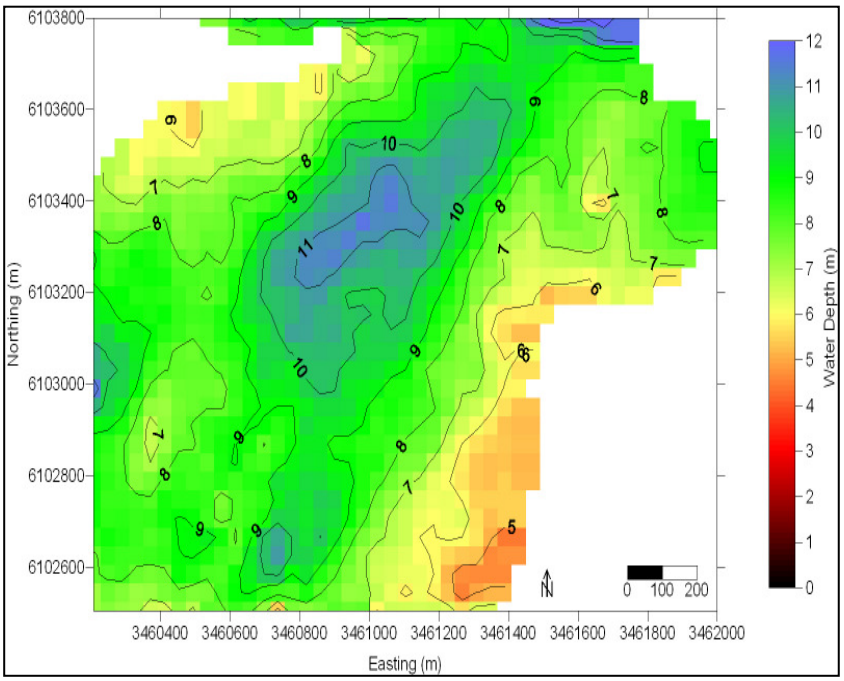

7th March 2002. 09:00

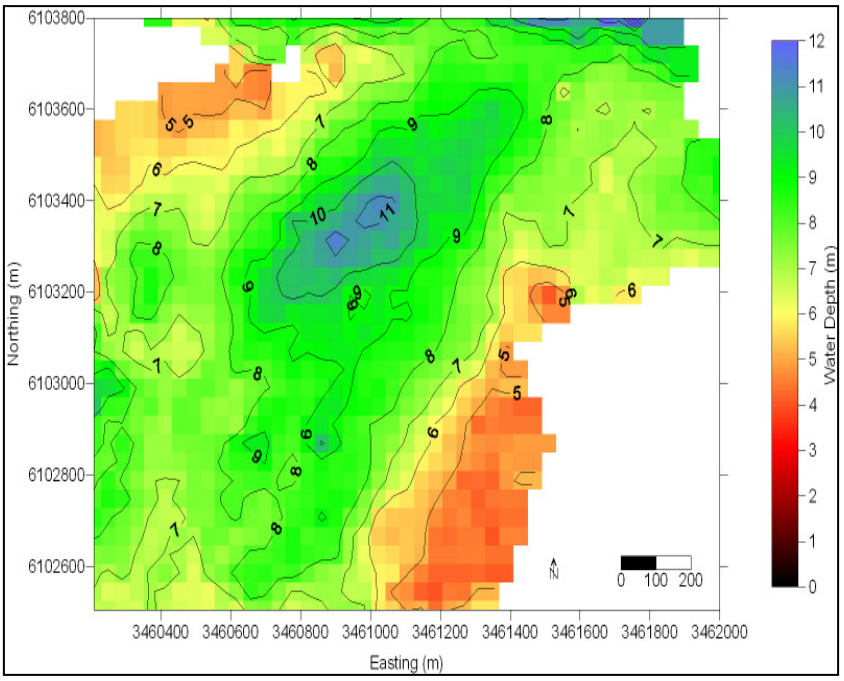

7th March 2002. 10:00

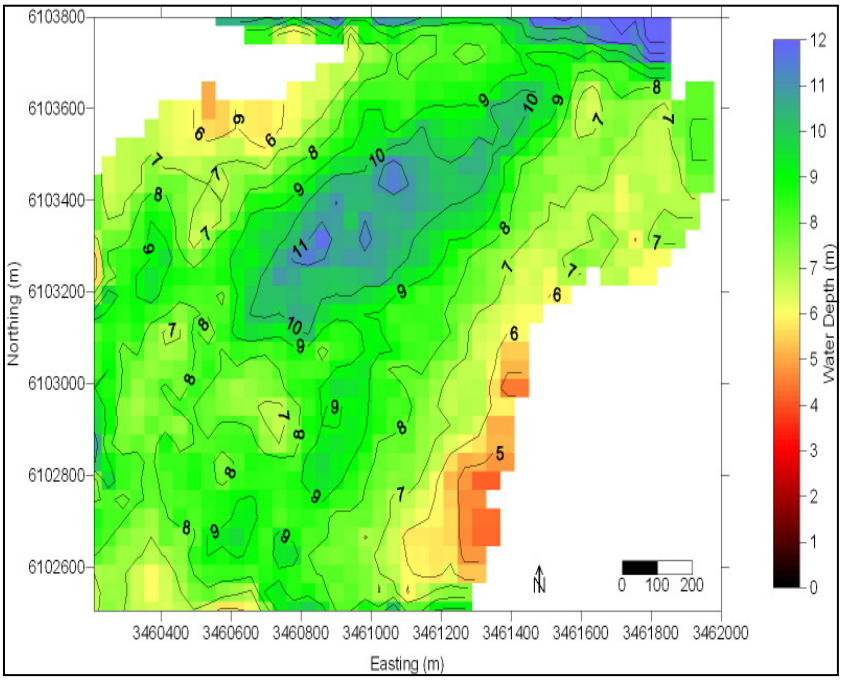

7th March 2002. 11:00

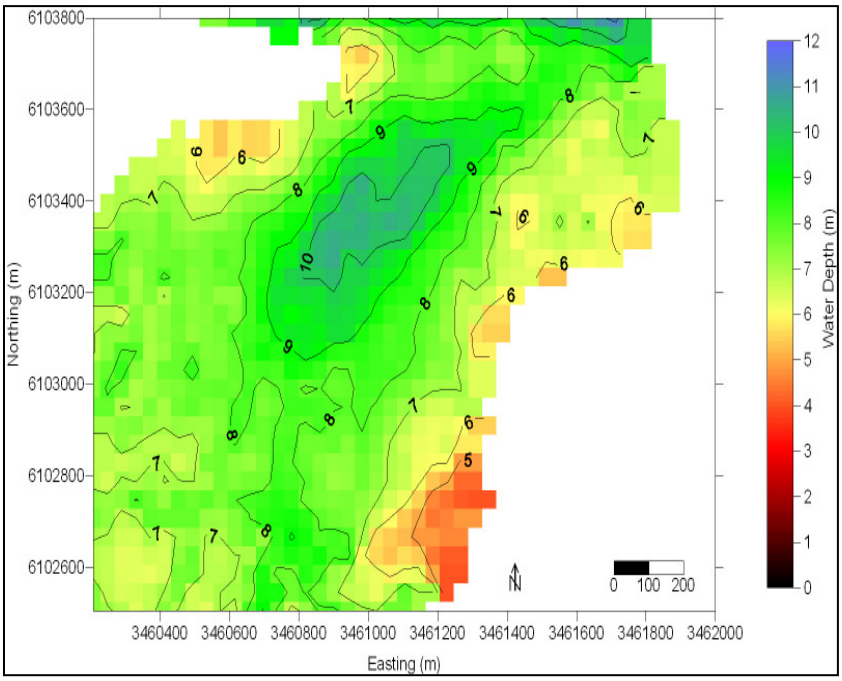

7th March 2002. 12:00

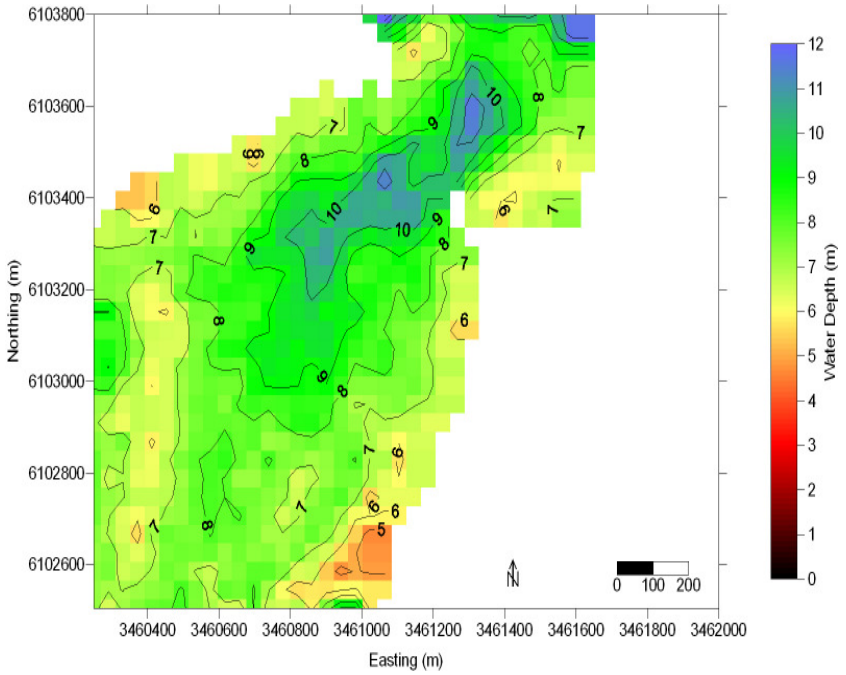

7th March 2002. 13:00

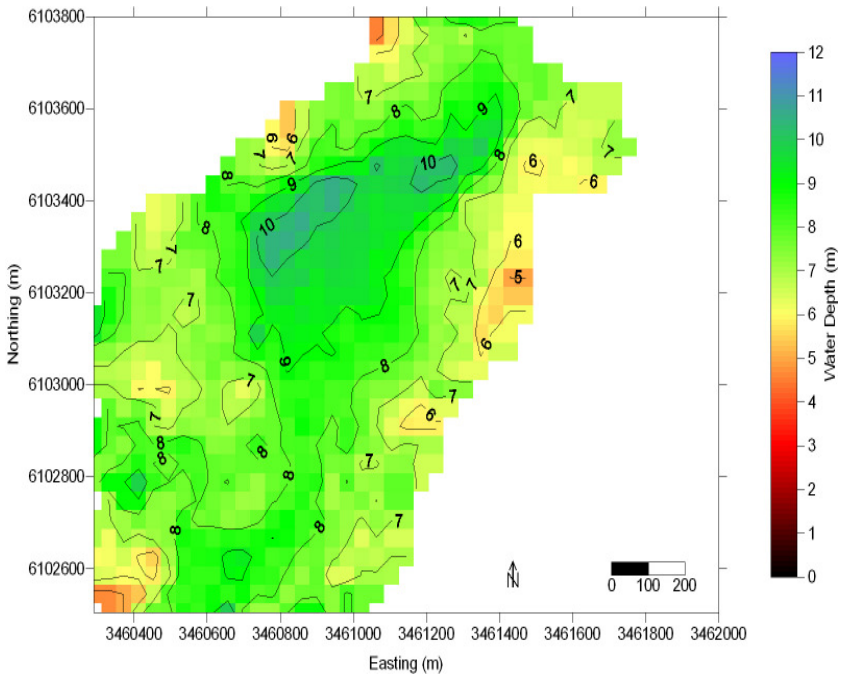

7th March 2002. 14:00

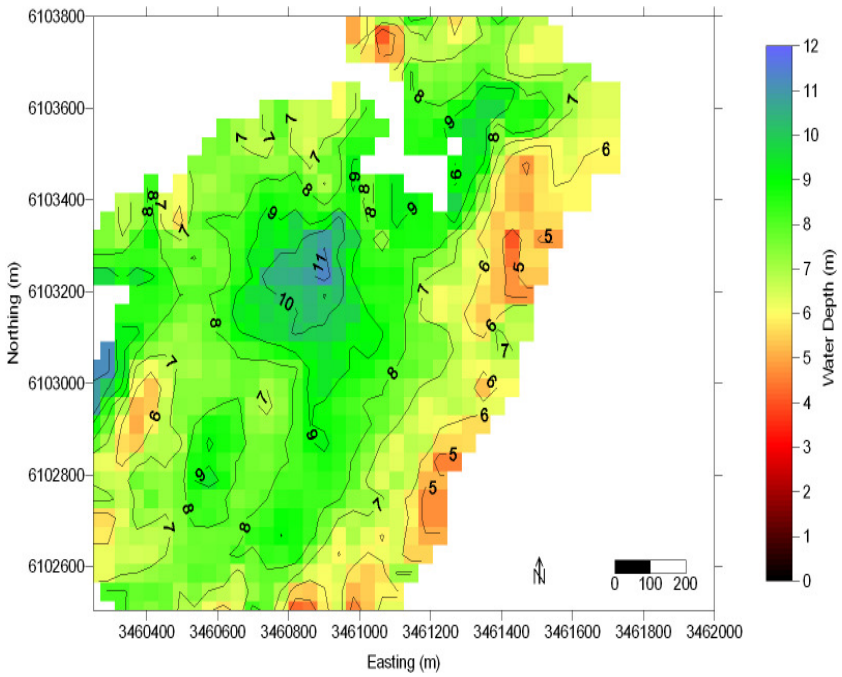

7th March 2002. 15:00

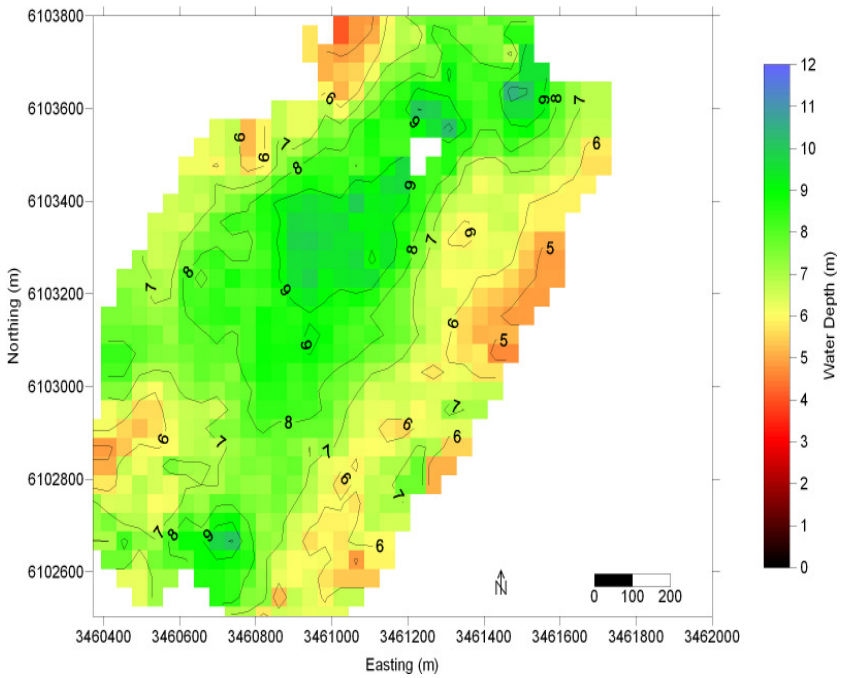

7th March 2002. 16:00

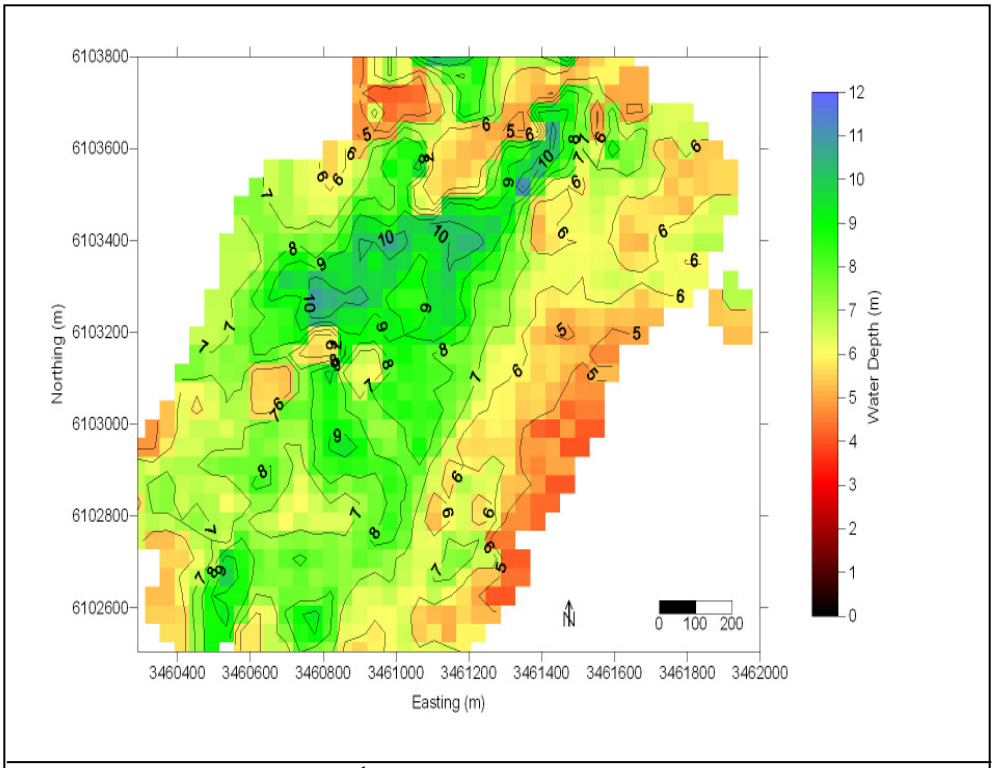

7th March 2002. 17:00

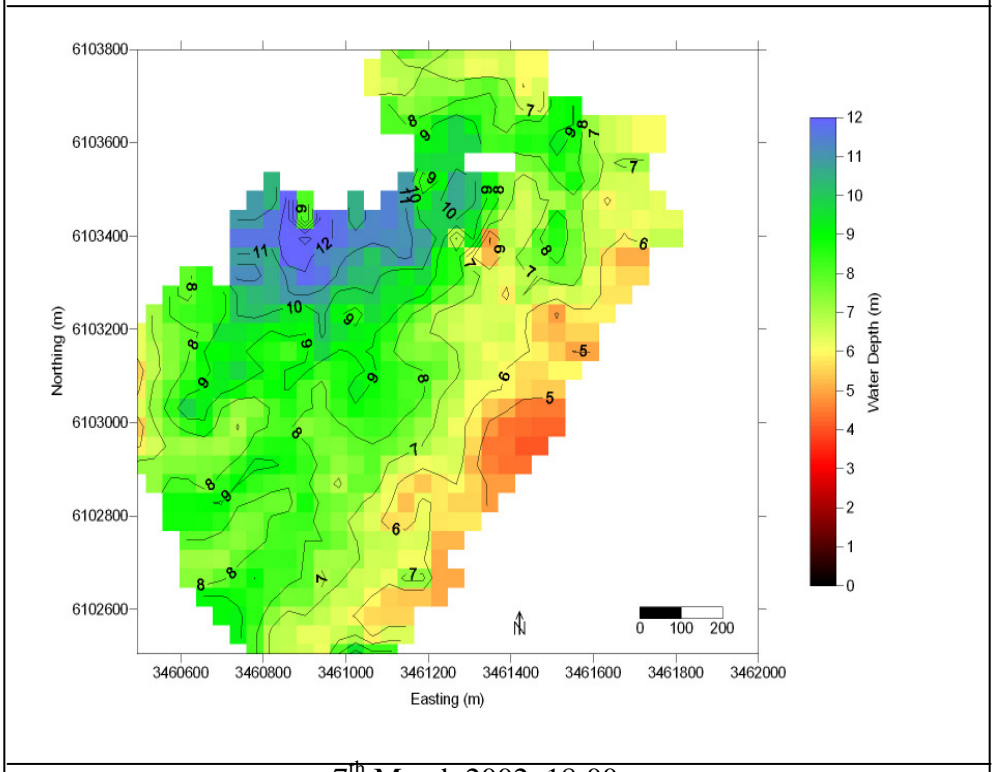

7th March 2002. 18:00

Figure IX-1: Visualization of hourly bathymetries of one tidal cycle, during period 2 (7th March 2002).

IX. Appendix

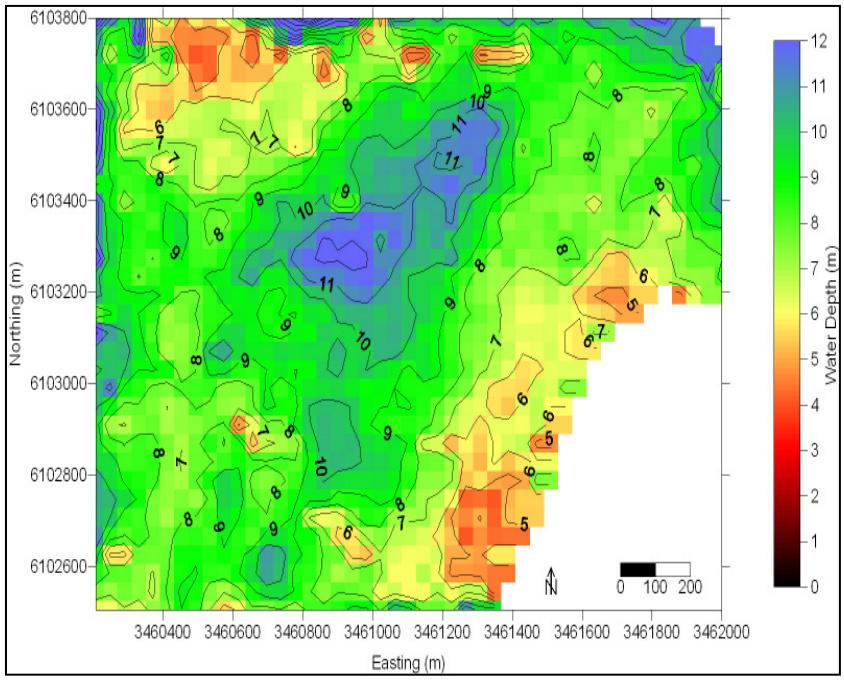

7th March 2002. 07:00

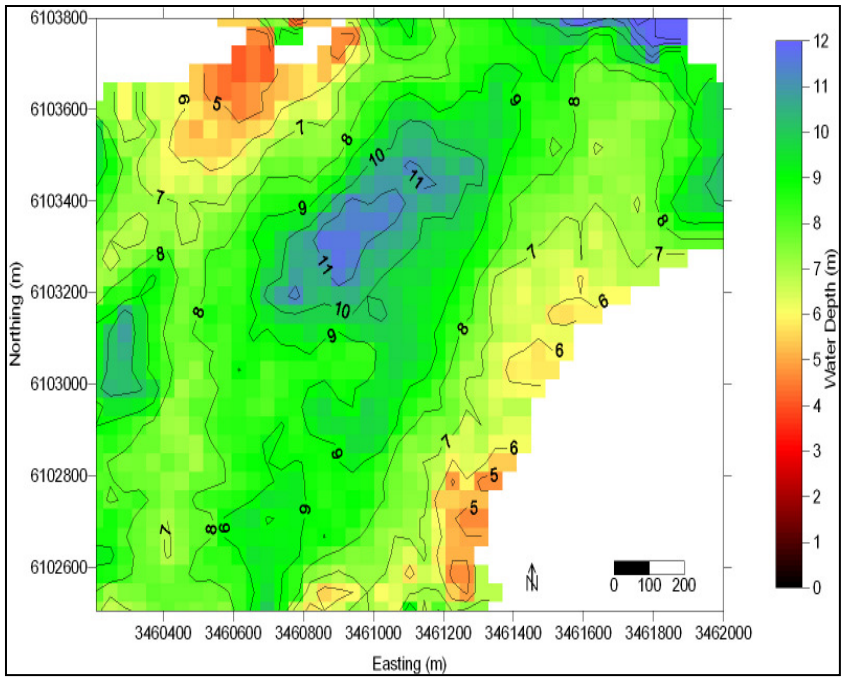

7th March 2002. 08:00

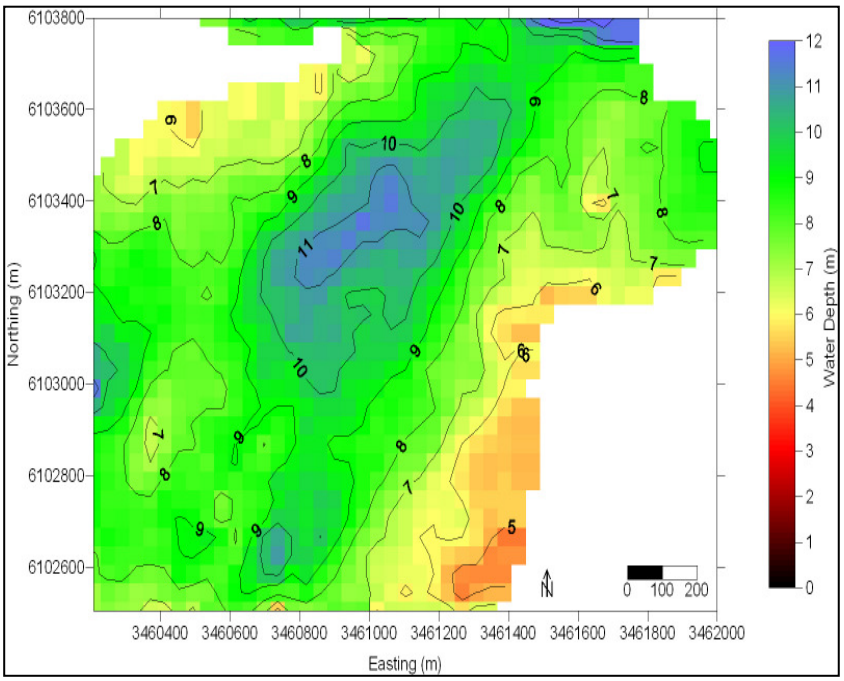

7th March 2002. 09:00

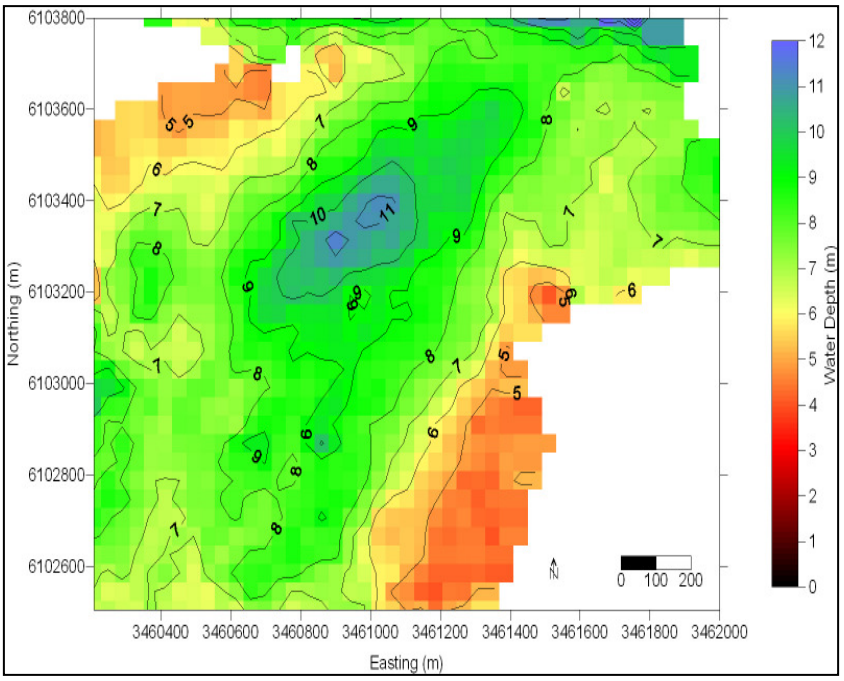

7th March 2002. 10:00

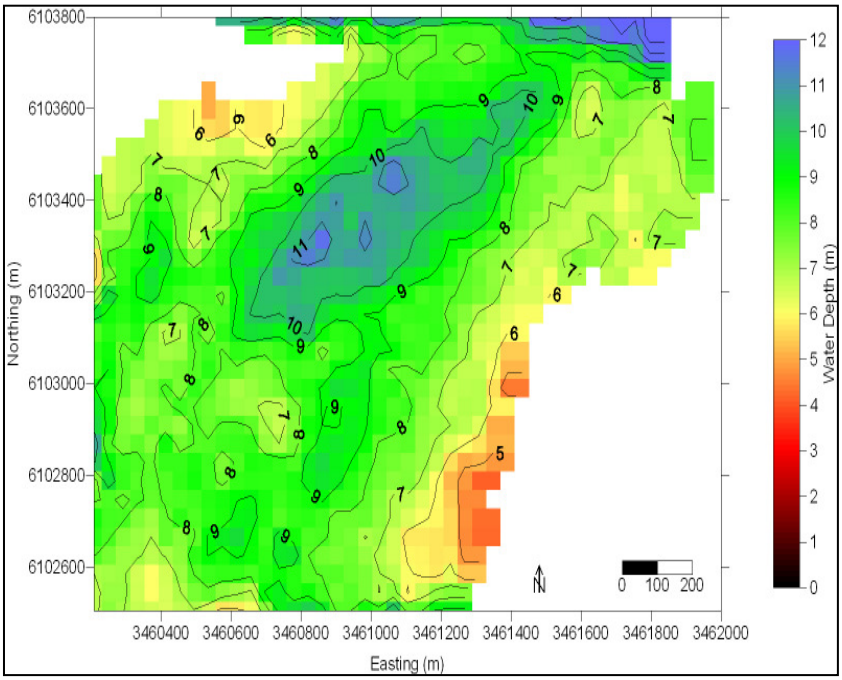

7th March 2002. 11:00

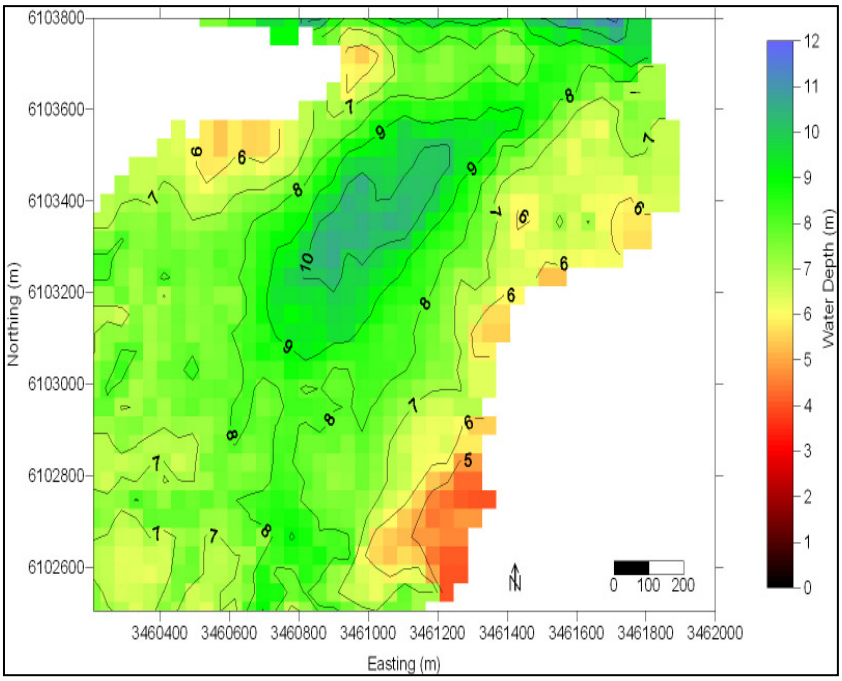

7th March 2002. 12:00

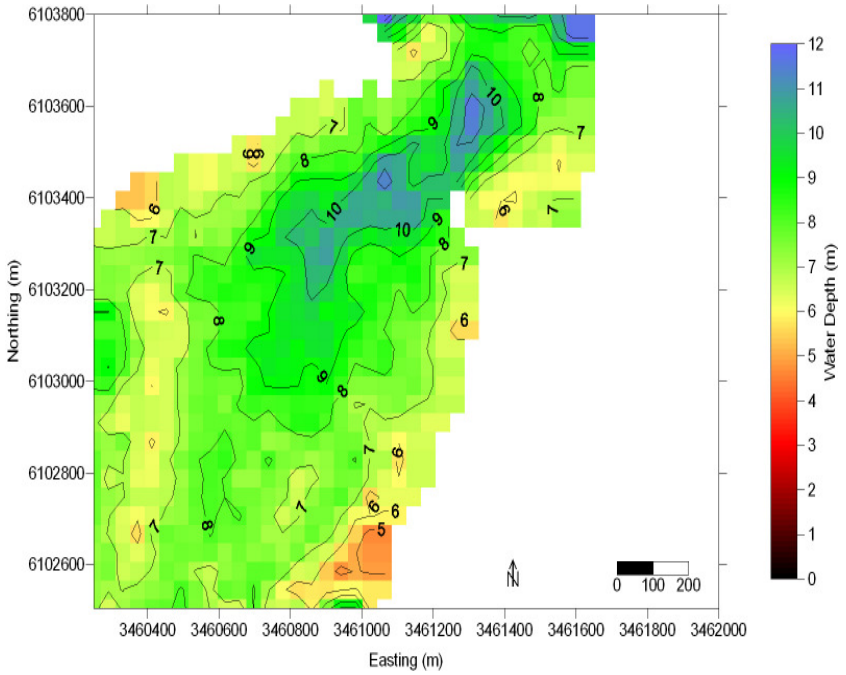

7th March 2002. 13:00

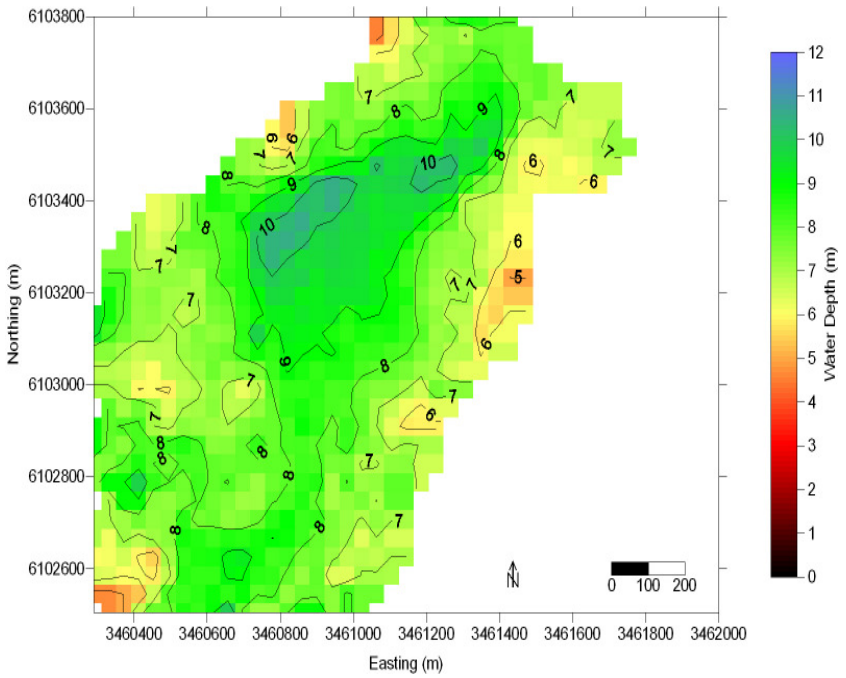

7th March 2002. 14:00

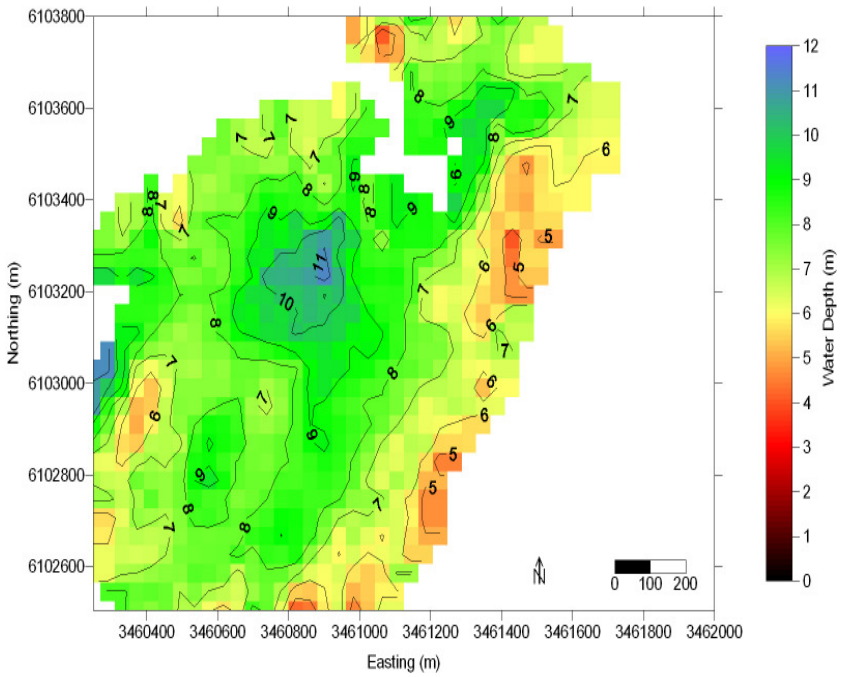

7th March 2002. 15:00

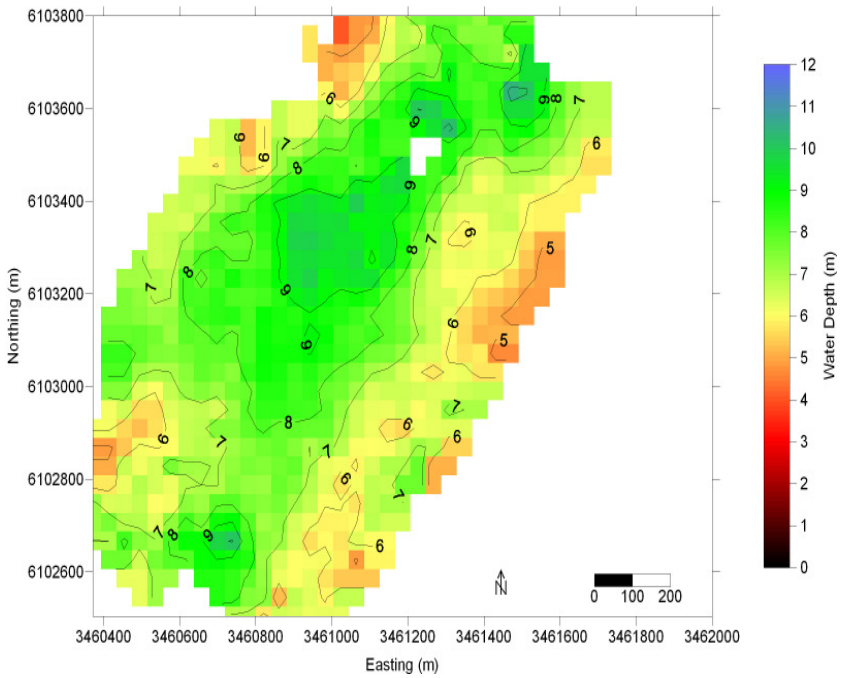

7th March 2002. 16:00

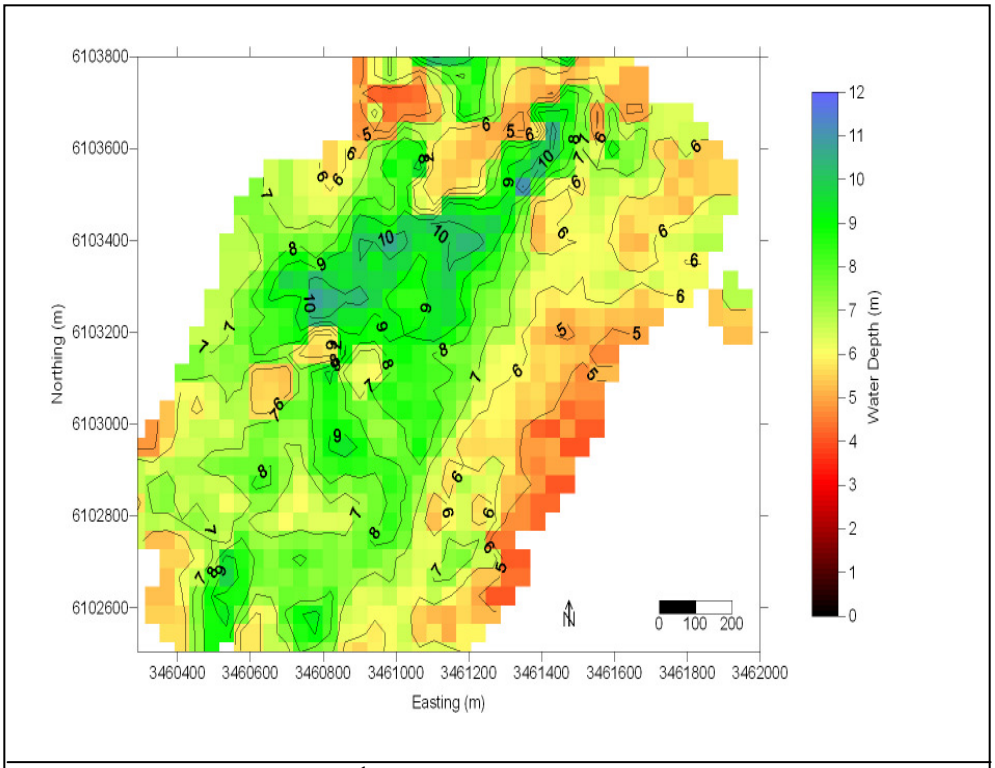

7th March 2002. 17:00

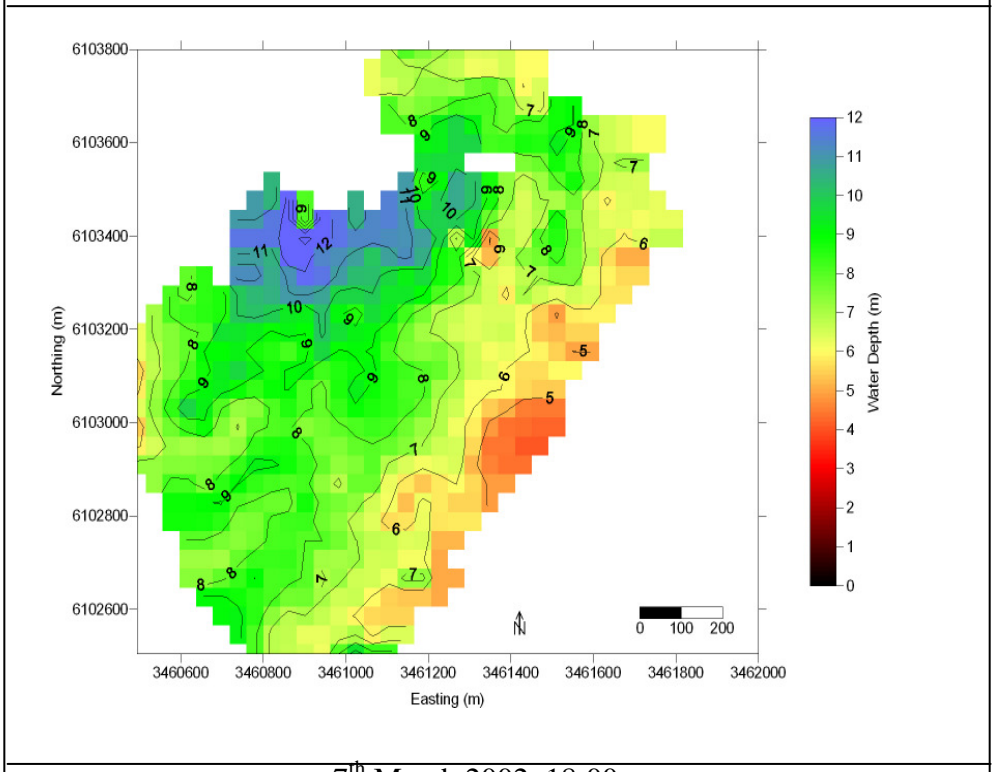

7th March 2002. 18:00

Figure IX-1: Visualization of hourly bathymetries of one tidal cycle, during period 2 (7th March 2002).

X. Appendix

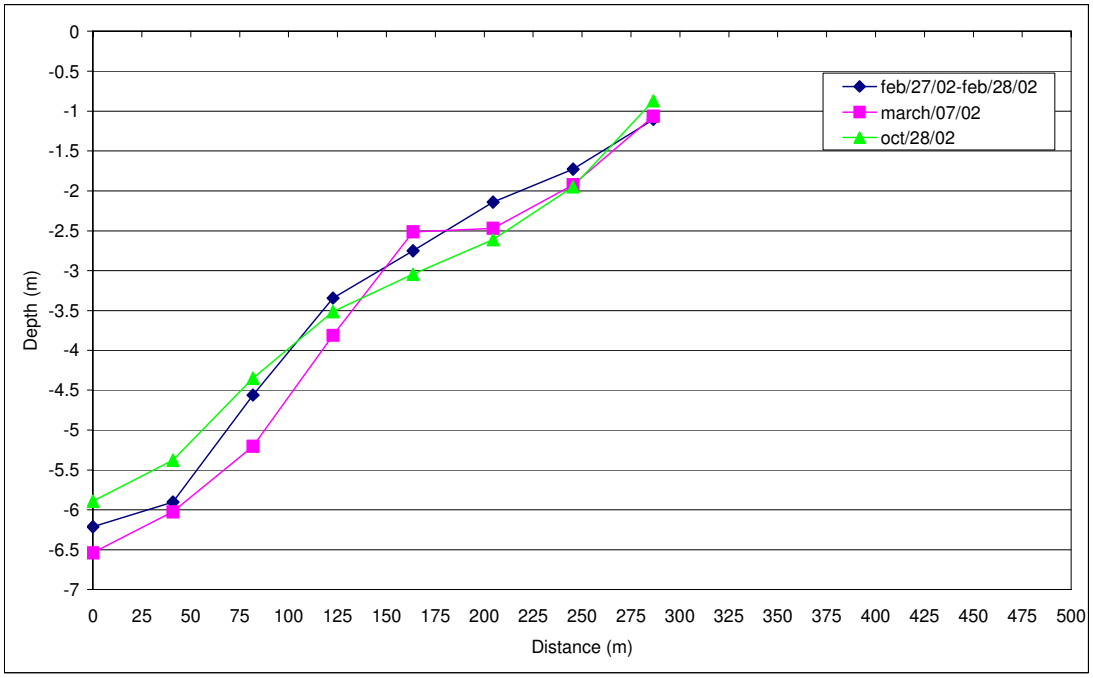

Figure X-1: The comparison of depth at the cross section C-D during the three difference periods; the reference is defined as the average of water level in 2002 (see figure 5.6).

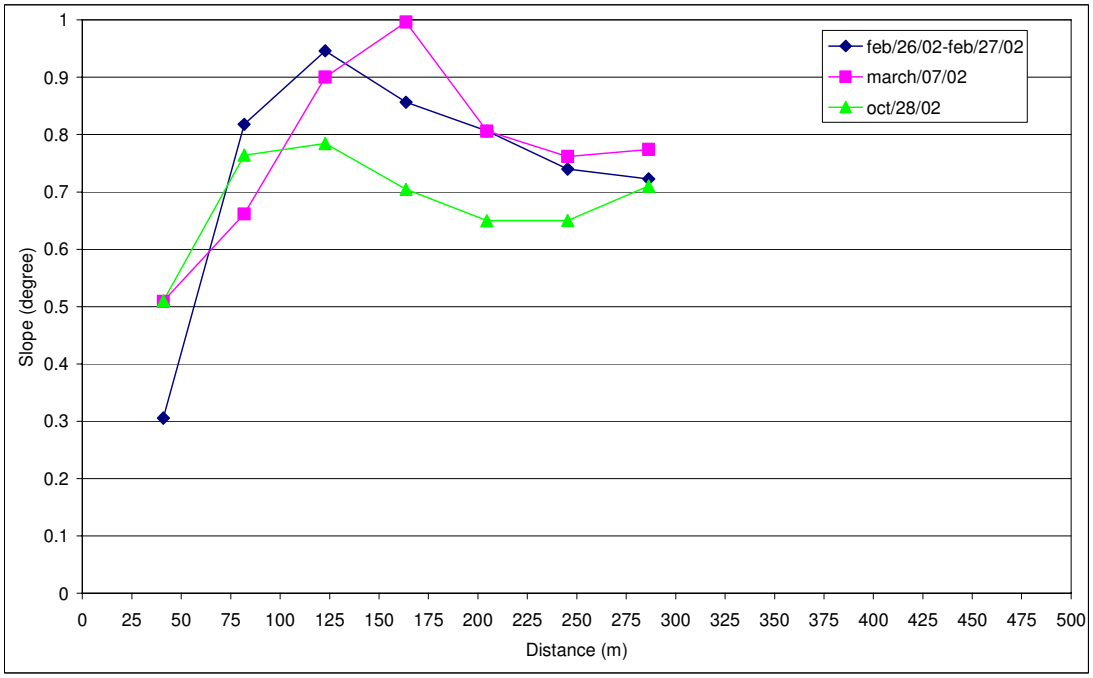

Figure X-2: The comparison of the slope over the cross section (C to D) for the three different periods (see figure 5.6).